10-29-2018

Mesoscale Modeling of Short Fatigue Crack Behavior in Metallic Microstructure and Application to the Structural Components

Hao Yuan
University of Connecticut - Storrs, hao.yuan@uconn.edu

Mesoscale Modeling of Short Fatigue Crack Behavior in Metallic Microstructure and Application to the Structural Components

Hao Yuan, PhD

University of Connecticut, 2018

Historically, many catastrophic failures of metallic structures, including steel structures most common for civil infrastructures, were found to originate from fatigue damages in local details. The progressive fatigue damages emerge to be short cracks in materials and grow into long cracks in components, finally lead to brittle structural failure. Meanwhile, the associated environmental effects such as corrosion and high uncertainties from many aspects including material microstructure and structural flaws also make it even more difficult to quantify the fatigue life of the components or structures. Partially overcoming the limitation of current experimental means and custom fatigue assessment methods, this dissertation develops a probabilistic multi-scale fatigue damage modeling framework to comprehensively analyze the short fatigue crack behavior in mesoscale microstructure and propagate the damage to component level and structural level analysis.

For statistical volume element (SVE) in mesoscale, a 2D short crack growth framework is proposed based on the microstructure-sensitive model and crystal plasticity based fatigue indicator parameters. Firstly, the transgranular crack growth method under constant amplitude load is developed and applied to weld microstructure as a demonstration. To incorporate the variable amplitude load, a nonlinear grain-based fatigue damage model is superposed. Then, the simulation algorithm evolves to Integrated Transgranular and Intergranular Crack Growth Method (ITICGM) and further to Corrosion-informed ITICGM.

As the natural linkage between short crack growth variability and long crack growth analysis of structural components, the time distribution to initial long crack is quantified by Deterministic Monte Carlo Simulations on mesoscale SVEs. With the help of order reduction technique, the quantification process is accelerated for regularized microstructures. In the application to single-site damage controlled structural component, pressure vessel has been taken as a representative to perform the fatigue crack growth simulation from microstructurally short crack to final failure. For components allowing multi-site damages

in a hotspot, the generation of time-deteriorated status has considered the crack initiation, growth and coalescence in multiple locations simultaneously. Some recommendations and a preliminary demonstration are also provided for surrogation of the time-deteriorated component with specific and damage-equivalent member for subsequent structural analysis.

Mesoscale Modeling of Short Fatigue Crack Behavior in Metallic Microstructure and Application to the Structural Components

Hao Yuan

B.S., Central South University, **2011**

M.S., Northwestern University, **2012**

A Dissertation

Submitted in Partial Fulfillment of the

Requirements for the Degree of

Doctor of Philosophy

at the

University of Connecticut

2018

APPROVAL PAGE

Doctor of Philosophy Dissertation

Mesoscale Modeling of Short Fatigue Crack Behavior in Metallic Microstructure and Application to the Structural Components

Presented by

Hao Yuan, B.S., M.S.

Major Advisor _____
Wei Zhang

Associate Advisor _____
Michael L. Accorsi

Associate Advisor _____
Jeongho Kim

Associate Advisor _____
Ramesh B. Malla

University of Connecticut
2018

DEDICATION

To my parents and grandparents

To my beloved wife Huiying Luo

To my entire family

ACKNOWLEDGMENTS

I would like to sincerely thank my major advisor, Dr. Wei Zhang, for his inspiring guidance, patient mentorship and enduring support during my Ph.D. study at UConn. His flexible personality allowed me more space and time to explore the research field freely. His encouragements helped me through the frustrating time during paper rejections and revisions. His strong support on attending conferences led me to the state of art in different related fields and helped to push forward my research. He always did all he can to ease my Ph.D. journey and setting out for a career. It has been my greatest experience to work with such an open-minded, diligent, comprehensive and helpful mentor.

I also want to thank my associate advisors and dissertation committee members: Dr. Michael L. Accorsi, Dr. Jeongho Kim, Dr. Ramesh B. Malla, Dr. Richard Christenson and Dr. Dianyun Zhang for reading this dissertation and offering constructive comments. I also want to express my particular gratitude to Dr. Gustavo M. Castelluccio (Cranfield University, UK) for his in-depth advice and corrections on partial contents forming the dissertation. I also appreciate the help and support on paper publications from Dr. Jeongho Kim, Dr. Amvrossios C. Bagtzoglou, Dr. Yongming Liu (Arizona State University), and Dr. Huijuan Liu (Guangxi University, China). And thanks to all other faculty and staff at UConn, who have taught me, helped me and supported me while pursuing my Ph.D. degree.

The graduate assistantship and fellowship support from several agencies, including UConn, UConn School of Engineering, UConn Graduate School, UConn Department of Civil and Environmental Engineering, National Science Foundation, and Eversource Energy Center, is fully acknowledged.

I thank all my fellows in Dr. Zhang's DM2L group for various academic support, and all friends at UConn for enriching my hard journey of doctoral study with colorful life and lots of laughter.

Last but not least, I am truly grateful to my big and close family for their dedicated nurture and endless support. I would offer my warmest thanks to my wife, Huiying Luo, for her companionship, follow, comprehension, compromise, forgiveness, support, and full of love embedded.

TABLE OF CONTENTS

LIST OF FIGURES

LIST OF TABLES

CHAPTER 1 INTRODUCTION

1.1 Research Scope and Motivation

Fatigue is one of the primary damage and failure mechanisms for many types of structures, such as aerospace, offshore, coastal structures or the associated structural components subjected to physical or chemical process related cyclic loadings and stresses/strains. For the high cycle fatigue (HCF) assessment in civil infrastructure, *S-N* curve approach combined with damage accumulation law still prevails under most circumstances and develops into different forms. The method does cover the crack initiation and growth until total failure; however, it lacks a physical base, and it is established upon empirical processing of mass experimental data. As for the explicit damage like fatigue crack growth, in the present codes or specifications for offshore engineering or aerospace engineering, an engineering critical assessment (ECA) approach or Fitness-For-Services (FFS) assessments are often used to evaluate the significance of the initial flaw or defects – by assessing the remaining fatigue life of the structural member or checking if the cracks are stable (API (American Petroleum Institute) and ASME (The American Society of Mechanical Engineers) 2016; BSI (British Standard Institution) 2013; EDF Energy 2009). However, the size and shape of the flaws or defects are usually based on assumptions, and Linear Elastic Fracture Mechanics (LEFM) based approaches (various modifications of Paris' law) are implemented to predict remaining cycles toward failure. In such process, the evolution of the flaws (mostly as initial crack) due to the dynamic interactions of the structures and the surrounding environments in the physical and chemical interaction process cannot be captured. However, significant uncertainties exist in the initiation phase and short crack regime especially when it could not be effectively detected by nondestructive testing (NDT) or nondestructive evaluation (NDE) techniques – due to the intrinsic neglect of heterogeneous microstructure of local material – make it extremely challenging for accurate prediction of remaining life of existing civil infrastructure. Physically speaking, crack growth is a very slow and continuous process that takes place on several different length scales with different phases, such as nucleation, microstructurally small crack (MSC), physically

small crack (PSC), and long crack (LC) for polycrystalline fatigue cracks. Due to the shared grain size variation, MSC and PSC are usually combined in the analysis (Castelluccio and McDowell 2014). Since the short crack nucleation and propagation regime could account for about 90% of the structural fatigue life, predictions of the short crack growth have been critical if such short cracks could not be detectable by the current state-of-the-art nondestructive examination methods (Krupp 2007). It is also technically impossible to performing detection at all critical locations of a large complex civil infrastructure using current NDT or NDE techniques. As a result, many historical catastrophic failures were found to originate from cracks in local details and these localized damages are usually identified as the main reasons for the failure of structural systems (Engelhardt et al. 2004). To better estimate the remaining life of the civil infrastructure and provide early warnings in advance for possible catastrophic failures, it is necessary to comprehensively analyze the short fatigue crack damage and propagate the damage to a structural component level analysis.

Since the most state-of-the-art NDT or NDE techniques is still challenging, if not impossible, to detect all short cracks such as those at the grain size level, the detection, diagnosis, and prediction of the short fatigue crack behavior usually is achieved by a probabilistic modeling method, which is also out of the capability of conventional code-based method. Ranging from macro-scale to micro-scale modeling techniques, several specific short crack nucleation and propagation methods were developed (Fricke 2014; Radaj et al. 2006). However, the continuum mechanics based structural/notch stress/strain approaches and strain analysis of structural detail can result in strong discontinuities, which make the continuum approach questionable in the crack initiation range (Lemaitre and Desmorat 2005; Liu and Mahadevan 2009). In addition, the scattering effect of fatigue data could not be captured by the model, due to the intrinsic neglect of heterogeneous data for microstructure in mesoscale, which are proven to be vital for the short crack nucleation and growth (Buirette and Degallaix 1998; Venkateswaran et al. 2005). Therefore, to balance the complexity in micro-scale models (molecular dynamics) and discontinuity-loss in macro-scale models (equivalent initial crack or continuum damage mechanics), mesoscale models based on crystal plasticity and continuous dislocation theory were developed (Dang-Van 1993; Mughrabi et al. 1981; Sehitoglu et al.

1989; Tanaka and Mura 1981). On this scale, microstructure (the grain configuration and grain boundary network) of polycrystalline material plays a key role in the evolution of micromechanical stresses and strains and consequent development of damage with the evolution of microstructurally short crack with a length scale from 10μm to 1mm. Random grain shapes and sizes, combined with different crystallographic orientations, inclusions, voids, or other microstructural features result in locally anisotropic and highly heterogeneous behavior of the microstructure with direct influence on the damage evolution. For practical usage in fatigue life prediction, consideration of variable amplitude load for short crack regime is also necessary. In addition, for some critical infrastructures, local environments for structural components or connections could be corrosive, such as coastal bridge connections with contact to de-icing chemicals or weldments for pressure vessels/pipelines in chemical infrastructures. At these critical locations, cracks will be more likely to initiate and could propagate much faster in a corrosive environment combined with cyclic stress cycles over its life cycle. Due to the complex nature of diffusion of chemicals and electrochemical reactions at the crack tip under the influence of remote stress and microstructure in plastic zone (Bathias and Pineau 2013), simulations of the simultaneous action of applied stress and a corrosive environment, termed as stress corrosion cracking (SCC) under dwelling load or corrosion fatigue under cyclic load, have been challenging (Davis 2006).

The link from short fatigue cracks in mesoscale to macro damages in a structural component may require multi-scale approaches such as concurrent method and the hierarchy method (Sun and Li 2014). However, although with the development of Extended Finite Element Method (XFEM) and Peridynamics, the multi-scale coupled finite element analysis is still unaffordable or even impossible due to the nonlinearity, multiple hotspots in multiple components, different microstructures and long-term cyclic loading. Since the remote stress field is not sensitive to the short crack growth (considered independent) in local details (Schijve 2009), coupled analysis can be avoided by using certain probabilistic approaches instead. These approaches could include Monte Carlo Simulation in mesoscale, initial macro crack sampling, and long crack growth through sophisticated techniques in component level. Using the surrogate

model of damaged components to facilitate structural analysis with simpler elements is also a promising topic, which is explored briefly for the current research.

In summary, the hidden nature of large uncertainty in the fatigue life prediction, the overlook of the short fatigue crack initiation and propagation under different operational and extreme loading conditions, and the gap between the varied local damages and the structure/component performance, are the motivations of the following research on the probabilistic modeling of the short fatigue crack in the metallic microstructure including the associated applications to structural components.

1.2 Literature Review of Research Background

This preposed and concise literature review provides a general background related to the present research. More detailed and targeted literature review can be found in each individual chapter.

1.2.1 Short fatigue crack concept and microstructure influence

Pearson first reported the anomalous behavior between short and long crack in an aluminum alloy (Pearson 1975). For a given ΔK, short cracks grow faster than long cracks (by at least one order of magnitude); short cracks grow with ΔK values lower than the propagation threshold ΔK_{th}. In long crack propagation regime, the Paris's Law that uses stress intensity factor range as fatigue drive force is widely used and verified by experiments. However, it cannot describe the low-stress range fatigue (i.e. Regime I near/under long crack threshold ΔK_{th}) or short crack initiation and propagation where the pre-conditions of linear elastic fracture mechanics, like similitude and small scale yielding, are not satisfied (Anderson 2005).

In nowadays research, the evolution of fatigue cracks is recognized as a continuous process that takes place on several different length scales with different phases, such as incubation, nucleation, and propagation, for the whole fatigue crack life (Dunne 2014). The total fatigue life in polycrystalline fatigue crack can be partitioned into four physically-based regimes with varied ranges for crack length associated with material type and microstructure: nucleation (10^{-7}m ~ 10^{-5}m), microstructurally short crack (MSC, 10^{-}

^{7}m ~ 10^{-5}m), physically short crack (PSC, 10^{-5}m ~ 10^{-4}m), and long crack (LC, > 10^{-3}m). Since sometimes MSC and PSC are hard to distinguish due to the grain size variation, the two regimes can be combined (Castelluccio and McDowell 2014):

$$N_f = N_{nuc} + N_{msc} + N_{psc} + N_{lc} = N_{nuc} + N_{msc|psc} + N_{lc} \tag{1-1}$$

It is noteworthy that, for high-cycle fatigue (HCF) loading conditions and high-strength materials, up to 90% of a component's fatigue life can be determined by the phase of crack nucleation and the propagation of MSC (Krupp 2007).

A crack can initiate in microstructural features such as pores, inclusions, slip bands (including PSB), grain boundaries, and surface with single slip system activation. Crack initiation along slip bands depends on the barrier strength, the crystallographic misorientation, and the structure of grain boundaries. Of particular significance for transgranular crack initiation are triple points. Often, triple points are the locations with of highest stress. The stress level may be further increased by the elastic anisotropy and the intergranular damages. Intergranular crack initiation at room temperature can be due to grain boundary precipitates or segregation, elastic anisotropy and plastic incompatibility. For short crack propagation, microstructure also generates significant influence. Due to microstructural barriers, grain or phase boundaries, immediately after crack initiation, the crack-propagation rate drops continuously. Once a short fatigue crack is not ultimately stopped by a microstructural barrier, the crack-propagation rate will increase again. It can be concluded that the abnormal crack propagation behavior of microstructurally short cracks is determined to a certain degree by metallurgical effects, such as the size and orientation distribution of the grains and precipitates. For residual stress, it is negligible to crack initiation but retard the crack propagation (Krupp 2007).

1.2.2 Models for short fatigue crack growth

In the macro scale, the short crack nucleation and propagation are simplified into an equivalent initial crack concept (Liu and Mahadevan 2009) or simulated by continuum damage mechanics (Lemaitre and Desmorat

2005). In the micro-scale method which is dealing with a crack under μm in length, the atomic mechanics or molecular dynamics are usually used to analyze the slip behavior and dislocation structure, while discrete dislocation theory is another tool to capture the highly slip localization (Dunne 2014). However, the microscale method is difficult to calibrate and characterize via conventional fatigue test with replica or in-situ microscope and is not practical for most of the practical engineering problems with complicated boundary conditions.

To bridge the gap between the micro and macro method, the mesoscale methods based on crystal plasticity and continuous dislocation theory were proposed (Dang-Van 1993; Mughrabi et al. 1981; Sehitoglu et al. 1989; Tanaka and Mura 1981). On this scale, microstructure (the grain w/o grain boundary network) of polycrystalline material plays a key role in the evolution of micromechanical stresses and strains and consequent development of damage with the evolution of MSC with a length from 10μm to 1mm. Random grain shapes and sizes, combined with different crystallographic orientations, inclusions, voids, and other microstructural features result in locally anisotropic and highly heterogeneous behavior of the microstructure with a direct influence on the damage initialization and evolution.

Several analytical models for describing short fatigue crack growth rate were demonstrated by Miller (Miller 1987), de los Rios (de los Rios et al. 1985), and Angelova (Angelova and Akid 1998) by analyzing the macroscale experimental data from small-specimen testing. Hussain (Hussain 1997) reviewed many analytical models of short fatigue crack growth behavior and summarized micro characteristics for short crack growth. Nowadays, Tanaka-Mura model (mostly for short crack initiation) (Tanaka and Mura 1981), Miller-Hobson model (Miller 1987), Navarro and de los Rios model (Navarro and de los Rios 1988) are still commonly used in the numerical simulations.

With the advanced computing technology and improved calculation capacity, more mesoscale models were developed. In the crack nucleation phase, several new local criteria, such as minimum total PSB energy, microscopic fracture stress at the grain boundary and ex/intrusion height, were proposed to consider local properties such as strain gradient and PSB substructure (Polák and Man 2014; Sauzay and Moussa 2013). As for MSC propagation, Lillbacka (Lillbacka et al. 2006) evaluated the fatigue crack

growth rate within the first two grains using a crystal plasticity model for an austenitic-ferritic duplex stainless steel idealized as a 2D microstructure with a predefined crystallographic growth path for the crack. The total crack growth rate was computed as a fraction of the integral of cyclic plastic deformation acting on the crystallographic planes along which the crack grows. Similarly, Duber (Düber et al. 2006) and Kunkler (Künkler et al. 2008) characterized the MSC crack growth rate using a cyclic shear-based 2D cohesive zone model along slip band segments. By assuming a crack growth rate proportional to the range of cyclic crack tip sliding displacement, the meandering crack path through multiple grains was determined, and the transition from single- and multi-slip crack growth was predicted.

Recently, the microstructure-sensitive model with fatigue indicator parameters (FIPs) has been a promising tool to describe both the MSC nucleation and growth with the non-local measure (Pineau et al. 2016). Many FIPs, such as those based on accumulated plastic strain and dislocation density (Kartal et al. 2014; Manonukul and Dunne 2004; Sweeney et al. 2013), energy dissipation (Sangid 2013; Sangid et al. 2011), averaged effective strain and tensile stress (Ghosh and Chakraborty 2013; Sinha and Ghosh 2006), are proposed based on different non-local measure and varied fatigue damage mechanism for short fatigue crack research (Dunne 2014). McDowell and co-workers (Castelluccio et al. 2014; Pineau et al. 2016) developed a systematic method namely microstructure-sensitive model to apply FIP into multiaxial MSC nucleation and growth based on accumulated plastic strain per cycle and normal stress. Due to the complexity of cyclic microplasticity and damage formation in HCF, the FIPs provide a computable parameter with which differing microstructures may be quantified in fatigue analysis. Extreme value hotspots that determine the low probability of failure in HCF are introduced which relate to weighting factors on the FIPs in spatial correlations between factors thought to drive fatigue (e.g. inclusions, grain size, misorientations).

1.2.3 Corrosion effect

Disastrous accidents have occurred due to fatigue cracks starting from corrosion damage, in several cases corrosion pits. In the gaseous environment, water vapor, oxygen, and hydrogen can accelerate the corrosion process. In a liquid environment, salt water is one of the most common corrosion sources. Corrosion fatigue as a problem of a structure in service is characterized by many variables which can be highly different from the material/environment system in the laboratory research.

Modeling the corrosion effect on fatigue behavior is challenging since the corrosion fatigue is a complex process associated with multiple damage mechanisms that have not been studied thoroughly. The earlier research of the author focused on the general corrosion effect of fatigue performance of existing bridges (Zhang and Yuan 2014). However, the corrosion model adopted is obviously oversimplified for nominal stress approach of fatigue assessment. Corrosion effect studies on the short fatigue crack models are especially limited due to the complex nature of diffusion of chemicals and electrochemical reactions at the crack tip under the influence of remote stress and microstructure in the plastic zone (Bathias and Pineau 2013). The most common mechanisms considered in corrosion fatigue model are anodic dissolution, hydrogen embrittlement, or a combination of both (Craig and Lane 2005). Anodic dissolution based corrosion fatigue studies started earlier and Macdonald et al. have built a systematically coupled environment corrosion fatigue model considering the electrochemical crack growth as a penetrating slot with moving wall boundaries (Macdonald and Engelhardt 2012). Akid et al. have combined the anodic dissolution with short crack growth models such as Hobson-Brown model and Navarro-de los Rios model with an empirical approach (Akid and Miller 1991; Angelova and Akid 1998; Murtaza and Akid 2000). However, for high strength steel, the hydrogen induced cracking dominates the corrosion fatigue mechanism (Mansor et al. 2014). Hydrogen-assisted cracking has to be more comprehensive because the electrochemical kinetics of the generation of hydrogen ions and subsequent absorption, the transport inside the metal, and the interaction of the metal with the dissolved hydrogen atoms have to be considered. The analytical models for hydrogen-assisted crack are reviewed by Boellinghaus and Hoffmeister (Boellinghaus 2000). Based on hydrogen diffusion simulation and certain experimental technique around the crack tip, Dmytrakh et al. form a relationship between fatigue crack growth behavior and local hydrogen

concentration near the crack tip (Dmytrakh et al. 2013). However, above corrosion fatigue crack models mainly focus on Paris regime or long crack. For MSC regime, microstructural effects play a role in hydrogen-informed corrosion fatigue analysis. In the fracture process due to hydrogen embrittlement in polycrystal like steel, the hydrogen preferentially attacks the grain boundaries (GB) rather than the inside of grain, since the diffusive velocity of hydrogen is much faster at GB (Shintaku et al. 2015). H atoms can diffuse in depths and trapped at grain boundaries. At slip transfer across GB, the presence of hydrogen increases the strain energy stored within the GB which could lead to the crack growth mode transition from the transgranular mode to the intergranular mode (Adlakha and Solanki 2016). Cohesive zone model (CZM) has been widely used for intergranular crack simulation while the degradation effect on CZM from hydrogen diffusion has been studied by several researchers (Alvaro et al. 2014; Moriconi et al. 2011; Rimoli and Ortiz 2010).

Based on the above discussion, under the early stage corrosion, the MSC path could be mixed transgranular and intergranular with little branching which was observed by Piascik and Willard, and Lee on aluminum and steel, respectively (Lee 1996; Piascik and Willard 1994). While most MSC growth models developed for either purely transgranular or intergranular cracking behavior, some researchers do consider this behavior through an implicit way such as adding the intergranular cycle to explicit transgranular crack growth using the stochastic method (Castelluccio and McDowell 2014). However, this mixed behavior has not been studied yet by explicit simulation with the mutual trans-intergranular transition. Thermal effect is not critical in common civil infrastructure even such as pipe in a chemical plant. Sometimes the corrosion models have temperature as a parameter such that the thermal effect is automatically embedded.

1.2.4 Cumulative damage from variable amplitude load

Fatigue damage increases cumulatively increases with applied load cycles. Cumulative fatigue damage analysis plays a key role in the life prediction of components and structures subjected to the load time histories. Many damage models and different quantifying parameters based on different physical

mechanisms have been developed in decades and reviewed by (Fatemi and Yang 1998). However, the damage accumulation rules are mainly used in macro continuum mechanics. Research on mesoscale or microscale damage accumulation from variable amplitude load is quite limited.

Coming to short crack initiation and growth under variable amplitude load (VA), the fatigue life prediction methods can be mainly grouped into two categories. One class of methods is to combine the short fatigue crack model under constant amplitude load (CA) with damage law and counting methods. The variable amplitude stress spectrum can be simplified to an equivalent constant amplitude stress range based on the root mean square approach, Miner's law or nonlinear damage law (Ghahremani et al. 2015; Li et al. 2002; El Malki Alaoui et al. 2009). To be employed in the local approaches under CA, the VA load can also be converted into local strain (Buch 1981; Lynn and DuQuesnay 2002), effective cyclic *J*-integral (Heitmann et al. 1984) or effective crack growth rate (Zheng et al. 1994) with certain damage rule and counting methods. The development of either CA model or damage rule from a variety of perspective promotes the fatigue prediction under VA. With inclusion of the notch and multiaxial effect, a new short-crack-growth-based fatigue assessment scheme was proposed (Döring et al. 2006; Hertel and Vormwald 2011). To consider microstructure influence like slip bands, a critical distance/plane method, as well as shear stress-maximum variance method, are presented to predict the fatigue life in short crack regime (Susmel et al. 2014; Susmel and Taylor 2012). Wei et al. (Wei et al. 2002) modified Newman's crack closure model to include the influence of grain boundaries on the crack opening level through introducing the concept of crack tip plasticity constrained by grain boundary blocking. With rigorous statistical analysis, a new physics-based, mathematically precise fatigue small-crack growth modeling method is proposed for scattering surface small-crack growth in heterogeneous metals (Xue 2010). To unify the short-long crack transition, long crack model analogy method (Endo and McEvily 2007) and UniGrow model (Mikheevskiy et al. 2015) were developed. For damage rule, Lautrou et al. (Lautrou et al. 2009) found that the accumulation of damage in the two-scale damage model tends to be linear if variations of amplitude are repeated many times. Recently, Zhang et al. (Zhang et al. 2016) proposed a new nonlinear continuous damage model that could include the effects of multiple over-loading on the damage accumulation and

describe the retardation influence on the short fatigue crack growth effectively. The other class of methods is a cycle-by-cycle short crack model which is mainly based on linear finite element analysis and analytical models like modified Wheeler model and Willenborg model (Hodapp et al. 2014; Romeiro et al. 2009). Code μcracksim without finite element analysis was also developed for microcrack and non-proportional multiaxial VA (Ahmadi and Zenner 2006). Wheeler model and Willenborg model are most widely used since they consider the load interaction (Maljaars et al. 2015; Romeiro et al. 2009). Fricke (Fricke 2014) and Remes et al. (Remes et al. 2012) addressed that the proposed frameworks seldom offer explicit simulation for short fatigue crack in weld microstructure and these processes still comprise primarily microstructural phenomena (moving dislocations, micro-crack initiation on slip bands and further crack growth by local slip mechanisms at the crack tip).

1.2.5 Multi-site damage on structural components

The Multi-site Damage (MSD) phenomenon has been widely studied since the famous Aloha accident on 28 April 1988. MSD approach is developed in aeronautical engineering for the purpose like aging aircraft structural assessment. MSD refers to the simultaneous presence of fatigue cracks in the same structural element, such as a large skin-panel. Thus most research is targeting for aircraft structure. Millwater established a comprehensive computational framework for MSD risk assessment (Millwater 1997). For the appearance of MSD, Jeong and Tong proposed the concept of MSD threshold (Jeong and Tong 1997). MSD under corrosion fatigue is also studied with a comprehensive seven-stage model (Shi and Mahadevan 2003). A probabilistic analysis method based on the statistical theory and fatigue characteristics of each structural detail is developed, and effect from a number of details and stress levels are explored (Zhang et al. 2010). Crack interaction and coalescence are characteristics of MSD. Effect of equivalent initial flaw size distribution in an MSD specimen is studied by using the extended finite element method (XFEM) to consider crack interaction (Kim et al. 2011). Short crack effect in MSD is also studied by quantitative

fractographic methods. Without the concept of MSD, multiple crack coalescence is limited examined in bridge component and offshore pipe (Ishihara et al. 1985; Wang 1990; Zhang et al. 2015).

1.3 Research Overview

Overall, the present research aims to develop a multi-scale numerical framework that enables probabilistic prediction of the short fatigue crack initiation and propagation in material level and transit the damage to the component level and even connect to the structural level. Multiple factors that influence the fatigue damage evolution, such as microstructure, defects, residual stress, variable amplitude load and environmental assistance (corrosion, temperature), need to be addressed in the framework. The main outputs of the study are the damage profiles of the statistic volume element (SVE), and the time-deteriorate component, which can be further used to build a surrogate model of equivalent damaged connections for incorporation into the structural analysis. The research objectives have been fulfilled after three major parts of accomplishment in sequence:

- **Part 1: 2D SVE-based mesoscale modeling of short fatigue crack in different scenarios**

  A comprehensive 2D SVE-based simulation framework for short fatigue crack nucleation and propagation has been proposed, setting on the microstructure-sensitive modeling and nonlocal crystal plasticity based fatigue indicator parameters (FIPs), being able to consider the scenarios with variable amplitude loads, trans-intergranular behavior, environmental effects, and the presence of defects. (Application of SVE scale simulation: short crack in the spatial-variant weld microstructures)

- **Part 2: Damage profile generation and quantification of time distribution to initial long crack**

  With the framework built up in Part 1, Deterministic Monte Carlo Simulation (DMCS) is performed on SVEs to establish the crack length vs. time curve cluster. From these damage profiles, the crack length distribution at any time and the consumed life distribution of any crack length can be obtained. A reduced order modeling (ROM) framework has been established to accelerate the quantification of time distribution to initial long crack for a simplified microstructure.

- **Part 3: From SVE to component – a probabilistic damage evolution framework**

  The cracking configuration is sampled from the damage profile from Part 2 and components with initial cracks at the hotspot are generated. Then, long crack growth simulation (such as finite element method (FEM) aided analytical approach) is performed to generate different time-deteriorated components. A simple single-site damage approach (SSD) is naturally formed for the single-site damage controlled components. For multi-site damage approach (MSD), the initial crack insertion is time-dependent with progressive evolutions, which will be coupled with long crack growth simulation due to crack coalescence. Finally, the damaged components at present are virtually tested for stiffness of local details. The hotspot in the structural model is surrogated with a time-dependent equivalent connection to consider the progressive damage evolutions. (Application of component scale simulation: crack growth in the pressure vessel/pipe and T-joint)

As shown in Fig. 1-1, these three major parts are integrated to be a multi-scale fatigue damage modeling framework, and some application examples with a major focus on steel structural components are presented for demonstration.

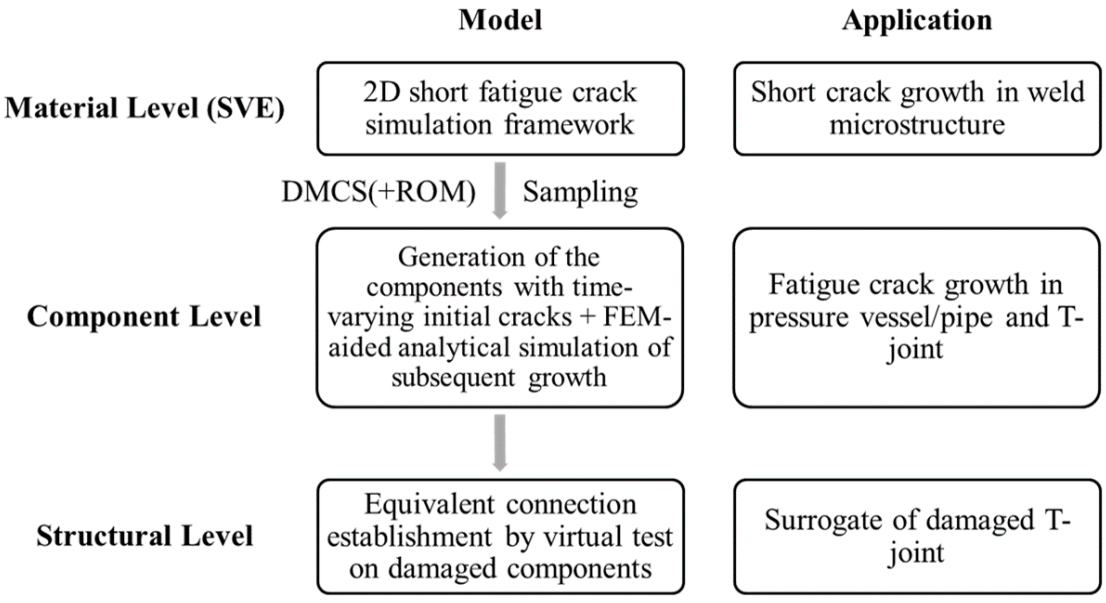

Figure 1-1. Multiscale fatigue damage modeling framework and application examples

1.4 Organization of the Dissertation

This dissertation consists of eight chapters. All chapters, except for the introduction (Chapter 1) and summary (Chapter 8), are based on papers that have been published, accepted, submitted or to be submitted to peer-reviewed journals, while some contents have already been published in extended abstract peer-reviewed conference proceedings. Therefore, each chapter is relatively independent. For this reason, "Introduction" part of each chapter may have some overlap. Some essential contents about framework may also be repeated in some individual paper. However, as a chapter in the dissertation, this part of contents is abbreviated but referred to previous chapters for conciseness. Briefly, this dissertation is structured and outlined as follows:

Chapter 1 introduces the background and motivation of the research, and the overview and structure of the dissertation. Chapter 2 builds up the 2D SVE-based transgranular crack growth method (TCGM) under constant amplitude load (CA) and applies it to the estimation of small fatigue crack growth in bridge weld microstructure (Yuan et al. 2018a). Chapter 3 extends the TCGM with the grain-based Miner's Rule, leading to a nonlinear grain-based damage model for civil infrastructure under variable amplitude loads (VA) (Yuan et al. 2017a). Chapter 4 evolves the TCGM to the Integrated Transgranular and Intergranular Crack Growth Method (ITICGM) and further to Corrosion-informed ITICGM (Yuan et al. 2017b). Chapter 5 presents the SVE-based damage profile generation with Deterministic Monte Carlo Simulation and a reduced order modeling framework to quantify time distribution to initial long crack for a simplified microstructure (Yuan et al. 2018b). Chapter 6 implements the single-site damage approach to evolve the damage profile from SVE to the components and demonstrates it with fatigue failure assessment of a pressure vessel. Chapter 7 presents the multi-site damage approach to generate the time-deteriorate components, and further explore the damage equivalent surrogation for structural model. Finally, Chapter 8 summarizes the dissertation and makes an outlook on possible future research.

The relationship between each chapter (Ch. 2~7) and the logical workflow of the research (based on Section 1.3) is illustrated as Fig. 1-2.

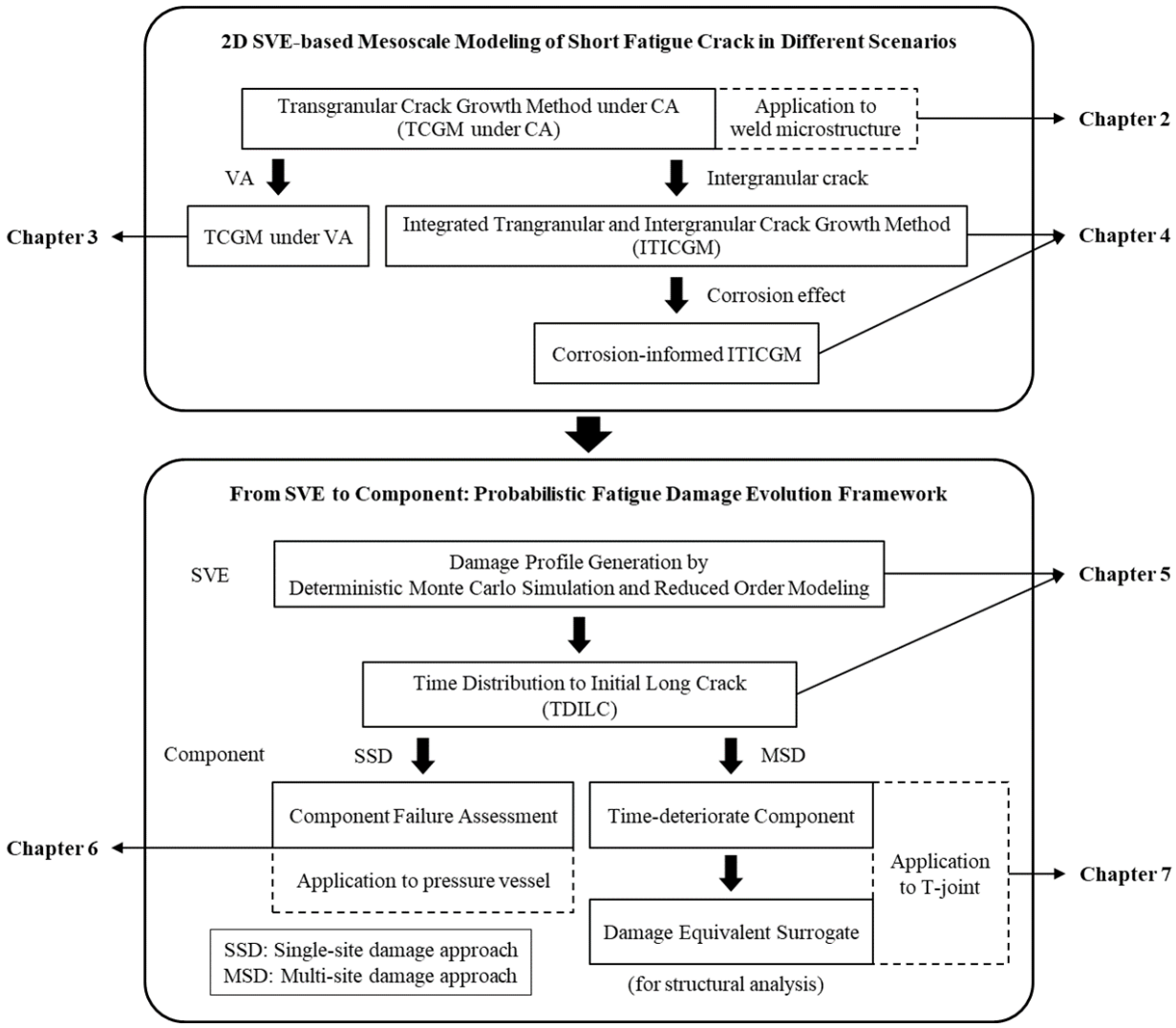

Figure 1-2. Relationship between chapters and logical workflow of the research

CHAPTER 2 MICROSTRUCTURE-SENSITIVE ESTIMATION OF SMALL FATIGUE CRACK GROWTH IN BRIDGE STEEL WELDS

2.1 Introduction

Coastal and offshore infrastructure is constantly evolving to span over increasingly larger water bodies and to exploit natural resources in remote areas. To mention a few examples, the challenge is to build economic and sustainable coastal bridges, ships, offshore floating structures, and subsea pipelines that can endure decades under harsh environments and unforeseen conditions. These structures usually employ welding as a method to connect metallic structural members, mainly made of high strength low alloy steel (HSLA) including bridge steel. Certainly, open or closed ribs are often welded to the deck plate in orthotropic deck design of bridges, ships or offshore structures, for enhancing the bending resistance of steel plates to carry lateral loads (AISC (American Institute of Steel Construction) 1963; Troitsky 1987; Zhang et al. 2013a). These joints resist cyclic deformations or repetitive service loads from heavy vehicles, hurricane-force wind, and destructive waves that can initiate and propagate fatigue cracks. In addition, welding procedures introduce material heterogeneity, mesoscale defects, residual stresses, and geometric distortions that are detrimental to fatigue and fracture resistance. The vast number of welds in orthotropic decks have raised safety concerns regarding localized fatigue failure (Ya et al. 2010). However, design codes for fatigue failure are usually based on nominal stress approaches that neglect local stress raisers, material heterogeneity, and weld profiles.

Many local approaches for fatigue assessment of welded joints have been developed since 1930s to estimate the fatigue crack propagation starting from discontinuities and notches (Fricke 2014; Radaj et al. 2006, 2009). The validity of these approaches depends on a preexisting defect that resembles a crack-like shape, which is not always present in current high-quality welding processes and post-weld improvement techniques. Certainly, the fatigue crack initiation phase usually dominates fatigue lives, especially in the high cycle fatigue (HCF) regime (Skorupa and Skorupa 1993), whereas fatigue cracks

usually initiate in welded toe under elastic nominal stresses below the fatigue limit of the base metal. Approaches discussed above are also unable to capture the intrinsic microstructural variability of fatigue failure due to the implicit assumption of isotropic homogeneous materials (Buirette and Degallaix 1998; Venkateswaran et al. 2005).

Recent advances on local approaches have attempted to predict the number of cycles to nucleate and propagate small fatigue cracks in base and welded metals (Ghosh et al. 1994; Lautrou et al. 2009; Radaj et al. 2009; Zheng et al. 1994). Fricke (Fricke 2014) and Remes (Remes et al. 2012) highlighted that most frameworks seldom offer explicit simulation of small fatigue cracks meandering through weld microstructures, a process that strongly depends on microstructural attributes and mesoscale irreversible processes (dislocation production and localization, micro-crack initiation along slip bands and further crack growth by local slip mechanisms at the crack tip). Therefore, the evaluation and prediction of the early fatigue behavior in weld requires microstructure-sensitive approaches.

Microstructure-sensitive models for fatigue crack initiation and propagation have been a matter of active research for decades (Krupp et al. 2007; Navarro and de los Rios 1987; Tanaka and Mura 1981), with particular focus on isotropic and homogeneous polycrystalline alloys for aerospace applications (e.g., Ni or Ti alloys). However, steel welds with strong gradients in their polycrystalline structure have received little attention. Welds typically present roughly three zones — base metal (BM), heat affected zone (HAZ) and fusion zone (FZ) — that may have different phases, grain size and morphology, which impact directly mechanical response (Castelluccio et al. 2012, 2013; Smith et al. 1989). Therefore, small crack nucleation and propagation methods developed for isotropic and homogeneous materials may be applied to the weld microstructure as long as the microstructural attributes of each zone are taken into account.

Mesoscale methods based on crystal plasticity are among the more effective approaches to link microstructure to component level response under complex loading conditions. At micro- and mesoscales, the microstructure plays a key role in the evolution of micromechanical stresses and strains and that leads to microstructurally small cracks (MSCs). Random grain morphology and size, crystallographic orientation,

inclusions, voids, and other microstructural features result in local anisotropy and highly heterogeneous stresses and strains.

Simple mesoscale models for MSC such as Tanaka-Mura (Tanaka and Mura 1981), Miller-Hobson (Miller 1987), Navarro and de los Rios (Navarro and de los Rios 1988) are still commonly employed in computational models, but they are limited in rendering realistic microstructures. Recent developed microstructure-sensitive models based on fatigue indicator parameters (FIPs) (Pineau et al. 2016) are a promising tool to describe both MSC nucleation and growth. Several FIPs, such as those based on accumulated plastic strain and dislocation density (Kartal et al. 2014; Manonukul and Dunne 2004; Sweeney et al. 2013), energy dissipation (Sangid 2013; Sangid et al. 2011), averaged effective strain and tensile stress (Ghosh and Chakraborty 2013; Sinha and Ghosh 2006), are based on non-local variables different for each damage mechanism (Dunne 2014). Due to the complexity of cyclic microplasticity and damage formation in HCF, the FIPs provide a computable parameter to quantify fatigue damage at a microstructural length scale for engineering applications.

In the present study, a probabilistic framework of small fatigue crack simulation is employed to quantify and differentiate the potential fatigue damage in steel welds for bridges. We employ a microstructure-sensitive fatigue model based on non-local crystallographic FIPs to estimate the number of cycles required to grow fatigue cracks along BM, HAZ, and FZ. The paper is organized in following sections: Section 2 introduces the 2D microstructure-sensitive computational model and FIP formulations. Section 3 discusses statistical volume elements (SVEs) for microstructures of each weld zone, including building crystal plasticity model, generation and mesh of Voronoi grain structure, and boundary conditions. Section 4 presents the framework implementation, calibration, and results. The framework is implemented in ABAQUS (DS SIMULIA 2011) with Python scripts for the whole process and user subroutine UMAT for crystal plasticity. The verification of the non-local FIP as a mesoscale fatigue driving force is carried out for single body center cubic (BCC) crystal structure. Afterward, a calibration of irreversibility parameters and prediction assessments are presented along with comparisons of crack length (a) vs.

predicted number of cycles (N), and crack growth rate da/dN vs. a for each weld zone. Section 5 and 6 discuss the validity of the results and summarize conclusions.

2.2 Small Fatigue Crack Model for Welds

The total fatigue life in polycrystals can be partitioned into four physically-based regimes: nucleation (10^{-7}m ~ 10^{-5}m), microstructurally small crack (MSC, 10^{-7}m ~ 10^{-5}m), physically short crack (PSC, 10^{-5}m ~ 10^{-4}m), and long crack (LC, > 10^{-3}m) (Castelluccio and McDowell 2014). These regimes are arbitrary constructions that have been historically useful to correlate macroscopic crack growth rates with crack length. Indeed, the physics that dominate MSC and PSC regimes are identical, but they differ in the number of grains controlling crack growth. Thus, some approaches combine both regimes:

$$N_f = N_{nuc} + N_{msc} + N_{psc} + N_{lc} = N_{nuc} + N_{msc|psc} + N_{lc} \tag{2-1}$$

It is noteworthy that, for high-cycle fatigue (HCF) loading conditions and high-strength materials, up to 90% of a component's fatigue life can be determined by the phase of crack nucleation and the propagation of MSC (Krupp 2007). Following experimental evidence in steel (Azar et al. 2015), we assume that MSCs are transgranular and are driven by the cyclic plasticity in the bulk of the grains. This assumption allows us to employ the microstructure-sensitive framework developed by Castelluccio and Mcdowell (Castelluccio and McDowell 2013, 2014, 2015a; Przybyla et al. 2013) and Fatemi and Socie's FIP to assess fatigue crack growth through weld microstructure.

2.2.1 Prediction of fatigue crack nucleation based on FIPs

Well-controlled and high-quality welding or post-weld treatment often results in low residual stresses and very few weld defects such as mesoscale inclusions and pores. Instead, crack nucleation usually occurs due to the irreversible accumulation of damage along crystallographic planes (so-called Stage I fatigue). Thus, we define crack nucleation as the number of cycles to fully develop a crack within the first grain. Following experimental findings (Fan et al. 2011), only crystallographic slip bands are considered as the mechanism

that nucleated cracks in welds. According to (Castelluccio and McDowell 2013), FIP proposed by Fatemi and Socie (Fatemi and Socie 1988) can be used as an effective surrogate measure for cyclic crack tip displacement range (ΔCTD) under the mixed mode loads in crystallographic cracks, i.e.

$$\mathrm{FIP}^{(\alpha)} = \frac{\Delta\gamma_p^{(\alpha)}}{2}\left[1 + k\frac{\sigma_n^{(\alpha)}}{\sigma_y}\right] \tag{2-2}$$

where $\Delta\gamma_p^{(\alpha)}$ is the cyclic plastic shear strain range on the α slip system, $\sigma_n^{(\alpha)}$ is the peak stress normal to the slip plane of this slip system, σ_y is the reference strength, k is a constant, usually between 0 and 2, but for steel weld we choose $k = 1$ according to (Stephens et al. 2000).

One of the most challenging aspects of studying the mechanical response of HSLA steels is the various phases the may arise during thermomechanical treatments like welding (Azar et al. 2015; Radaj et al. 2006). To overcome these difficulties, this work assumes that weld zones contain only a stable ferritic phase with BCC crystalline structure. As discussed later on, this assumption should not have a major impact on the fatigue predictions since experimental evidence indicates that cracks nucleate and propagate along persistent slip bands (PSBs) in ferritic grains in the three weld zones (Azar et al. 2015; Fan et al. 2011). Thus, FIP values are averaged over predefined SBs, which subdivide a grain into layers that are parallel to the prime slip system. Each SB has a nominal thickness of two elements, and transgranular crystallographic failure is assumed to occur along plastic deformation localized in these bands.

The mesoscale fatigue model defines the crack nucleation period N_{nuc} as the minimum number of cycles required to crack the first grain and follows the semi-empirical relation (Tanaka and Mura 1981),

$$N_{nuc} = \frac{\alpha_g}{d_{gr}}\left(\mathrm{FIP}_{meso}^{(\alpha)}\right)^{-2} \tag{2-3}$$

in which $\mathrm{FIP}_{meso}^{(\alpha)}$ is the SB-averaged FIP for α slip system, α_g is an irreversibility coefficient, and d_{gr} is length scale of the microstructure, such as the order of the grain size, which can be calculated by revising Eq. (24) in (Castelluccio and McDowell 2013) for 2D microstructure,

$$d_{gr} = D_{st} + \omega D_{nd} \tag{2-4}$$

where D_{st} is the length of the band in the current grain and D_{nd} is the length of intersecting bands in the adjacent grain. The disorientation factor ω is calculated according to (Castelluccio and McDowell 2013) and is zero for most grains since the misorientation with neighbor grains exceeds 20° based on grain cluster with random crystal orientation.

Based on prior research (Castelluccio and McDowell 2013) and convergence studies not included for the sake of brevity, our model shows that two computational loading cycles are enough to estimate the dominant shape of the stress and plastic strain range fields that contribute to crack formation, i.e., at the time the FIP is stable for a long cyclic life under HCF. Of course, the number of computational cycles required depends on the ability of the constitutive model to reach saturation and the desired accuracy of the fatigue estimation. In this case, we attempt to roughly quantify fatigue evolution in different zones of welds rather than an accurate prediction on each zone.

2.2.2 MSC propagation by microstructure-sensitive crack growth equation

The MSC crack growth rate can be understood as the net number of dislocations emitted from a crack tip after a cycle, or equivalently the ΔCTD. As shown by Castelluccio (Castelluccio and McDowell 2014), the SB-averaged mesoscale FIP can serve as a more efficient fatigue indicator for MSC growth, i.e.

$$\left.\frac{da}{dN}\right|_{msc}^{(\alpha)} = \phi \left\langle A \frac{d_{gr}}{d_{gr}^{ref}} \mathrm{FIP}_{meso}^{(\alpha)} - \Delta\mathrm{CTD}_{th} \right\rangle \tag{2-5}$$

where ϕ is a measure of the mechanical irreversibility at the crack tip process zone (typically 0.01 ~ 0.1) and $\Delta\mathrm{CTD}_{th}$ is a threshold that recognizes a minimum required ΔCTD for dislocation emission (on the order of the Burgers vector). In between the Macaulay bracket, A = 2 μm is a scaling constant that correlates FIP_{meso} with ΔCTD, and d_{gr}^{ref} is a reference distance that nondimensionalizes the grain size effect (mean grain size).

The simplification of grain-by-grain crack growth requires a strategy to predict the evolution of the FIP as the crack growth progresses inside a grain. When computing MSC crack growth rate in Eq. (2-5),

we assume that the FIP depends on the crack length within a grain as stated in Eq. (2-6). Such an equation should be understood as a mesoscale self-similar dependence of the fatigue driving force on the fraction of grain that has been fractured. Compared to sub-grain element-by-element growth method, the grain-by-grain approach based on SB-averaged FIP can provide statistically-equivalent predictions with significantly lower computational effort (Castelluccio and McDowell 2013).

$$\mathrm{FIP}_{meso}^{(\alpha)} = \mathrm{FIP}_{0}^{(\alpha)}[1 - R_{GB}(a / D_{st})^{m}] \tag{2-6}$$

In Eq. (2-6), FIP_0 is the FIP value before any crack growth occurs in a grain; R_{GB} and m can be taken as a resistance measure of the grain boundary (GB) to the crossing crack (Musinski and McDowell 2016). Although these parameters depend on complex GB conditions such as twist/tilt angle, grain morphology, and other material properties, for the current study R_{GB} is treated as a deterministic parameter that characterizes the mean value of mesoscale crack growth. Regarding the parameter m, Table 2-1 and Fig. 2-1(a) present various alternatives to represent the evolution of the FIP as a crack grows along an SB within a grain. Case (1) corresponds to a constant FIP as the crack progress throughout a grain; Case (2) indicates the constant influence form the GB independent of the crack length within the grain; Case (3) and (4) assume linear and parabolic decay of the FIP as the crack grows within the grain due to the influence of GBs. Accordingly, the number of cycles needed to fully crack a grain (after nucleating a crack in the first grain) can be calculated by analytical integration of Eq. (2-5) with Eq. (2-6), and the results are listed in Table 2-1. Here, $C(1 - R_{GB}) > \Delta\mathrm{CTD}_{\mathrm{th}}$ is assumed to evaluate the Macaulay bracket in Eq. (2-5).

Table 2-1 Different self-similar evolutions of FIPs inside grain and corresponding cycle number N after integrating Eq. (2-5)

Case	Condition	$\mathrm{FIP}_{meso}^{(\alpha)}$	$N\big\|_{msc}^{(\alpha)}$ $\left(C = A\frac{d_{gr}}{d_{gr}^{ref}}\mathrm{FIP}_{0}^{(\alpha)}\right)$
(1)	$R_{GB} = 0$	$\mathrm{FIP}_{0}^{(\alpha)}$	$\frac{D_{st}}{\phi}\left(C - \Delta\mathrm{CTD}_{th}\right)^{-1}$
(2)	$R_{GB} \neq 0$, $m = 0$	$(1 - R_{GB})\mathrm{FIP}_{0}^{(\alpha)}$	$\frac{D_{st}}{\phi}\left[C(1 - R_{GB}) - \Delta\mathrm{CTD}_{th}\right]^{-1}$

(3)	$R_{GB} \neq 0$, $m = 1$	$(1 - R_{GB}\frac{a}{D_{st}})\text{FIP}_0^{(\alpha)}$	$\frac{D_{st}}{\phi C R_{GB}} \ln \frac{C - \Delta\text{CTD}_{th}}{C(1-R_{GB}) - \Delta\text{CTD}_{th}}$
(4)	$R_{GB} \neq 0$, $m = 2$	$\left[1 - R_{GB}\left(\frac{a}{D_{st}}\right)^2\right]\text{FIP}_0^{(\alpha)}$	$\frac{D_{st}\tanh^{-1}\left[(CR_{GB})^{1/2}(C-\Delta\text{CTD}_{th})^{-1/2}\right]}{\phi(CR_{GB})^{1/2}(C-\Delta\text{CTD}_{th})^{1/2}}$

Note: We consider m = 0, 1, and 2 to demonstrate the variability that can be attributed to the mesoscale crack growth evolution. For $m \geq 3$, the integration of Eq. (3-5) becomes significantly more complicated.

Fig. 2-1(b) compares MSC grain lives, N, for different FIP evolutions in Table 2-1, normalized by FIP_0 (Case (1)) and assuming that $R_{GB} = 0.5$ is representative of the average GB resistance. The normalized grain life drops rapidly when $C = A\frac{d_{gr}}{d_{gr}^{ref}}\text{FIP}_0^{(\alpha)}$ increases from 2 to 4; after that, the normalized grain life stabilizes to a constant, such as 1.25 for Case (4). Fig. 2-1(b) shows that the number of cycles to crack a grain is bounded by Cases (1) and (2), with the former being more conservative. Furthermore, a higher exponent m results in the curve closer to that for Case (1); for $m \geq 3$, these trends holds but are not drawn for consistency with Table 2-1. In summary, these results suggest that the details of the parameterization in Eq. (2-6) affect the most the near fatigue threshold regime ($C \approx \Delta\text{CTD}_{th}$). Lives for higher cyclic deformation tend to saturate and only differ in a scaling factor in different cases.

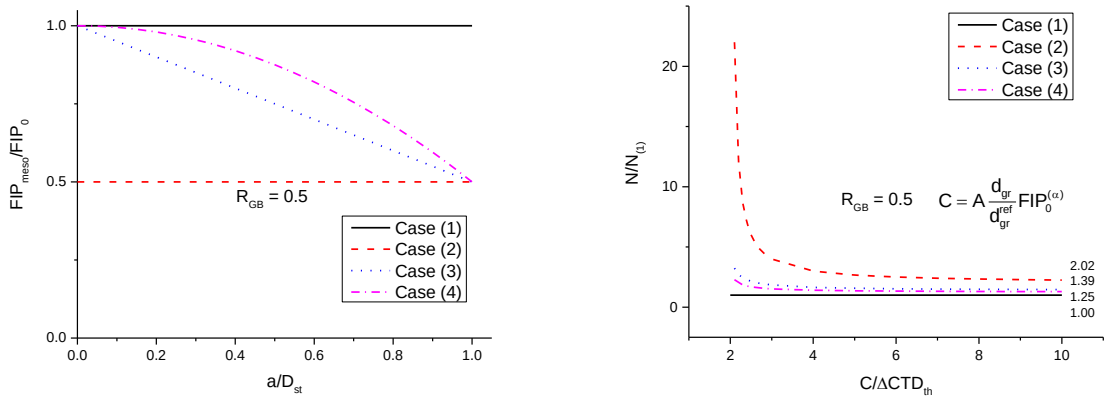

(a) (b)

Figure 2-1. Normalized sub-grain FIP variation (a) and corresponding fatigue life of a grain (b)

When incorporated into the whole framework, the Macaulay bracket in Eq. (2-5) is evaluated at the beginning of the crack starting with the FIP_0. If $C(1 - R_{GB}) > \Delta\text{CTD}_{th}$, Case (1), (3) or (4) can be used; if

$C > \Delta CTD_{th}$ and $C(1 - R_{GB}) < \Delta CTD_{th}$, Case (1) will be used instead and the cracks stop growing at the next boundary; if $C \leq \Delta CTD_{th}$, crack is arrested at the current tip location.

Inspired by Fig. 2-1(b), a simple scheme is adopted to calculate N for different cases while R_{GB} = 0.5. Assuming that $C/\Delta CTD_{th}$ is outside of the range between 2 to 3, then conservatively, all N can be evaluated as Case (1) firstly and multiplied by the stable normalized N (1.39 for Case (3), and 1.25 for Case (4)) to get the fatigue life considering the sub-grain FIP variation. Therefore, in the following sections, all simulations are performed under Case (1).

Since the dominating transgranular MSC controls fatigue life, only one crack is assumed to nucleate per realization; after nucleation, the crack extends to the next grain along the closest SB that intersects with the crack tip elements, while at most time the SB has the minimum fatigue life.

2.3 Weld Zone Microstructures

2.3.1 Voronoi tessellation for different weld zones

Our modeling framework relies on the explicit representation of grain morphology and a mesoscale domain to compute a microstructure-sensitive driving force that controls MSC growth. As shown by Castelluccio and McDowell (Castelluccio and McDowell 2015b), an adequate mesoscale domain helps mitigating mesh sensitivity and reduces the need for fine meshes. Furthermore, Sauzay et al. (Sauzay et al. 2014) showed minimum differences in the distributions of internal state variables between coarse cubic grains and refined conformal meshes; this characteristic is particularly relevant for transgranular fatigue failure. Thus, we recreate synthetic microstructures generated with a Poisson-Voronoi tessellation algorithm, which has been extensively used for modeling polycrystalline material. An open-source quasi-random polycrystal generator Neper (Quey et al. 2011) is used to distribute grain seeds that build the microstructure together with a Python script that regulates the grain morphology and subdivides the microstructure in SBs.

Fig. 2-2(a) compares synthetic and experimental microstructures from a single-pass weld (Ghomashchi et al. 2015); grain size in the synthetic microstructure is enlarged for clarity. From each weld

zone with in Fig. 2-2(a), SVEs of grain aggregates are sampled with size according to commonly used characteristic transition length to PSC or LC and drawn schematically in Fig. 2-2 (b) with predefined SBs (or potential locations of PSBs) shown as dark/white lines. These microstructures represent different zones of the weld profile of shield metal arc weld (SMAW) (Ghomashchi et al. 2015) which is a typical process in bridge welding. Compared to the grains in BM, the grains in HAZ may be coarser (CGHAZ) or finer (FGHAZ) due to the recrystallization and subsequent thermally activated grain growth processes. Since larger grains are usually more prone to fatigue cracking than smaller grains (Boumerzoug 2010), this work assumes that the HAZ is fully composed of coarse ferritic grains (worse scenario). Grains in the FZ have columnar shape due to the directional heat flow in the solidification process. Similar grain morphologies were found in experiments (Ballesteros et al. 2015; Ghomashchi et al. 2015).

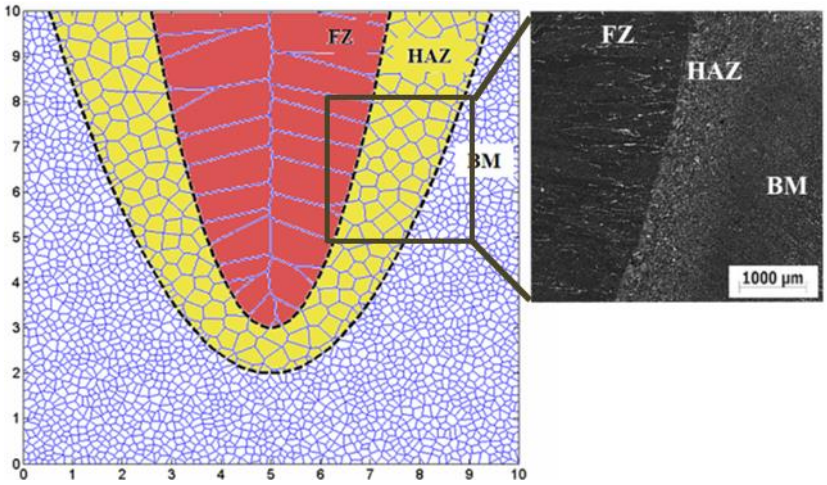

(a) Numerical generation and a comparative photo of a cross-sectional-bead-shape weld profile of single-pass SMAW

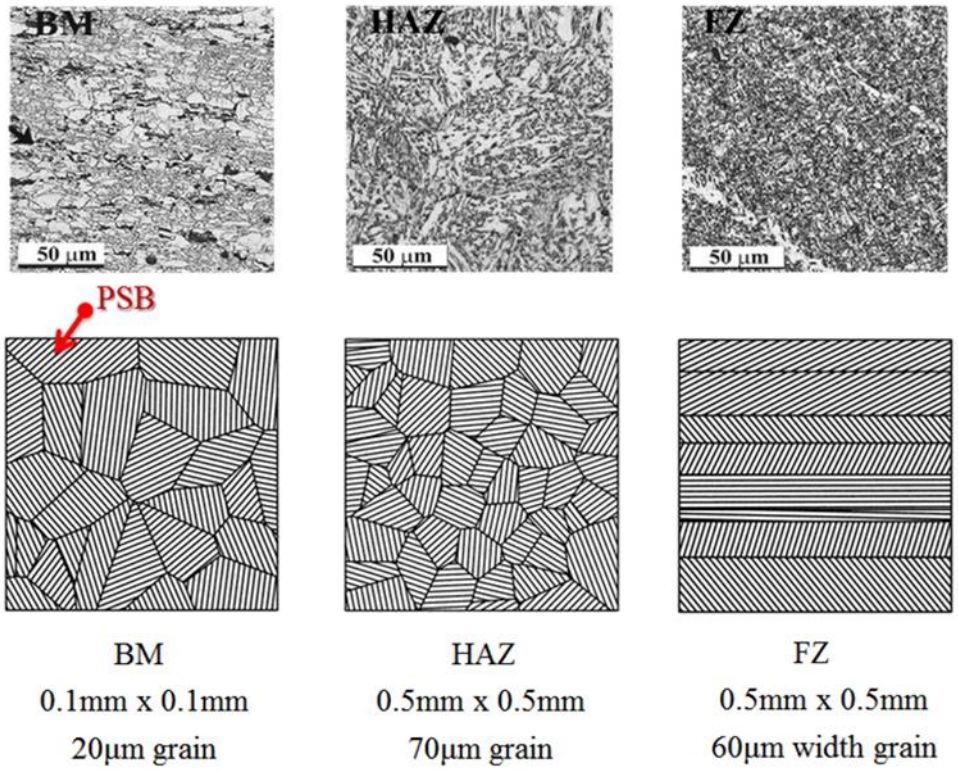

(b) Schematic SVEs with typical grain size and morphology from SMAW

Figure 2-2. Schematic SVEs with typical grain size and morphology from SMAW

(Black and white lines in SVE represent the mesoscale domains (SBs) in which mean FIPs are computed. Experimental images are from an Open Access article[1] (Ballesteros et al. 2015))

2.3.2 Grain property assignment, boundary conditions, and mesh of SVE

Each grain corresponds to a crystal with cubic elastic properties, a predefined crystallographic orientation, and impenetrable grain boundaries. In 2D implementations of crystal plasticity, the slip systems degrade to a planar mode that accommodates plane stress/strain state. To reproduce the stochastic effect of grains on fatigue damage, each grain has a random prime slip orientation defined by an angle θ subtended from the x

[1] This Open Access article is distributed under the terms of the Creative Commons Attribution Non-Commercial License which permits unrestricted non-commercial use, distribution, and reproduction in any medium provided the original work is properly cited.

geometrical axis, where $0^{\circ} \leq \theta < 360^{\circ}$ (non-directional solidification is assumed). A uniform distribution is considered for grain orientations, which assumes there is no crystallographic texture.

Periodic boundary conditions (PBCs) are imposed to reproduce the constraint of the bulk material from a large domain. Furthermore, we perform multiple microstructural realizations of SVEs with a finite number of grains to estimate the distributions of true representative volume elements (which are much larger and computationally unfeasible). Note that a true representative volume element (RVE) for FIP would require thousands of grains (Castelluccio and McDowell 2015b). Following the approach by Wu (Wu et al. 2014), we employ PBCs on finite element meshes built with CPE3 plane strain element generated with Neper and ABAQUS.

2.3.3 Crystal plasticity finite element method (CPFEM)

We employ a crystal plasticity model introduced by Huang (Huang 1991), but modified to account for Bauschinger effects. Inelastic crystal deformation arises from crystalline slip as a result of dislocation nucleation and glide. The shear rate ($\dot{\gamma}$) follows a power law expression for each slip system α,

$$\dot{\gamma}^{(\alpha)} = \dot{\gamma}_0^{(\alpha)} \operatorname{sgn}(\tau^{(\alpha)} - B^{(\alpha)}) \left| \frac{\tau^{(\alpha)} - B^{(\alpha)}}{g^{(\alpha)}} \right|^n \tag{2-7}$$

where τ is shear stress, g is the drag strength, $\dot{\gamma}_0$ is the reference shear strain rate, $B^{(\alpha)}$ is the back stress that accounts for Bauschinger effect, and n is the strain rate sensitivity parameter (a larger value of n ensures the rate independent case, such as $n = 50$). The values of these material properties are listed in Table 2-2.

The drag strength rate for each slip system is given by,

$$\dot{g}^{(\alpha)} = \sum_{\beta} h_{\alpha\beta} \dot{\gamma}^{(\beta)} \tag{2-8}$$

where the matrix $h_{\alpha\beta}$ contains the hardening modulus for each slip system, $h_{\alpha\alpha}$ is known as self-hardening while $h_{\alpha\beta} (\alpha \neq \beta)$ is known as latent hardening.

Our approach modifies the hardening modulus employed by Huang (Huang 1991) and considers three stages (Equation 2-9) of hardening in crystalline materials (Wu et al. 1991). The self and latent hardening coefficients depend on the shear strains $\gamma^{(\alpha)}$ of all slip systems as follows:

$$\begin{aligned} h_{\alpha\alpha} &= \left\{ (h_0 - h_s)\mathrm{sech}^2 \left[\frac{(h_0 - h_s)\gamma^{(\alpha)}}{\tau_s - \tau_0} \right] + h_s \right\} G(\gamma^{(\beta)}; \beta \neq \alpha) \\ h_{\alpha\beta} &= q h_{\alpha\alpha} (\beta \neq \alpha) \\ G(\gamma^{\beta}; \beta \neq \alpha) &= 1 + \sum_{\beta \neq \alpha} f_{\alpha\beta} \tanh(\gamma^{(\beta)} / \gamma_0) \end{aligned} \tag{2-9}$$

where h_0 is the initial hardening modulus, τ_0 is the initial yield stress, τ_s is the saturation stress, $g^{(\alpha)}$ is the total shear strain in system α, h_s is the hardening modulus during stage I deformation, $f_{\alpha\beta}$ is the interaction strength between slip system α and β, and $\gamma^{(\beta)}$ is the total shear strain in slip system β.

A nonlinear hardening-recovery evolution rule is set for the back stress rate by Ref. (Xie et al. 2004),

$$\dot{B}^{(\alpha)} = c\dot{\gamma}^{(\alpha)} - dB^{(\alpha)} \left| \dot{\gamma}^{(\alpha)} \right| \tag{2-10}$$

where c and d are material parameters identical for all slip systems. The fading memory term $dB^{(\alpha)} \left| \dot{\gamma}^{(\alpha)} \right|$ introduce the Bauschinger effect of materials.

The above model is implemented in ABAQUS using a user subroutine UMAT. Different material parameters for each weld zone can be calibrated considering polycrystal or single crystal response (monotonic or cyclic, shear or normal) along with optimization algorithms (Siddiq and Schmauder 2006). Since the present study focuses on the mesoscale effects of ferritic grains (which dominate fatigue), the same material parameters are employed for three weld zones, and the values are adopted from HSLA 50 in the literature (Xie et al. 2004); material parameters are summarized in Table 2-2. The constitutive model assumes that slip occurs along three families of slip systems for BCC crystal, i.e. {110}<111>, {112}<111>, and {123}<111>. However, only {110}<111> slip systems are assumed to nucleate cracks due to their highest closest atomic density (Fong and Fields 1988).

To validate the proposed modeling scheme, Fig. 2-3 compares the cyclic stress-strain curves from simulations and experimental data from the literature (Xie et al. 2004). Simulations consider an SVE of 400 μm×400 μm in size, 150 grains, with 1386 CPE4 elements and periodic boundary condition. Deformation is strain-controlled by displacing the right edge of nodes (see Fig. 2-3) with a fully-reversed triangular waveforms and peak strain of 0.015 at a constant strain rate of 5.83×10^{-4}/s. The constitutive behavior from simulations saturates rapidly and the stress-strain loop after two computational cycles matches the saturated experimental curve. By assuming identical material properties and limiting the slip systems that nucleate cracks, our approach reduces the complexity of the physical model without sacrificing the engineering applicability to predict the crack growth and fatigue life with the aid of statistical calibration and post-processing.

Table 2-2 Material and crystal plasticity parameters

Elastic stiffness	Flow parameters	Isotropic hardening parameters		Kinematic-hardening parameters
C_{11} = 253.1 GPa	n = 13.58	h_0 = 570.1 MPa	γ_1 = 0.48	c = 855 MPa
C_{12} = 132.4 GPa	$\dot{\gamma}_0$ = 10 s^{-1}	τ_s = 177.1 MPa	$f_{\alpha\beta}$ = 3.3	d = 71
C_{44} = 75.8 GPa		τ_0 = 118.1 MPa	$f_{\alpha\beta1}$ = 2.1	
		h_s = 0.002 MPa	q = 0.3	
		γ_0 = 0.0075	q_1 = 0.2	

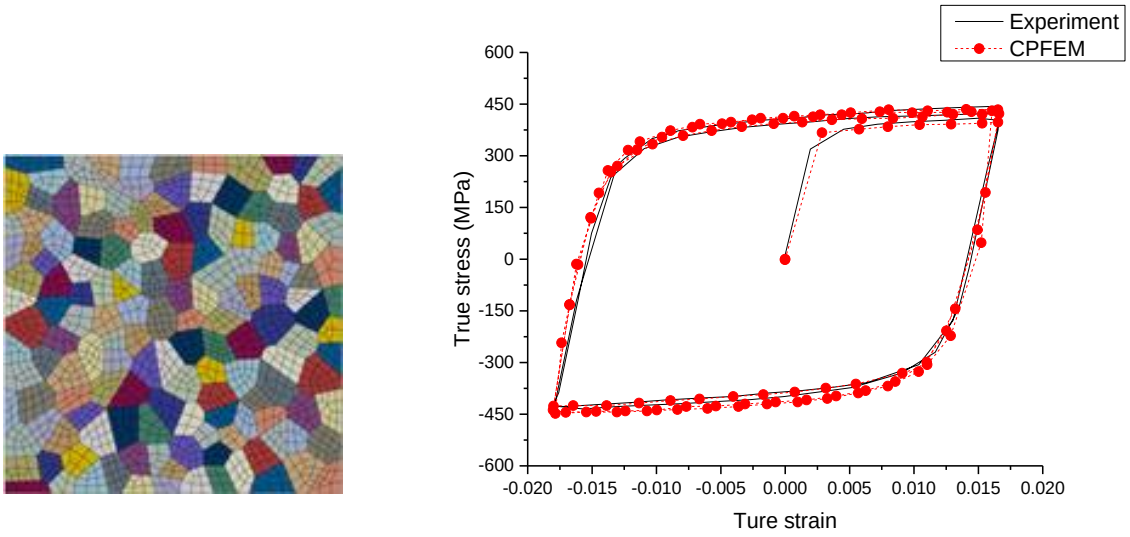

(a) (b)

Figure 2-3. (a) FE mesh for a 400 μm×400 μm model with 150 grains, 1386 CPE4 elements, and fully periodic boundary condition (b) Stress-strain response from simulations and experiments ((Xie et al. 2004)). Note that the constitutive behavior from simulations saturates rapidly and the stress-strain loop after two computational cycles matches the saturated experimental curve.

2.4 Implementation in ABAQUS and Example Test

2.4.1 General procedure for implementation in ABAQUS

Random realizations of synthetic microstructures are generated for each weld zone. Each grain is entirely subdivided into several SBs parallel to the {110}<111> slip systems that correspond to potential PSBs. After applying two computational cycles, cracks initiate at the SB with the largest SB-averaged FIP, and the corresponding nucleation life is obtained from Eq. (2-3). Next, the elastic stiffness for the elements along the cracked SB is reduced isotropically up to 99.9%, and the cyclic loading process continues to promote stress redistribution. The path for the crack extension is assumed to be transgranular along the SBs and the number of cycles required to fully crack each subsequent grain is evaluated based on the method discussed in Section 2.2.2. Crack arrest at grain boundaries is automatically captured if $da/dN = 0$. The

flowchart of the modeling approach is included in the previous work (Yuan et al. 2017a), and Fig. 2-4 presents a schematic representation of the crack growth sequence based on the proposed approach.

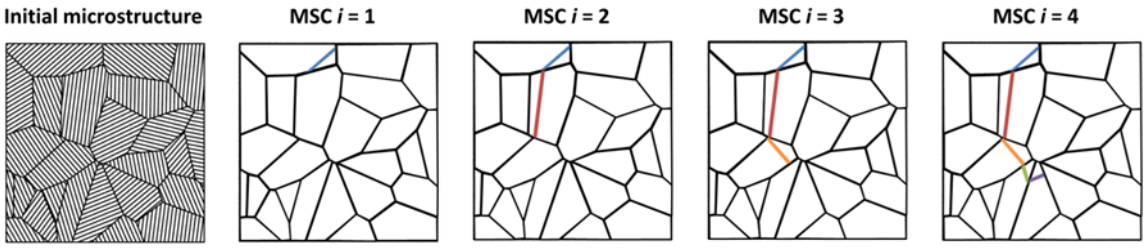

Figure 2-4. Schematic representation of the nucleation and growth of a fatigue crack along predefined SBs (Black and white lines in the initial microstructure correspond to crystallographic SBs and colored bands correspond to the grain-by-grain crack growth (SBs not shown for clarity upon crack nucleation and growth)).

2.4.2 Verification of non-local FIP for BCC single crystal

Prediction of fatigue crack growth resistance of individual grains is based on computing mesoscale FIPs, particularly the Fatemi-Socie parameter averaged over SBs. This fatigue driving force was originally proposed to predict crack initiation in macroscopic experiments in FCC and BCC metallic alloys (Fatemi and Kurath 1988; Fatemi and Socie 1988). More recently, a crystallographic version of the Fatemi-Socie FIP was validated at the mesoscale by comparing FIPs with cyclic crack tip displacements ΔCTD in OFHC Cu and RR1000 Ni-base alloy (Castelluccio and McDowell 2012; Przybyla et al. 2013). These investigations demonstrated a correlation between FIP and ΔCTD under shear and mixed mode loading.

To further support the validity of the crystallographic Fatemi–Socie FIP in BCC metals, this study performs a similar verification applied to BCC BM steel, with a predefined crack plane and extension direction along with {110}<111> slip system. Simulations consider a single crystal with a blunt crack tip adjacent to an SB as shown in Fig. 2-5. The ΔCTD corresponds to the displacement between two nodes in red in the detailed view of the crack tip in Fig. 2-5. Two computational cycles were applied to different crack lengths and loading directions to investigate the relationship between FIP and ΔCTD following the

same procedure as in Ref. (Castelluccio and McDowell 2012). The FIP was averaged in this case within a uniform band of 2 μm thickness parallel to the crack, shown in gray in Fig. 2-5.

Results in Fig. 2-6 indicate, in logarithmic scale, a linear relationship between the ΔCTD and the FIP for both loading modes. This relation breaks down for ΔCTD values below the magnitude of the Burgers vector (~$2.5\text{x}10^{-4}$μm). A least square analysis in logarithmic scale to fit the power law,

$$\text{FIP} = A\left(\Delta\text{CTD}\right)^{b} \tag{2-11}$$

results in an exponent b of 0.75 under shear mode and 0.69 under mixed mode while the other fitting parameter A is 1 and 0.72, correspondingly. Conversely, it means FIP is equivalent to ΔCTD with exponent larger than one. Therefore, taking FIP ~ ΔCTD is still conservative since FIP is mostly small than one. In this case, the verification suggests that non-local FIP can be used as a substitution of local driving force for fatigue in both BCC and FCC metal safely.

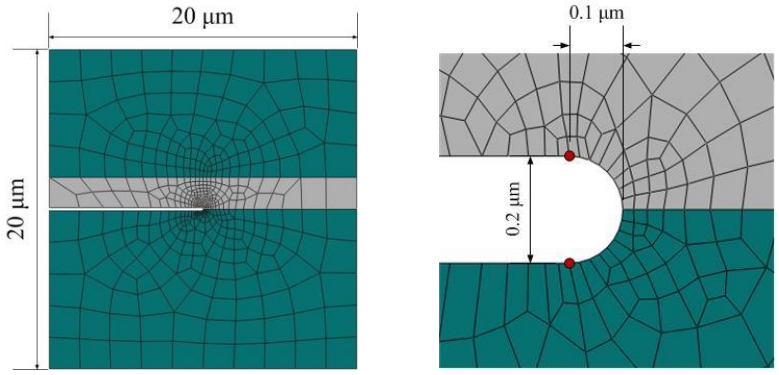

Figure 2-5. Finite element model with a deep crack in a single crystal

Shear or mixed mode loading is applied to the upper and bottom boundaries (similar model as Fig. 4 in (Castelluccio and McDowell 2012)).

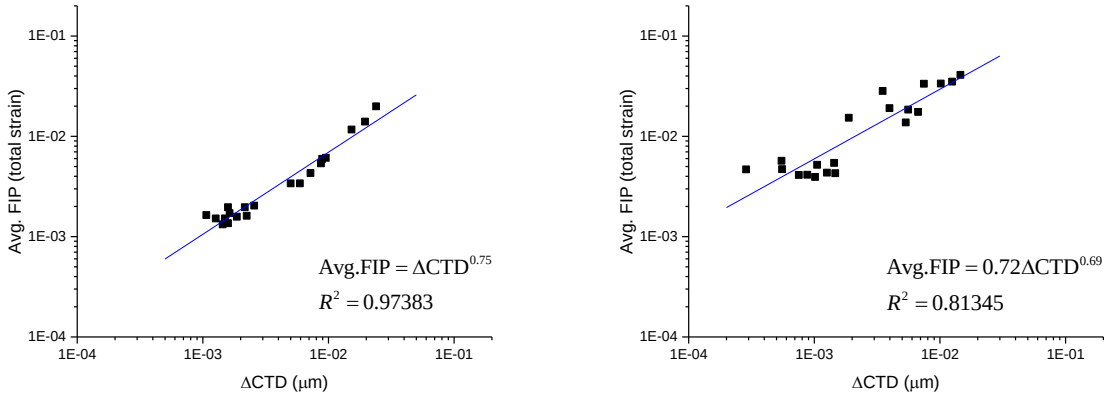

Figure 2-6. Comparison of computed SB-averaged FIP vs. ΔCTD for (left) shear and (right) mixed mode loading

2.4.3 Estimation of irreversibility parameters

In addition to the calibration of the constitutive model, three irreversibility parameters in Eqs. (2-4) and (2-6) need to be calibrated to estimate fatigue lives: irreversibility coefficient α_g, mechanical irreversibility measurement ϕ at the crack tip process zone and cyclic CTD threshold for dislocation emission ΔCTD_{th}. A precise estimation of the parameters would require crack growth data from small crack fatigue experiments or bottom-up multiscale simulations, which are extremely scarce, especially for welded material. Due to the unavailability of small crack fatigue data for typical bridge welds, our calibration relies on reference experiments from the literature for comparable materials and environments. In addition, we assume that all the weld regions have identical α_g, ϕ and ΔCTD_{th}, which follows from the fact that irreversibility is controlled by atomistic rather than mesoscale processes (e.g., dislocation emission, cross slip, adsorption of species, etc.). These processes are similar among the weld zones and other metallic materials with similar, environments, composition and phases. For instance, the minimum possible crack growth from a crack tip controls ΔCTD_{th} and it is related to the emission of a dislocation. Thus, the magnitude of the ΔCTD_{th} is on the order of the Burgers vector for BCC crystal of iron, $\Delta CTD_{th} \approx 4 \times 10^{-4}$ μm. This magnitude is indeed the same for all weld zones.

The reference experiments (Buirette and Degallaix 1998) were carried out for Al-killed Nb-V microalloyed Grade S550 MC high strength steel that is widely used materials in transportation infrastructure and is comparable to SAE J1392 X80 or API 5L X80 HSLA. The test specimen was ground to 5.2mm thick and grooved at the HAZ (4mm radius and 0.5mm depth) as shown in Fig. 2-7(a). The mean grain size of the HAZ is roughly 10 μm.

To quantify the stress intensification induced by the groove we modeled the specimen in Fig. 2-7(a) assuming a elastoplastic material response (Buirette and Degallaix 1998). A BCC model is used since the ferrite-bainite microstructure is present after MAG (metal active gas) welding process. The results in Fig. 2-7(b) show that stress gradient, σ_{xx}, is relatively smooth compared to the grain size. Thus, instead of modeling the entire grooved specimen, we consider a 100μm x 100μm crystal plasticity domain in Fig. 2-7(c) subjected to a loading condition equivalent to that at the root of the groove. Multiple SVE realizations under constant cyclic load equivalent to that at the groove are employed to reproduce the small fatigue crack variability.

The SVE has a top boundary free of constraint, a bottom boundary constrained to move along the Y-axis, and periodic boundaries along the X-axis. The maximum and minimum longitudinal stress at the groove bottom is 610 MPa and 75 MPa based on pre-mentioned macroscopic analysis. Considering the residual stress profile obtained from the same set of referred experiments (Buirette and Degallaix 1998), which has a representative value of -117 MPa at at the root of the groove, the load on the side edge of the SVE is taken as 493 MPa to -42 MPa and triangle loading at 10,700 MPa/sec (according to the fatigue test frequency of 10 Hz), which assumes linear elastic addition of stress fields.

A total of 150 microstructural realizations were simulated to compute FIPs distributions, whose mean values are employed to estimate the irreversibility parameters. In addition, another set of simulations were performed using the calibrated parameters to estimate fatigue life predictions. The distribution of maximum FIPs for the first six cracked grains is shown in Fig. 2-8. and Fig. 2-9, which compiles the same information boxplots. At each box, the central mark (Q2) is the median, while the edges of the box are the 25th and 75th percentiles (Q2 and Q3, respectively). The whiskers extend to the most extreme data points

with the range Q1−1.5 (Q3−Q1) ~ Q3+1.5 (Q3−Q1) and outliers are plotted individually by mark "+". As shown in Fig. 2-11, the FIPs for the first grain cracking are significantly higher than those in subsequent crack growth, while the FIPs are comparable among these grains. Moreover, FIP distributions are not symmetric and have a longer tail towards larger values; these extremes indeed dominate fatigue lives.

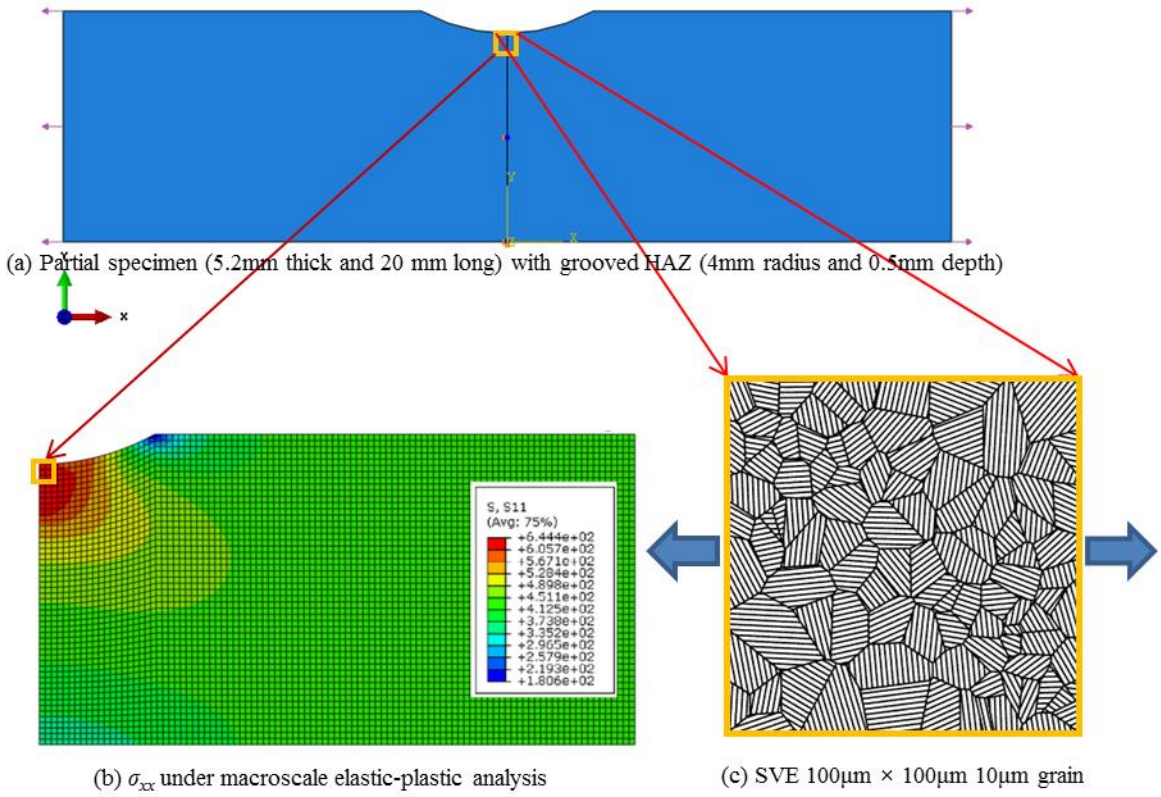

Figure 2-7. Grooved specimen and meshes used for calibration of irreversibility parameters

An elastic model estimated the applied load in a subdomain at the bottom of the groove, which corresponds to the SVE analyzed with the crystal plasticity and fatigue models.

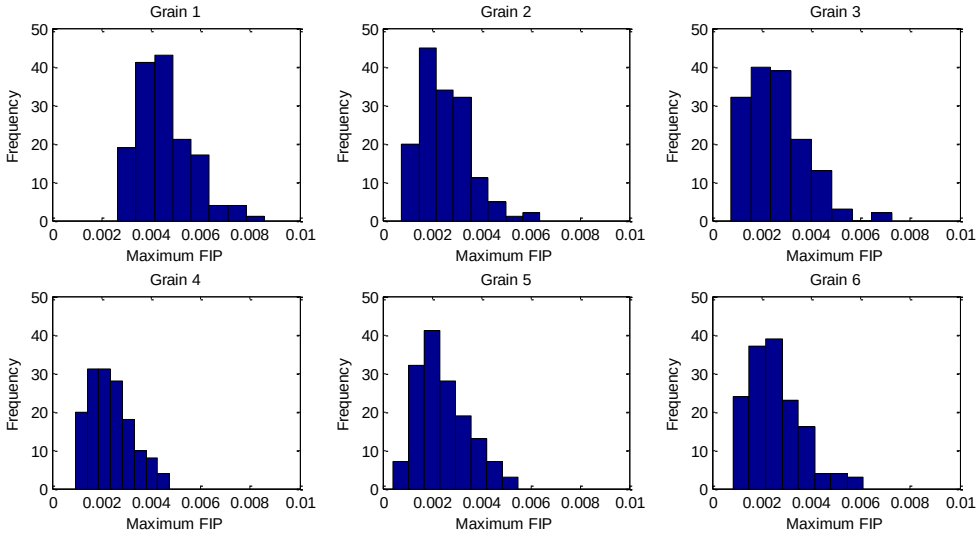

Figure 2-8. Distribution of maximum FIPs for the first six grains that failed from among all 150 simulations

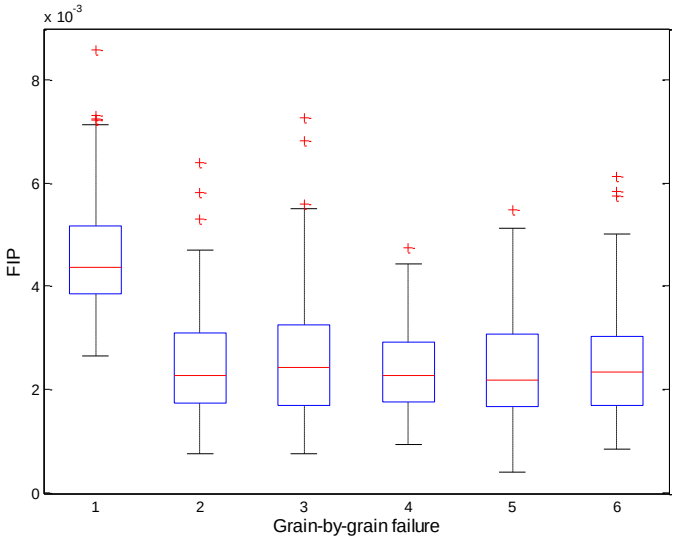

Figure 2-9. Boxplot by compiling the FIP distributions from Fig. 2-8 for the first six grain fractured on a grain-by-grain basis

Parameter α_g for the nucleation regime is determined by assuming a value for each unknown in Eq. (2-3). Thus,

$$\alpha_g = N_{nuc} d_{gr} (\mathrm{FIP}_{meso}^{(\alpha)})^2 = 47.1 \text{cycles } \mu\text{m}, \tag{2-11}$$

by assuming that,

- N_{nuc} = 70,000 (Buirette and Degallaix 1998), which corresponds to the fatigue life consumed when the dominant crack reaches one mean size grain in length.
- D_{st} = 10 μm; taken as mean grain size (Buirette and Degallaix 1998).
- ω = 0; since most misorientation exceeds 20°, as estimated from the random grain generations.
- $\mathrm{FIP}_{meso}^{(\alpha)} = 0.0092$, which is the extreme value obtained in Fig. 2-9.

The calibration of ϕ in Eq. (2-5) for the MSC growth regime is based on the crack growth rate data from (Buirette and Degallaix 1998), reproduced and shown in Fig. 2-10. The curve starts with an initial decreasing crack growth rate which is assumed to correspond to the nucleation regime. From the fluctuating small crack growth rate due to GB crossing, the minimum crack growth rate is estimated as 5×10^{-6} μm/cycle, and the average maximum rate when a grain begins to crack is taken as about 8×10^{-4} μm/cycle.

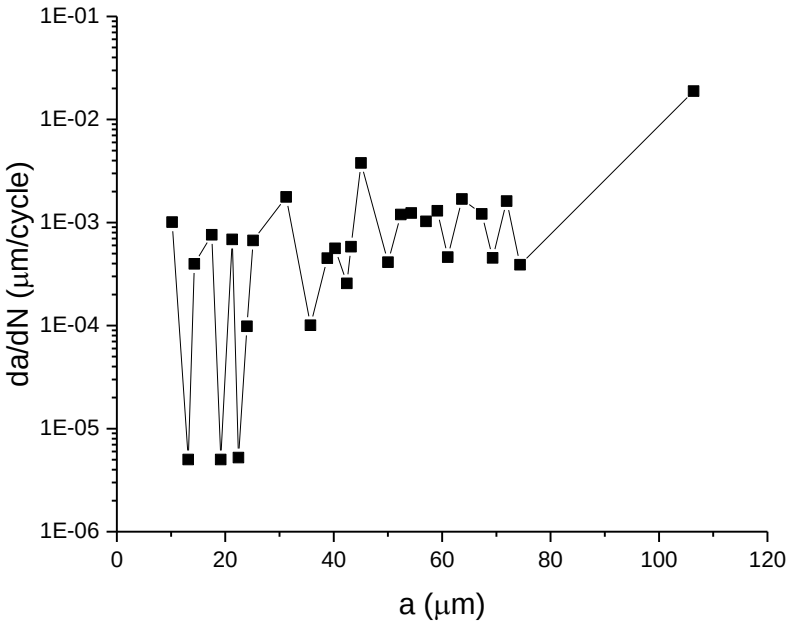

Figure 2-10. MSC growth rate data of HAZ

(reproduced from Figure 14 in (Buirette and Degallaix 1998))

The calibration of constant ϕ assumes that

- $\left.\frac{da}{dN}\right|_{msc}^{(\alpha)} = 8\times10^{-4}\ \frac{\mu\text{m}}{\text{cycle}}$, which is roughly the average crack growth rate after crack cross the GB.
- D_{st} = 10 μm and ω = 0; following the same arguments considered for the calibration of α_g.
- $\text{FIP}_{meso}^{(\alpha)} = 0.0065$, which is the average remaining FIP after the reduction on the FIP of nucleation regime in Fig. 2-9.

Therefore, the transgranular irreversibility factor becomes ϕ = 0.063 which is within the custom range of 0.01 ~ 0.1 (Castelluccio and McDowell 2014).

2.4.4 MSC simulation and statistics of results

This section assesses the early fatigue lives for different weld regions, which are all assumed to be located at a macroscopic stress raiser (worse case scenarios) and cracks nucleate on surface grains (prescribed for only one crack nucleation and subsequent growth). Sixty microstructural realizations are carried out assuming that the top surface is free of constraint, a bottom surface constrained to move along the Y-axis, and periodic boundaries along the X-axis. A triangular cyclic strain is applied along the X-axis, with peak strain 0.5%, at a rate of 0.5%/sec, and strain rate $R_\varepsilon = 0$.

An example of the grain-by-grain crack growth sequence is presented in Fig. 2-11 for microstructure. The figure presents a sequence of strain localization, crack nucleation, stress redistribution, and crack propagation and arrest. In some cases, the SB with the highest FIP plastic strain may occur below the surface grain in the nucleation regime. However, the assumption that the first crack starts at surface grain is still appropriate due to the influence of the environment on the irreversibility parameters, which were calibrated for an active atmosphere, not vacuum. Indeed, subsurface crack initiation only becomes more likely in the very high and ultra-high cycle fatigue regimes, in which the marked heterogeneity in plastic deformation competes with the irreversibility of the environment.

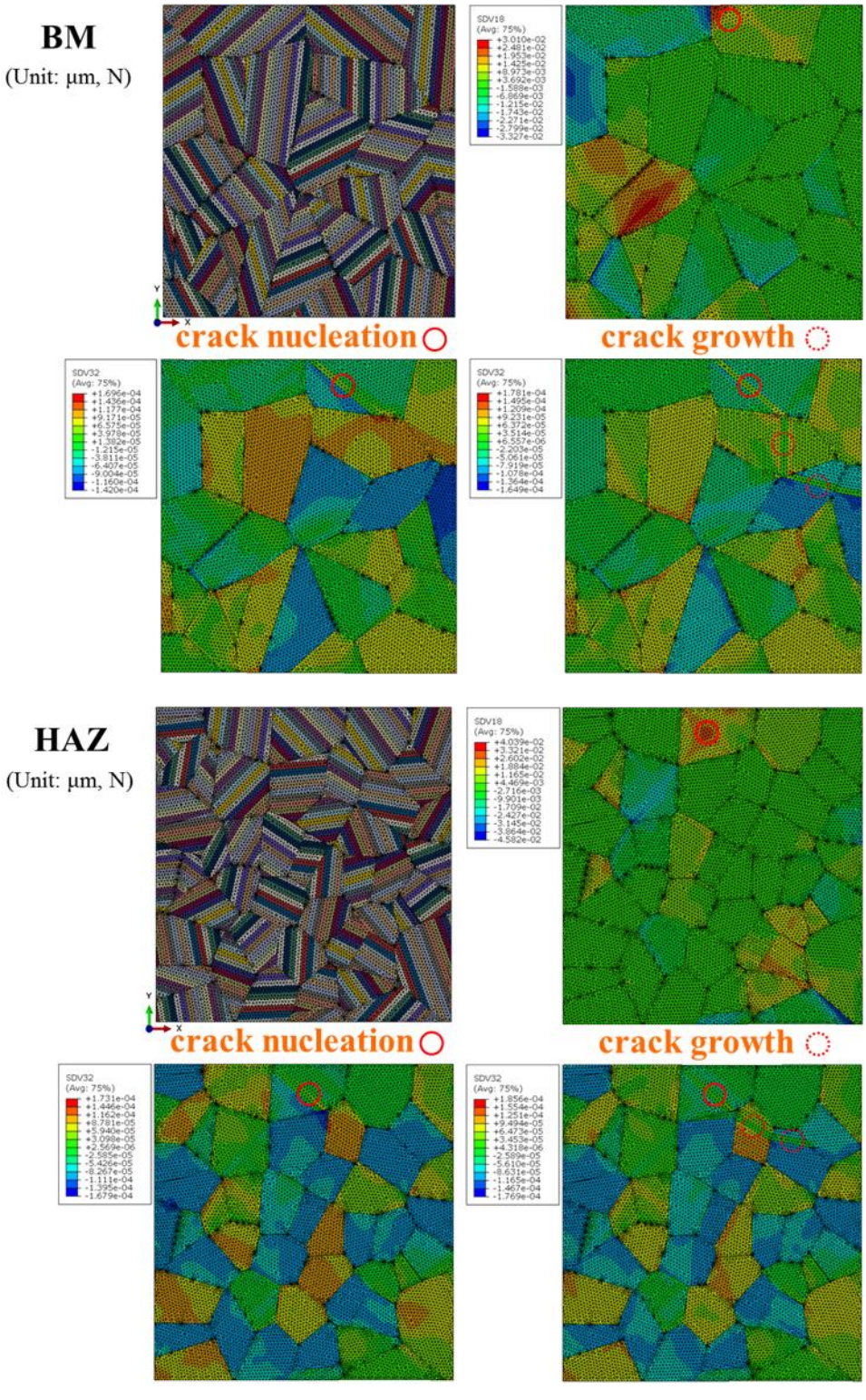
BM
(Unit: μm, N)
crack nucleation
crack growth
HAZ
(Unit: μm, N)
crack nucleation
crack growth

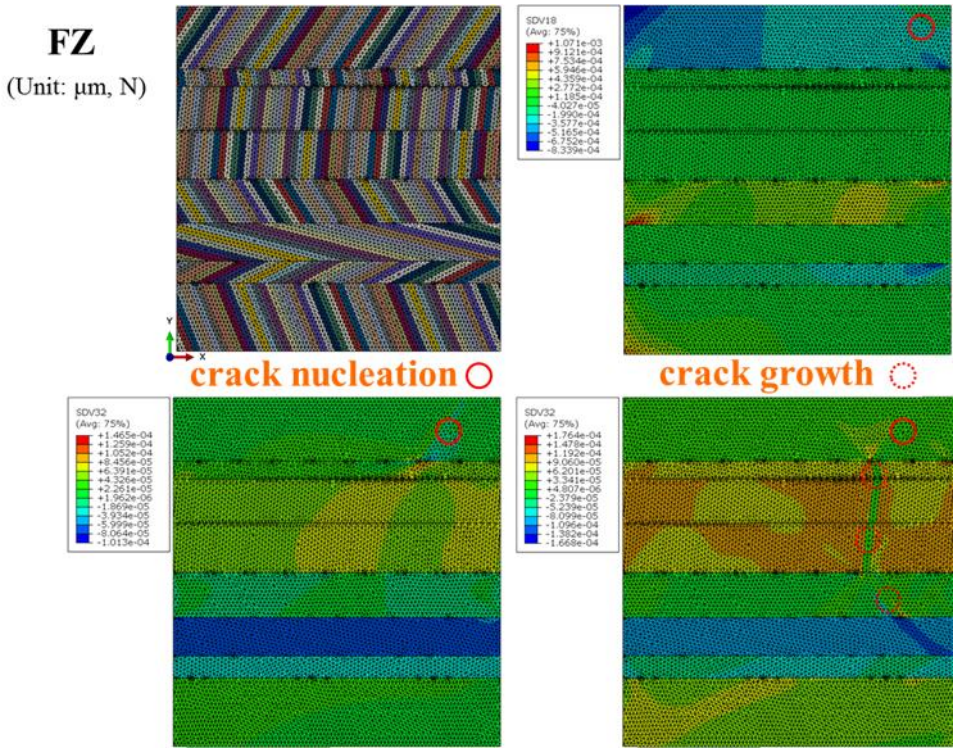

Figure 2-11. Crack growth, strain and stress in weld zones for one simulation (upper left – SB distribution, upper right – plastic shear strain (SDV18) after two load cycles, lower left – resolved shear stress (SDV32) at two cycles after nucleation, lower right – MSC path at the end)

The Y-axis projected crack length *a* vs. *N* diagrams for three weld zones are plotted in Fig. 2-12. Each data point represents extending the crack by one grain until arrested or reaches the SVE boundary. Furthermore, each line that connects dots represents one simulation, and the slope indicates the crack growth rate. The crack growth rates oscillate (as expected for MSC), but the trend is increasing until encountering a strong barrier. Seldom can the crack grow through the entire SVE, but a direct comparison with experiments of the crack arrest probability should consider 3D models. As shown in the Fig. 2-12, the span of nucleation lives are is shorter for BM than for HAZ and FZ, which suggests that grain morphology has a detrimental effect crack nucleation. In comparison, crack growth in BM seems to present wider spread compared to the FZ and HAZ. Meanwhile, the cracks in FZ are arrested more often than those in BM and HAZ as shown in the figure.

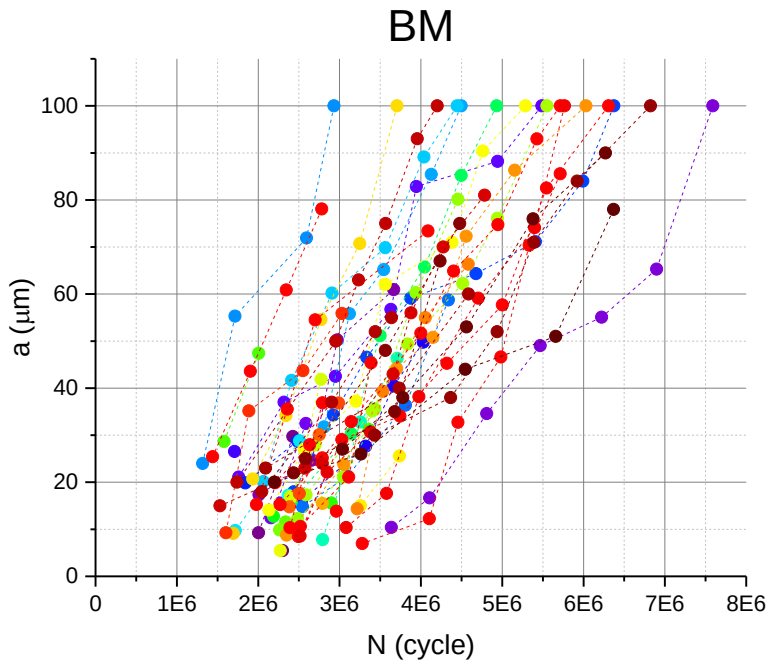
BM
a (μm)
N (cycle)
0
20
40
60
80
100
0
1E6
2E6
3E6
4E6
5E6
6E6
7E6
8E6

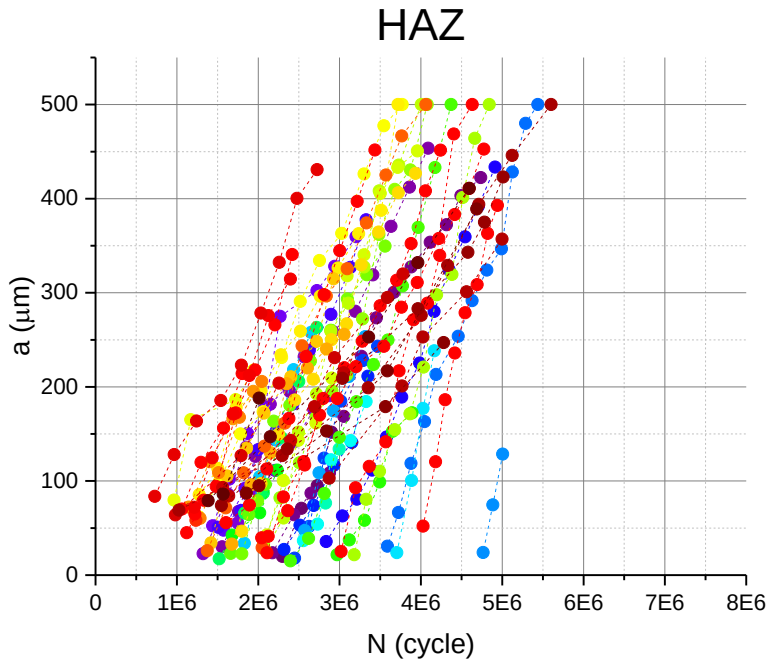
HAZ
a (μm)
N (cycle)
0
100
200
300
400
500
0
1E6
2E6
3E6
4E6
5E6
6E6
7E6
8E6

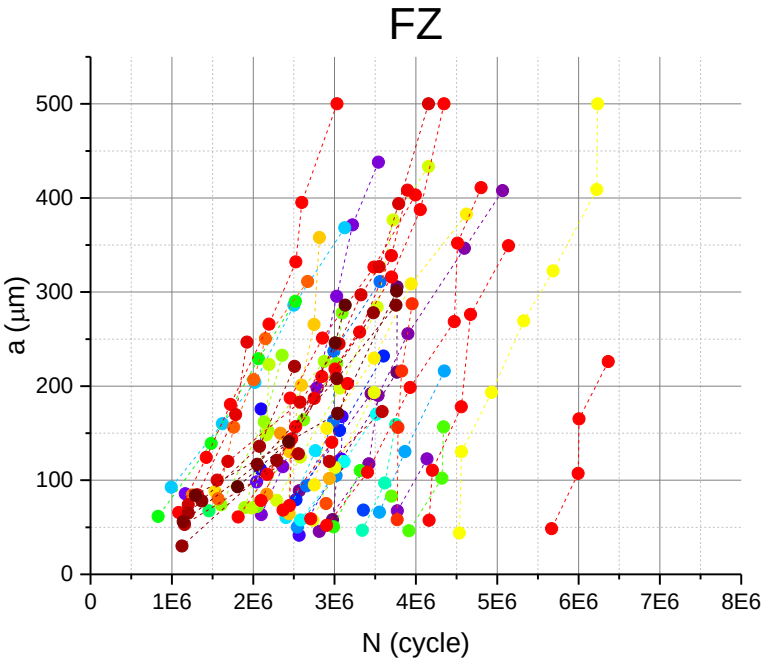

Figure 2-12. Crack length (projected) vs. number of load cycles for three weld zones

Table 2-3 presents some significant statistics: Min N_{nuc} and Max N_{nuc}, represent the maximum and minimum crack nucleation life in the surface grain in all simulations for each zone, respectively, the 5% nucleation probability corresponds to the third shortest nucleation life computed, and the average cycle numbers to form a 100 μm crack.

The results show that the number of cycles for BM to develop a 100 μm crack can double those for HAZ and FZ, while the FZ has the smallest value. These differences result from different grain size and morphology between the HAZ and the FZ.

Table 2-3 Most significant statistics for MSC nucleation and growth in welds

	BM	HAZ	FZ
Min N_{nuc}	1,316,966	728,618	832,034
Max N_{nuc}	3,637,766	4,765,911	5,669,326
5% prob. N_{nuc}	1,529,173	982,348	1,084,039
Avg. N for 100 μm crack	5,353,025	2,258,445	2,599,180

To compare the effects of the microstructure on crack growth, Fig. 2-13(a) presents the crack length normalized by the SVE size. As shown in the figure, at the crack nucleation stage (first grain crack), the distributions for the crack nucleation (first grain crack) are similar for the three zones. However, as more grains are cracked, the slope of the curves, which is the ratio of the normalized crack to the cracked grain numbers, shows more variability. In comparison, BM has a higher ratio than those for HAZ and FZ, which suggests that the SVE in BM gets fully cracked with less number of grains. Such differences are due to the grain size, SVE size (characteristic transition length to PSC or LC), and the grain shape (lath-like grain shape in FZ ends up with much less grain to be fully cracked). Fig. 2-13(b) shows the crack growth rate (CGR) for the three zones. It is noteworthy that the vertical axis is in a logarithmic scale. As shown in the figures, CGR increases after nucleation. In the three zones, BM has the smallest value of CGR compared with those for FZ and HAZ. Compared with those for BM and HAZ, FZ has the largest variations of CGR. Additionally, a large overlap of CGR values for FZ and HAZ can be found, as well.

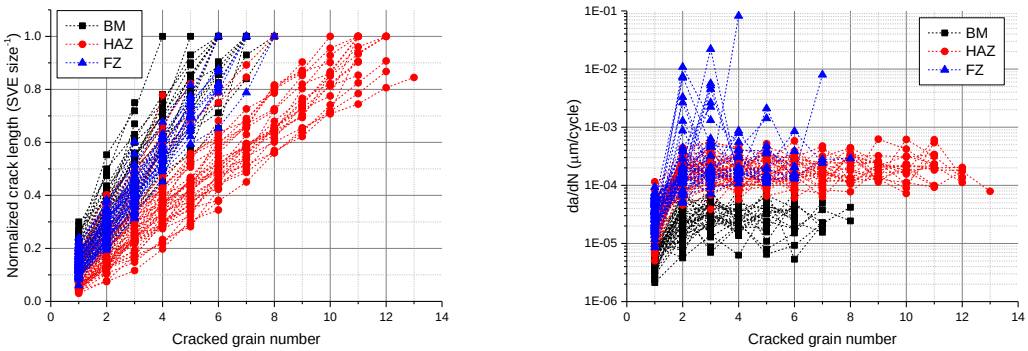

(a) (b)

Figure 2-13. Crack growth variation with cracked grain number in three weld zones

(a) is the SVE size-normalized crack length growth;

(b) is the variation of the crack growth rate along the crack path.

To compare the scattering, Fig. 2-14 presents the coefficient of variations (COVs) of the number of cycles ΔN to crack a grain, the crack extension Δa, and CGR da/dN for each cracked grain. Most COVs fall into the range between 0.1 and 1, and it has a general slightly decreasing trend but increasing fluctuation with increasing grains cracked. Among three weld zones, BM shares similar trends with HAZ but the FZ has a larger discrepancy. We argue that the morphology rather than the size of the grain is responsible for such differences.

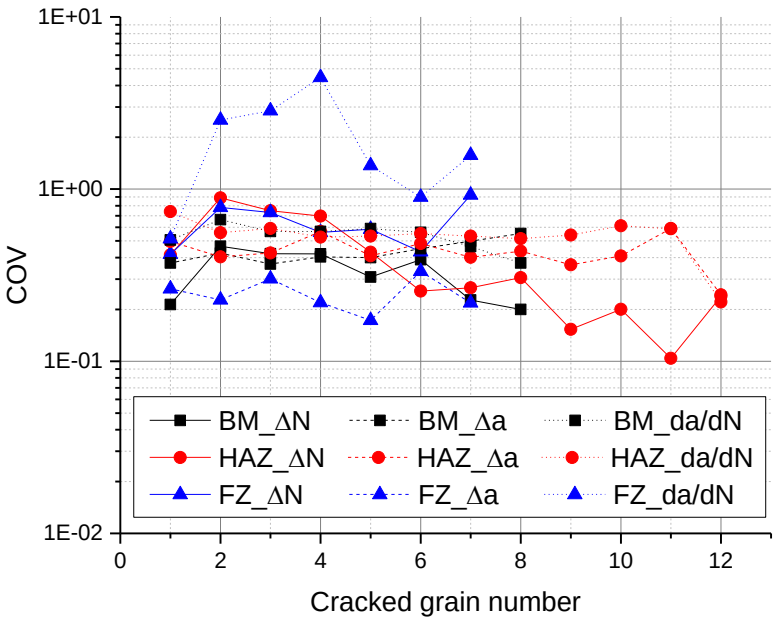

Figure 2-14. COVs of ΔN, Δa, and da/dN in three weld zones

For a further study of CGR with relation to the macro-scale measure, CGR is plotted versus crack length in Fig. 2-15. To eliminate the size effect, the SVE size-normalized crack length is used. The shape of the line is stepped since the CGR is considered to be constant in subgrain growth (refer to Section 2.2.2). After the normalization, a major part of the curves from three weld zones are overlaid. Most of the HAZ curves overlap, while the curves for FZ show largest variability. These discrepancies mainly come from the grain shape and deviation of the grain size.

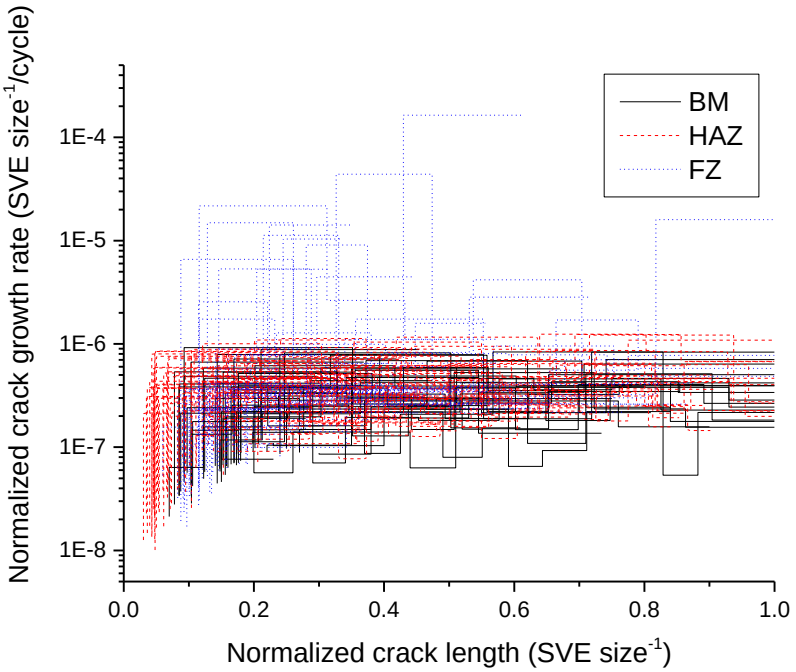

Figure 2-15. Crack growth rate vs. normalized crack length in three weld zones

Finally, these simulations provide the means to compute probabilistic MSC growth curves in Fig. 2-16 where linear interpolation is applied to get the cycle number for a specific crack length. A special normalized standard deviation (NSTD) is used to integrate the comparison of the fatigue life variability in one weld zone and across three weld zones, namely, the standard deviation of cycle number consumed by a specific crack length is normalized by cycle number value averaged from all data points of each weld zone (refer to Fig. 2-12). As shown in Fig. 2-16, the range of mean value of fatigue life N (cycle number consumed) is between 1.5×10^6 and 5.5×10^6, and the range of NSTD is between 0.2 and 0.5. Overall, the mean N increases almost linearly for all zones. NSTD shows a different trend for each zone — slightly increasing for BM, slightly decreasing for HAZ, and slightly decreasing and then increasing for HAZ. In the very early phase of fatigue (mainly nucleation regime), the mean value and NSTD of N for BM is slightly smaller than that for HAZ and FZ. During the MSC propagation regime, the mean value of N for BM increases faster and exceeds that for HAZ and FZ, while its NSTD of N slightly increases and exceeds

that for HAZ. These phenomena are related to the grain size to SVE size ratio or the number of grains. For the mean value of *N*, the lower number of grains in BM reduces the chance to have severe strain concentration, leading to longer fatigue life. For NSTDs, to crack the first surface grain, the HAZ has a larger NSTD because of more grains on the surface compared with BM. Then the NSTD drops to a plateau since more grains in the subsequent cracking steps mean more chances to develop the same crack length until stabilization. However, as for BM, with fewer further cracking paths (through potential grain sequence ahead) but the large variability of grain size, an increasing NSTD is expected. Compared with BM/HAZ, the thickness variation of lath-like grain in FZ also introduced larger variations for FZ.

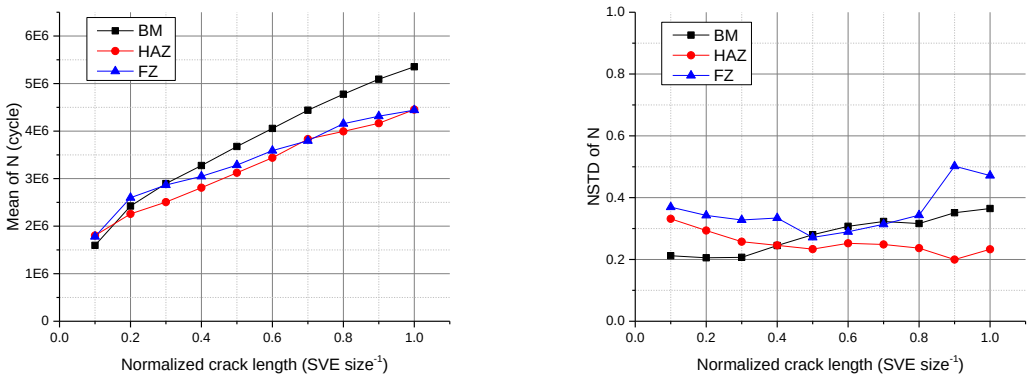

(a) (b)

Figure 2-16. Mean value (a) and variability (b) of the fatigue life vs. crack length

2.5 Discussions

- *Simplification of 2D models*

  The representation and solution of the MSC problem in 2D is a significant simplification, but it does not prevent us from assessing a few key effects of the microstructure on fatigue cracks. Certainly, we do not aim for precisely modeling crack growth to qualify the life of a component but to compare the relative detrimental effects on fatigue of the various weld zones in joints. A 2D model is a balanced effort that can incorporate complex microstructure information and request statistical realizations to

compute low probability fatigue cracking event. Having proved the usefulness of the framework, future work will implement the approach in this paper to study welds with 3D models.

- *Constitutive model*

  The quality of the constitutive model affects the quantification of the fatigue driving force and introduces some uncertainty. The crystal plasticity model is a continuum description of the crystal behavior that partitions the strain among the slip planes based on the phenomenological description of dislocation glide. Here, the crystal plasticity model has parameters calibrated to reproduce the cyclic stress-strain curve, but these parameters may not be unique. Lack of uniqueness does not preclude the use of these parameters to estimations of the final damage. Although the model has not been validated for a specific crystal orientation, there is much higher confidence that the response of an ensemble of grains can be predicted. This explains why we do not focus on the local grain environment that initiates/propagates a crack, but on the trends from the ensemble. Future work should aim for a formulation informed by physical bottom-up approaches (such as first principle calculation by atomic mechanics).

- *Fatemi-Socie model and k parameter*

  The Fatemi-Socie parameter (Fatemi and Socie 1988) is widely applied for critical plane approach and depends on a material constant *k*, which can be found by fitting fatigue data from simple uniaxial tests to fatigue data from simple torsion tests. Generally, $k = 1$ is suggested as a first approximation if test data not available (Stephens et al. 2000). However, *k* may differ from 1 or not be constant for the different number of cycles, i.e., different *k* for different material and different *k* under different crack length criteria for defining failure of one material. The range of *k* can be from 0 ~ 2 for a variety of steel using different failure definition based on Park and Nelson's research (Park and Nelson 2000). For steels similar to that considered on the paper — Ck45, 30CrMiMo 8, 42CrMo4, X 10 CrNiTi 18 9, and 1% CrMoV — *k* has been found to be 0.4, 1.0, 1.0, 1.4, 1.2 under small crack length criterion (Park

and Nelson 2000; Reis et al. 2009). Therefore, for bridge steel weld, k = 1.0 is taken as a good approximation for the Fatemi-Socie damage parameter.

In the integration with crystal plasticity for crystallographic cracks, Castelluccio (Castelluccio and McDowell 2012) has shown that k only plays a significant role when considering multiaxial loading. Hence, within a single grain equally good damage predictions (based on crack tip displacements) can be obtained with various k as long as the same loading is applied (e.g., tensile or shear), but an optimal k (close to k = 1) arises for using a single parameter for multiple loading directions (which was indeed the original intent from Fatemi and Socie). Furthermore, the paper considers a single nominal loading direction, although grains will naturally have a local multiaxial component. Further understanding of the physical meaning of Fatemi-Socie parameter would be beneficial, but it is beyond the scope of the present paper. Furthermore, different k will impact the FIP and mean fatigue life, but less likely the spread and ranking of microstructures.

- *Fatigue model formation, calibration, and validation*

  The microstructure-sensitive fatigue model (Eqs. (2-6)) is based on FIPs and irreversibility parameters. Like Paris' law, the model form needs to be tested by many practices and experiences to be accepted. Regarding the irreversibility coefficients, the situation is similar to the constitutive model in the sense that crack growth trends would hold even if these parameters are modified. The quantitative interpretation of the atomistic process in crack tip zone would help to quantify these parameters with an additional validation from small crack growth tests. For the current paper, due to the limited experimental data, especially for crack growth for infrastructural material like bridge steel, a better calibration and validation for our current model is not able to be performed. Therefore, the experimental work is scheduled for the authors now. Due to the large uncertainties, experiments need to repeat for multiple times for a cluster of crack length vs. cycle number (time) curves to compare with the one

from proposed model. There is a clear trend that the calibration and validation need to shift to probability based.

- *RVE vs. SVE*

  Traditionally, the size of RVE are validated based on the stress-strain response, and they are constructed as a deterministic representation of a material using the microstructure data from experiments or simulations. However, fatigue crack growth problem is dominated by extreme rather than mean values, which implies that the RVE for FIP prediction needs to be much larger than that to reproduce the stress-strain curve. Such a large RVE carries an unfeasible computational cost. Instead, we opt to model SVEs and multiple realizations, which provide a scalable and efficient estimation of crack growth and fatigue life in a stochastic sense. The optimal SVE size and number of realizations that yield accurate prediction for each weld zone should be analyzed in future work.

2.6 Conclusions

This paper employs a small crack simulation framework built on the microstructure-sensitive model and crystal plasticity to predict the early fatigue lives of weld zones with different microstructures. Firstly, a non-local FIP is verified to be suitable for mesoscale driving force in BCC structures. Considering the uncertainty of the microstructure, a probabilistic approach is proposed to calibrate the model for which limited experimental data is available. Simulations study the growth of small microstructure cracks under constant cyclic load by modeling a grain-by-grain crack path.

The results show larger deviations of *a*-*N* data for BM than those for HAZ and FZ in MSC regime. Furthermore, the crack growth rate in the FZ has largest variability among the three zones, while the HAZ has the lowest. Future work will focus on performing a full characterization of crack growth rate distributions to quantify the characteristic transition length between small and long cracks. In addition, the whole framework can be easily extended to include residual welding stress inside microstructure and environmental effects, and can serve as a part of multi-scale fatigue prognosis system if variable amplitude

loads can be covered. However, there are some limitations such as simplified nucleation, SB based mechanism, and 2D microstructure, etc. Despite these, the proposed framework can still serve as a promising local approach for early fatigue assessment of high-quality weldment. As future work for peers, the full validation of the model requires extensive statistical technique and physical test data throughout the weld microstructure in specific structural components like U-rib joints of an orthotropic deck.

CHAPTER 3 A NONLINEAR GRAIN-BASED FATIGUE DAMAGE MODEL FOR CIVIL INFRASTRUCTURES UNDER VARIABLE AMPLITUDE LOADS

3.1 Introduction

During the life cycle of steel bridges, local details like weldments are often subjected to time-variant stress cycles induced by ambient environmental or service loads from heavy vehicles, hurricane-force winds, or destructive waves, etc. Fatigue damages are accumulated gradually, starting from crack initiation, short crack propagation to possible failure of the structural components or the entire structure. Among the entire fatigue life of structures, crack initiation regime could account for about 90% of the total fatigue life and cracks in this regime could hardly be detected even with the current state-of-the-art nondestructive evaluation methods (Krupp 2007). In addition, the stress status of the welding details could be much more complicated where fatigue cracks could most likely initiate. Material heterogeneity, micro-defects, residual stresses, distortion and geometric weld characteristics (weld toe/root) in these areas are more favorable for fatigue and fracture. Although the fatigue assessment under VA by crack growth method is mature with many sophisticated codes if an initial long crack is prescribed (Stephens et al. 2000), modeling of the fatigue damage accumulation during the initiation regime till long cracks still remain challenging especially under VA loading.

In the current practice, when dealing with VA in crack initiation problems, the stress ranges are usually simplified by using an equivalent constant amplitude stress range, Miner's rule or nonlinear damage rule with corresponding *S-N* curve or ε-*N* curve, or a local strain approach with certain counting methods (Ghahremani et al. 2015; Li et al. 2002; Lynn and DuQuesnay 2002; El Malki Alaoui et al. 2009; Zheng et al. 1994). In 1998, Fatemi and Yang reviewed many cumulative damage rules and theories (Fatemi and Yang 1998) and concluded that most rules lack clear physical basis. To capture the nonlinear nature of crack initiation, Miner's law was modified to consider stress effect and still maintain its simplicity (Liu and Mahadevan 2007). In addition, nonlinear damage approach based on continuum damage mechanics are also

getting increasing applications, such as fatigue damage assessment of existing bridges (Zhang et al. 2013b). However, damage under macro fatigue limit, local microstructure effect, and notch effect are often sacrificed using above method, which can bring significant error in some circumstances (Schijve 2009). The continuum-mechanics based analysis of structural detail can result in strong discontinuities, which make the continuum approach questionable in the crack initiation range (Lemaitre and Desmorat 2005; Liu and Mahadevan 2009).

Crack initiation is a very slow and continuous process that takes place on several different length scales with different phases, such as nucleation, microstructurally small crack (MSC), physically small crack (PSC) for polycrystalline fatigue cracks. Due to the shared grain size variation, MSC and PSC are usually combined in the analysis (Castelluccio and McDowell 2014). Therefore, the crack initiation problem is inherently a problem of short fatigue crack nucleation and growth in the local microstructure. Coming to the short crack initiation and growth under variable amplitude load (VA), the fatigue damage accumulative model can be mainly grouped into two categories. One class of methods is to combine the short fatigue crack model under constant amplitude load (CA) with damage rules and cycle counting methods. The development of either the CA model or the damage rule promotes fatigue prediction under VA. Considering the notch and multiaxial effect, a new short-crack-growth-based fatigue assessment scheme was proposed (Döring et al. 2006; Hertel and Vormwald 2011). To consider microstructure influence like slip bands, a critical distance/plane method and a shear stress-maximum variance method were presented to predict the fatigue life in the short crack regime (Morel 2000; Susmel et al. 2014; Susmel and Taylor 2012). Wei et al. (Wei et al. 2002) modified Newman's crack closure model to include the influence of grain boundaries on the crack opening level through introducing the concept of crack tip plasticity constrained by grain boundary blocking. With rigorous statistical analysis, a new physics-based, mathematically precise fatigue small-crack growth modeling method is proposed for scattering surface small-crack growth in heterogeneous metals (Xue 2010). For the damage rule, Lautrou et al. (Lautrou et al. 2009) found that the accumulation of damage in the two-scale damage model tends to be linear if variations of amplitude are repeated many times. Recently, Zhang et al. (Zhang et al. 2016) proposed a new nonlinear

continuous damage model that could include the effects of multiple over-loading on the damage accumulation and describe the retardation influence on the short fatigue crack growth effectively. The other class of methods is cycle-by-cycle based or with small time scale which is either based on linear finite element analysis (Lu and Liu 2010) or analytical models, such as modified Wheeler model and Willenborg model (Hodapp et al. 2014; Romeiro et al. 2009). Code μcracksim without finite element analysis was also developed for microcrack and non-proportional multiaxial VA (Ahmadi and Zenner 2006). Wheeler model and Willenborg model are most widely used since they consider the load interaction (Maljaars et al. 2015; Romeiro et al. 2009). Fricke (Fricke 2014) and Remes et al. (Remes et al. 2012) addressed that the proposed frameworks seldom offer explicit simulation for short fatigue crack in weld microstructure and these processes still comprise primarily microstructural phenomena (moving dislocations, PSB behavior, micro-crack initiation on PSBs and further crack growth by local slip mechanisms at the crack tip).

Since a crack from initiation to propagation crosses several length scales, multi-scale analysis is more reasonable for fatigue assessment. Fatigue damage accumulation in mesoscale could be a key-chain link between the macro-scale and micro-scale. In (Li et al. 2012), effects of variable stress amplitude on cyclic plasticity and microcrack initiation are discussed by using the mesoscale model. In the mesoscale, PSBs are the favored physical sites for crack nucleation and transgranular crack growth. PSB associated fatigue damage measures such as PSB density/population were proposed to describe the fatigue initiation, damage mechanism, and process (Fatemi and Yang 1998). However, these indices are a general representative of fatigue status while short crack growth along these PSBs is a rare, very localized, and microstructure-sensitive event with strong discontinuity induced especially under high cycle fatigue. Therefore, a better model is needed to quantify the fatigue damage accumulation under VA when short crack propagates along PSBs till the characteristic length of the initial long crack. Recently, the microstructure-sensitive model with fatigue indicator parameters (FIPs) has been a promising tool to describe both the MSC nucleation and growth with the non-local measure (Pineau et al. 2016). Several FIPs, such as those based on accumulated plastic strain and dislocation density (Kartal et al. 2014; Manonukul and Dunne 2004; Sweeney et al. 2013), energy dissipation (Sangid 2013; Sangid et al. 2011), averaged

effective strain and tensile stress (Ghosh and Chakraborty 2013; Sinha and Ghosh 2006), are proposed based on different non-local measure and varied fatigue damage mechanism for short fatigue crack research (Dunne 2014). Due to the complexity of cyclic microplasticity and damage formation in HCF, the FIPs provide a computable parameter with which different microstructures may be quantified for the fatigue analysis.

In the present study, a two-fold grain-based fatigue damage accumulative model is proposed. It consists of two interrelated parts: PSB-based short crack growth model for grain-by-grain growth and grain-based Miner's rule describing the fatigue damage accumulation in a sub-grain regime under VA. The 2D PSB-based short crack growth model is based on the current state-of-art microstructure-sensitive fatigue model and non-local fatigue indicator parameter (FIP) concept. The grain-by-grain damage accumulation with FIP as the driving force and statistical representative elements (SVE) as the platform can automatically include the load sequence effect on the grain scale as well as the mean stress effect, damage under macro fatigue limit and the notch effect. The Miner's rule is assumed to hold for the sub-grain damage since its deficiency in the macroscale prediction can be avoided by using the mesoscale model. The paper is organized in the following sections. Section 2 introduces the two-fold grain-based fatigue damage accumulative model. Section 3 discusses the implementation of PSB-based short crack growth model. The framework is implemented in ABAQUS with Python scripts for the whole process and user subroutine UMAT for crystal plasticity. In Section 4, the approaches of processing repeated stress blocks are presented. For civil infrastructures such as bridges or offshore structures, the varied large dynamic loads, such as wind and wave loading, during extreme weather conditions can dramatically reduce the fatigue life of components. Based on the proposed framework, a demonstration example is provided for the bridge beam hotspot under stress history induced by vehicle and wind in Section 5. Section 6 provides a summary and some discussions.

3.2 Two-fold Grain-based Fatigue Damage Accumulative Model

3.2.1 PSB-based short crack growth model

The model proposed is to describe the short fatigue crack growth along PSBs under constant amplitude load. The short crack length consisted of several linked PSBs can be used as the fatigue damage accumulative measure. The model details have been elaborated in Chapter 2 Section 2.

3.2.2 Grain-based Miner's Rule

The physical base of Miner's rule is constant energy absorption or dislocation generation per cycle, and this linear damage rule is widely used with the *S-N* curve approach for crack initiation research (Stephens et al. 2000). In the sub-grain scale, the Miner's rule is reasonably assumed to hold for the sub-grain damage for the constrained single crystal under VA. The deviation of experimental results from Miner's rule in the macroscale prediction can be reduced by the probabilistic mesoscale simulations. The grain-based Miner's rule can be expressed as

$$D_{bj} = \sum_i \frac{n_{bi}}{N_{ij}} = \frac{C}{N_{bj}} \tag{3-1}$$

where D_{bj} is the damage from a stress block on grain j with physical meaning of relative PSB crack length, N_{bj} is the number of blocks to crack the grain j, n_{bi} is the cycle number for stress range i, N_{ij} is the failure cycle number for grain j under stress range i. C is the critical damage accumulation index which can be taken as a random variable. C is often set as 1 in the codes. However, experiments suggest that it could be within the range between 0.7 and 2.2 for structural steel (Fatemi and Yang 1998). In practice, certain distribution can also be assigned, such as lognormal distribution with a median value of 1.0 and coefficient of variation of 0.3 (Wirsching 1984). Together with the grain-based Miner's rule, traditional rain flow counting is used, which is suitable for short crack due to less crack closure induced sequence effect (Schijve 2009).

3.3 Implementation of PSB-based Short Crack Growth Model under CA

3.3.1 Crystal plasticity finite element model of SVE

In the present study, the crystal plasticity model defined by Huang (Huang 1991) is employed and modified to include the Bauschinger effect which is essential for cyclic loading. The inelastic deformation of a single crystal is assumed to arise only from crystalline slip, and the deformation flows via dislocation. The model detail and crystal plastic material parameters have been illustrated in Chapter 2. The construction, grain property assignment, boundary conditions and mesh of microstructural SVE have also been elaborated in Chapter 2. For the current study, since the surface SVE is of particular interest to identify crack initiation, mixed boundary conditions are used: the top edge is free, and the bottom edge is simply supported; and the left and right edges are equipped with periodic boundary conditions (PBCs).

3.3.2 Fatigue damage calculation under CA

In the initial model, the random SVE is generated while each grain is divided into several persistent slip bands (PSBs). During the loading process, cracks initiate at the PSB with the largest FIPs and the nucleation life is obtained using Eq. (2-3). The elements in the cracked PSB are updated with a reduced stiffness, and the cyclic loading process continues to get stress redistribution. The isotropic reduction by 0.999 is adopted for the stiffness of the cracked PSB. The path for the crack extension is assumed to be transgranular along the PSBs, and the cycle number needed to crack the neighbor grain is evaluated using the corresponding FIP-based crack growth rate equation. The crack will extend along the PSB with the minimum cycle number. The crack that arrests at the boundaries will be automatically captured by $da/dN = 0$. As a simplified approach implementing the microstructure-sensitive model and FIP concept (Castelluccio and McDowell 2015b), the general procedures provided could be summarized in the flowchart and the crack growth scheme in Fig. 3-1.

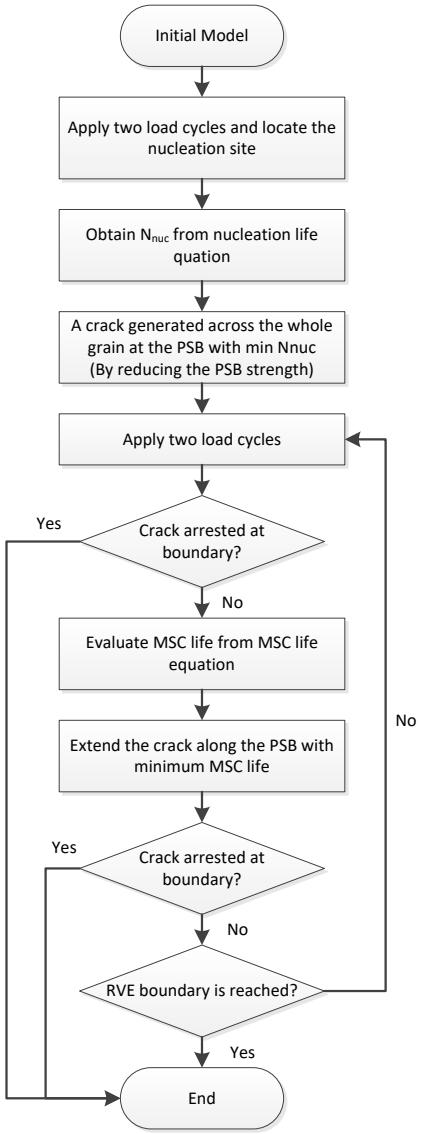

Figure 3-1. Flowchart for PSB-based short crack growth model

3.4 Implementation of Fatigue Damage Accumulation under VA

During the service life of the civil structure, ideally, a long stress history can be processed to crack the grains one by one by applying a searching method together with the proposed model. However, the large computational cost is needed to process the long-time histories. In fact, the VA would more or less have patterns or characteristics which help simplify the damage accumulation approach. In the present study,

two different VA scenarios are considered. One is repeated stress blocks. And the other is VA that consists of large fractions of the subcritical load with few critical loads.

3.4.1 Approach I – targeting at repeated stress blocks

If targeting at stress history that consists of repeated variable stress blocks (commonly happening in flight and car operation), the following approach will be used:

1) The stress history in a block is rainflow counted to obtain several mean-range pairs and cycle number n_{bi} for counted stress range i.
2) PSB-based short crack growth simulation will be performed under each counted stress range i and the failure cycle number N_{ij} for grain j will be obtained. D_{bj}, the damage from a stress block on grain j and N_{bj}, the number of blocks to crack the grain j can be calculated by Eq. (3-1).
3) N_{bj} will be added together and be converted to time scale to obtain the fatigue life.

It is noteworthy that a precondition here is that path for a given microstructure is the same under any different loads with the same stress or strain rate. At most time, the condition holds for high cycle fatigue (Castelluccio and McDowell 2015a).

3.4.2 Approach II – targeting at daily subcritical loads with extreme event loads

For civil infrastructures such as a bridge or an offshore platform, continuous repeat of critical stress blocks is unrealistic since these load conditions may only happen for few times during the entire life cycle of the structure. However, these low probability events could remarkably reduce the fatigue life. In other words, the structural lifetime load history shown in Fig. 2 consists of a large fraction of subcritical load (daily load) and few critical stress blocks (extreme event load). In this scenario, the large fraction of the subcritical load can be treated as CA with overall effective stress range (cubic root mean for the bridge details), while each of the critical stress blocks is processed separately with the first two steps in the above approach. Meanwhile,

the sequence effect of VA on fatigue performance can be overcome by processing each load fraction in order.

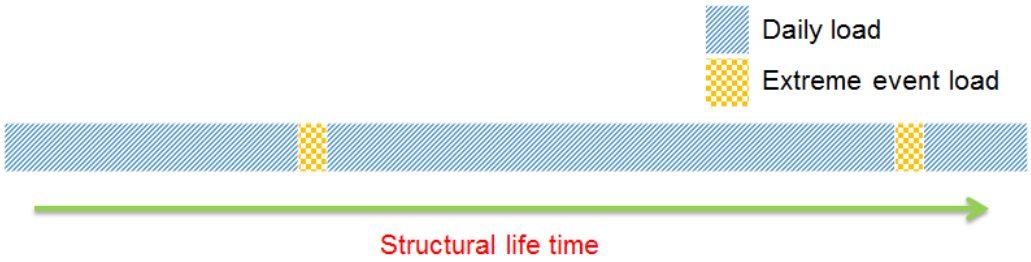

Figure 3-2. Schematic diagram of stress history for civil infrastructure

3.5 Case Study

A case study is presented in this section to evaluate fatigue damage accumulation on a bridge beam hotspot, such as web to flange weldment, by the proposed model. The dynamic stresses of the bridge are adopted from the resolution of a vehicle-bridge-wind coupled dynamic system. The stress is extracted from the bridge deck at the middle of the bridge's main span and the detailed information about the simulation could be found in the literature (Zhang et al. 2014). To consider the local stress effect, such as a typical weld toe of Category D, the stress concentration factor (SCF) is taken as 3.6 (Anderson 2005). The peak-valley local stress history shown in Fig. 3-3 can be used to get reversals for rainflow counting and the mean – range pairs.

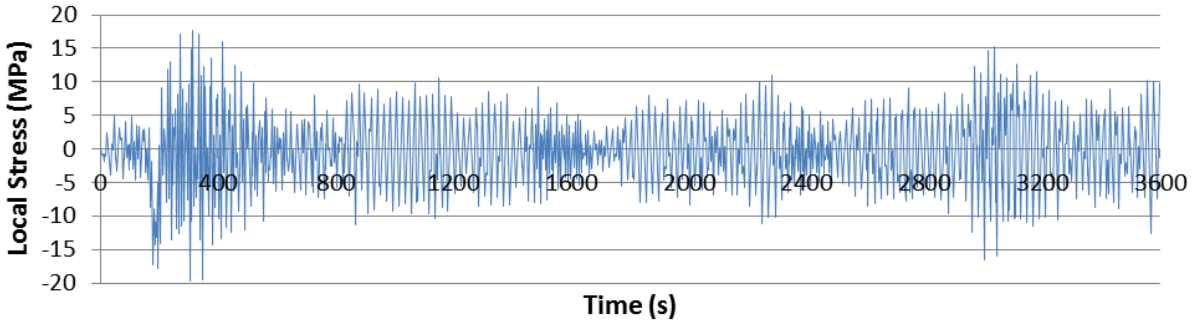

Figure 3-3. 1-hour peak-valley local stress history as loads for mesoscale model

In the first demonstration, considering the repetition of the above stress block, the Approach I is applied. In the grain-based Miner's rule, i.e., Eq. (3-1), *C* is taken as a fixed value 1 for the present study.

In the PSB-based short crack growth model for one SVE (see Fig. 3-4) under each counted stress range cycle, the parameters for the welding details are adopted from the literature and are listed below, namely, α_g = 400 cycles μm, ϕ = 0.055 and ΔCTD_{th} = 2.5 x 10^{-4} μm (Castelluccio and McDowell 2014; Mughrabi 2013; Venkateswaran et al. 2005). In the present study, cracks nucleate inside the surface grain (prescribed for one-way crack). Specified boundary conditions (free top surface and periodic boundary for other sides) and the loading conditions (uniaxial triangle loading at 0.01MPa/sec) are adopted for the simulation under each counted stress range. The whole process of one simulation under CA is plotted in Fig. 3-5. Crystal strain localization, crack nucleation, stress redistribution and crack propagation and arrest can be observed. Sometime the plastic strain may not localize in the surface grain in the nucleation regime, possibly due to the very heterogeneous grain distribution. However, the assumption that the first crack starts at the surface grain is still appropriate because of the uniform side strain load. In reality, the stain still has a larger value on the surfaces, and this condition reduces the chance to nucleate subsurface crack.

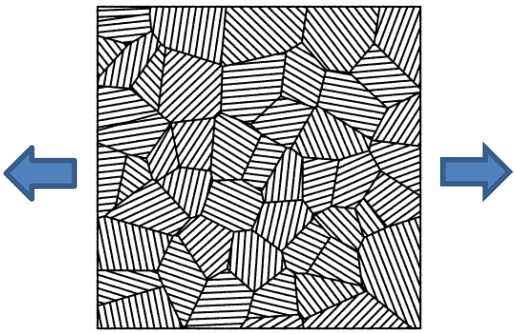

Figure 3-4. SVE under uniaxial load

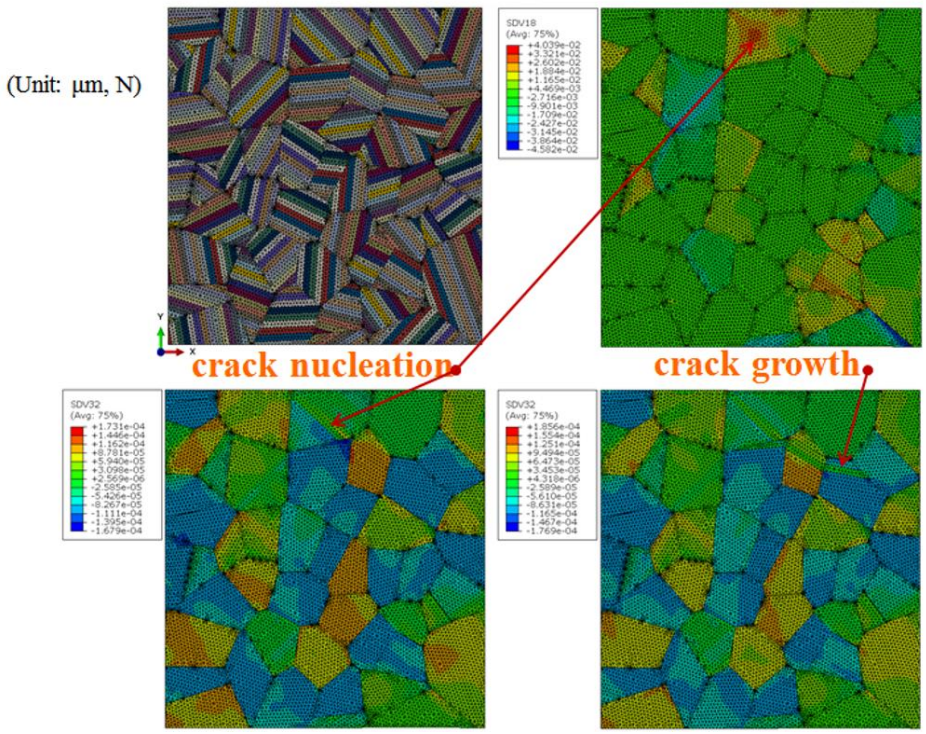

Figure 3-5. The PSB-based short crack growth under CA (-6.89 MPa ~ 6.24 MPa)

(upper left – PSB distribution, upper right – plastic shear strain (SDV18) after 2 load cycles, lower left – resolved shear stress (SDV32) at 2 cycles after nucleation, lower right – MSC path at the end)

The fatigue assessment results after the whole simulation are summarized in Table 3-1. It takes 31 years to crack the entire SVE. It is comparable with the literature (Zhang et al. 2014), which provided 44-year total fatigue life by using the linear fatigue damage rule. Compared with the typical Miner's rule, the proposed method could better capture the nonlinear damage accumulation during the structure's life-cycle. Meanwhile, the projected crack length *a* vs. *time* diagrams is plotted in Fig. 3-6 and nonlinear fatigue damage accumulation can be observed. It is noteworthy that the result in Table 3-1 is only for a demonstration purpose. The calculated fatigue is obtained based on the expanding of the 1-hour stress block to the whole life cycle, which is not realistic but similar to the approach used in the literature (Zhang et al. 2014).

Table 3-1 The fatigue damage assessment for each grain and the whole SVE

Grain #	D_b	N_b	*Life* (yr)
1	6.50E-06	153959	17.6
2	2.08E-05	47994	5.5
3	7.29E-05	13709	1.6
4	3.47E-05	28796	3.3
5	4.30E-05	23281	2.7
Whole SVE	—	267739	≈ 31

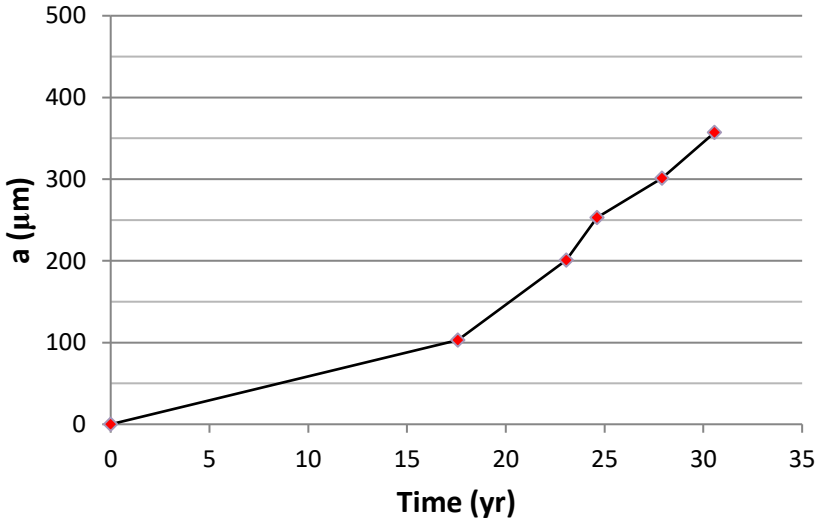

Figure 3-5. The short crack growth with time

In the second demonstration, the structural load history containing both critical loads and subcritical loads is applied to SVE in the previous example with following specific input:

- Daily load: overall effective stress range $\Delta\sigma$ = 15.8 MPa (zero mean stress) with a 2s period;
- Extreme event load: to be conservative, typical 6h hurricane event (50-year recurrence interval) with six repeated largest 1h stress history (Fig. 3-3) is used.

The simulation results for different scenarios are summarized in Table 3-2. As shown in the table, with the inclusion of extreme events, the fatigue life drops drastically. In addition, if the occurrence time

for the extreme event also affects the fatigue life significantly. For example, with two hurricanes, if the hurricanes hit the structure at 25 and 75 years, the fatigue life is 973 years. However, if the hurricanes hit the structure at 50 and 100 years, the fatigue life drops to 467 years.

Table 3-2 The whole SVE fatigue life for different hurricane scenarios

Scenario	Whole SVE fatigue life (yr)
Pure daily load	1649
One hurricane at 25 year	1367
One hurricane at 100 year	840
Two hurricanes at 25 and 75 year	973
Two hurricanes at 50 and 100 year	467

The extreme events (periodic overloads) seems to reduce the predicted fatigue life by increasing the strain in the SVE simulation, which leads to a small *N*. Due to the different pre-existing crack status, different hitting time of the extreme load has a different effect. Longer pre-existing crack induces larger strain in the grain ahead of the crack tip. In the present study, only one tested SVE is randomly generated in the present study for the demonstration purpose. To get a more realistic prediction, several SVEs need to be tested for extreme value statistical analysis to identify the low probability event of fatigue crack initiation.

3.6 Summary and Discussions

In the present paper, a two-fold nonlinear grain-based fatigue damage accumulative model is proposed by solving a crack initiation problem. The new model can be used to process the VA induced fatigue damages by combining PSB-based short fatigue crack model and grain-based Miner's rule. In the modeling scheme, the 2D short crack growth model built on the microstructure-sensitive model and crystal plasticity based FIP is applied. In the sub-grain regime, linear damage accumulation is adopted. Crack associated damage

are accumulated on a grain by grain basis until the crack reaches characteristic length of a long crack. The fatigue damage accumulation model is demonstrated by an example of a typical bridge subjected to multiple dynamic loads.

Compared with traditionally used linear damage rule, the two-fold nonlinear grain-based fatigue damage model incorporates physics-based short crack growth model. Uncertainties from microstructure can be included in the model to consider the stochastic nature of crack initiation process. The grain-by-grain damage accumulation with FIP as the driving force and statistical representative elements (SVE) as the platform can automatically include the load sequence effect on the grain scale as well as the mean stress effect, damage under macro fatigue limit and the notch effect. The deficiency of the application of Miner's rule in macroscale fatigue damage accumulation is avoided in the model via only applying for the damage accumulation in the sub-grain damage.

With a more sophisticated realistic stress history either from numerical simulations considering different environmental conditions statistically or from structural health monitoring with effective data processing techniques, a more realistic fatigue life prediction result is expected. However, it is noteworthy that different levels of validation of the model are required with extensive statistical analysis technique and multiple carefully designed physical tests. Considering the random nature of the mesoscale material behavior, it is more likely to be pertinent to validate the model results considering an ensemble of microstructures rather than one particular microstructure realization.

CHAPTER 4 MESOSCALE SIMULATION OF CORROSION FATIGUE BY AN INTEGRATED TRANSGRANULAR AND INTERGRANULAR CRACK GROWTH METHOD

4.1 Introduction

Fatigue is one of the primary damage and failure mechanisms of structures or the structural components subjected to cyclic loadings. Meanwhile, under the exposure to corrosive liquid or gas, fatigue crack nucleation and propagation behavior could become more complex. Disastrous accidents like the 1968 transport aircraft crash have occurred due to fatigue cracks interacting with corrosion damage at bulkhead (Schijve 2009). Whenever corrosion damage can occur to the material surface of a dynamically loaded structure, the complex interactions of the chemical process of corrosion and cyclic stress ranges could significantly affect crack initiation and growth and lead to corrosion fatigue. Since short crack regime accounts for 90% of the high-cycle fatigue life, it is of great importance to evaluate the effects of early-stage corrosion on the short crack growth (Krupp 2007). Despite recent development of various nondestructive techniques for short cracks, many short cracks still could not be detected. Many cracks develop quickly once becoming detectable, which brings some safety concerns of the structures or their components with undetectable short cracks. Therefore, it is of great importance to effectively assess fatigue damage in the short crack regime.

Several short crack nucleation and propagation methods were developed in a range from macro-scale to micro-scale. To balance the complexity in micro-scale models (molecular dynamics) and discontinuity-loss in macro-scale models (equivalent initial crack or continuum damage mechanics), meso-scale models based on crystal plasticity and continuous dislocation theory have been developed. On this scale, microstructure (the grain with or without grain boundary network) of polycrystalline material plays a key role in the evolution of micromechanical stresses and strains. Consequently, damage gradually develops and the microstructurally short crack (MSC) gradually increase in a length scale from 10μm to 1mm. Random grain shapes and sizes, combined with different crystallographic orientations, inclusions,

voids, and other microstructural features result in locally anisotropic and highly heterogeneous behavior of the microstructure with direct influence on the damage initialization and evolution. Recently, the microstructure-sensitive model with FIPs has been a promising tool to describe both the MSC nucleation and growth with the non-local measure (Pineau et al. 2016). Due to the complexity of cyclic microplasticity and damage formation in HCF, the FIPs provide a computable parameter with which different microstructures may be quantified in fatigue damage analysis.

Modeling the corrosion effect on fatigue behavior is difficult since the principle for the complex corrosion fatigue process has not been studied thoroughly with a consensus mechanism to describe and simulate it. Specifically, the complex nature of diffusion of chemicals and electrochemical reactions at the crack tip under the influence of remote stress and microstructure in the plastic zone has not been fully realized (Bathias and Pineau 2013). The most common mechanisms considered in corrosion fatigue (CF) model are anodic dissolution, hydrogen embrittlement, or a combination of both (Craig and Lane 2005). Studies on the anodic dissolution based corrosion fatigue studies started first. Recently, Macdonald et al. built a systematically coupled environment corrosion fatigue model considering the electrochemical crack growth as a penetrating slot with moving wall boundaries (Macdonald and Engelhardt 2012). Akid et al. have combined the anodic dissolution with short crack growth models such as Hobson-Brown model and Navarro-de los Rios model with an empirical approach (Akid and Miller 1991; Angelova and Akid 1998; Murtaza and Akid 2000). However, for high strength steel, the hydrogen induced cracking dominates the corrosion fatigue mechanism (Mansor et al. 2014). Hydrogen-assisted cracking has to be more comprehensive because the electrochemical kinetics of the generation of hydrogen ions and subsequent absorption, the transport inside the metal, and the interaction of the metal with the dissolved hydrogen atoms have to be considered. The analytical models for hydrogen-assisted crack are reviewed by Boellinghaus and Hoffmeister (Boellinghaus 2000). Based on hydrogen diffusion simulation and certain experimental technique around the crack tip, Dmytrakh et al. form a relationship between fatigue crack growth behavior and local hydrogen concentration near the crack tip. However, above corrosion fatigue crack models mainly focus on Paris regime or long crack. For MSC regime, microstructural effects play a

role in hydrogen-informed corrosion fatigue analysis. In the fracture process due to hydrogen embrittlement in polycrystal like steel, the hydrogen preferentially attacks the grain boundaries (GB) rather than the inside of grain, since the diffusive velocity of hydrogen is much faster at GB (Shintaku et al. 2015). H atoms can diffuse in depths and trapped at grain boundaries. At slip transfer across GB, the presence of hydrogen increases the strain energy stored within the GB which could lead to the crack growth mode transition from the transgranular mode to the intergranular mode (Adlakha and Solanki 2016). Cohesive zone model (CZM) has been widely used for intergranular crack simulation while the degradation effect on CZM from hydrogen diffusion has been studied by several researchers (Alvaro et al. 2014; Moriconi et al. 2011; Rimoli and Ortiz 2010).

Based on the above discussion, under the early stage corrosion, the MSC path could be mixed transgranular and intergranular with little branching which was observed by Piascik and Willard, and Lee on aluminum and steel, respectively (Lee 1996; Piascik and Willard 1994). While most MSC growth models developed for either purely transgranular or intergranular cracking behavior, some researchers do consider this behavior through an implicit way such as adding the intergranular cycle to explicit transgranular crack growth using the stochastic method (Castelluccio and McDowell 2014). However, this mixed behavior has not been studied yet by explicit simulation with the mutual trans-intergranular transition.

In this paper, an integrated transgranular and intergranular crack growth framework is proposed for the 2D mesoscale finite element simulation based upon the microstructure-sensitive fatigue model and non-local FIP concept. The integrated transgranular and intergranular crack growth method (ITICGM) consists of the crack initiation phase by crystal plasticity and the corresponding FIP, the transgranular crack part by persistent slip band (PSB) model, the intergranular crack part by inherent cohesive zone, and the manipulation scheme at the GB. Corrosion effect is primarily accounted for intergranular crack segments by introducing the hydrogen-diffusion informed cohesive zone model. The paper is organized in the following sections. Section 2 introduces the microstructure-sensitive model, FIP concept, and the associated equations, with focus on intergranular crack. Section 3 discusses the implementation of the ITICGM and. The framework is implemented in ABAQUS with Python scripts for the whole process and user subroutine

UMAT for crystal plasticity. Section 4 presents the incorporation of corrosion effect and demonstration results including comparison among transgranular crack growth, mixed crack growth with and without corrosion. Section 5 draws some remarkable conclusions.

4.2 Short Fatigue Crack Model

4.2.1 FIPs for transgranular crack and intergranular crack

For transgranular crack, as effective surrogate measures for cyclic crack tip displacement range (ΔCTD) under the mixed mode loads in crystallographic cracks, the non-local parameter FIP can be computed by reasonably coarser FE mesh (Castelluccio and McDowell 2013; Fatemi and Socie 1988). The FIPs for individual slip systems are particularly appropriate for the measurement of crystallographic growth of Stage I fatigue cracks, in which the growth is driven by the shear slip along a single plane. To numerically regularize the local FE mesh and to represent the physical scale of the process zone for crack formation, FIP values are averaged over PSBs, and the PSBs subdivide a grain into layers that are parallel to prime slip planes. Each layer has a nominal thickness of two elements. Transgranular failure is assumed to occur and localize in slip bands.

For the intergranular crack, the similar Zener FIP parameter is employed (Miller and McDowell 1992):

$$\mathrm{FIP}_{\mathrm{int}} = \mathrm{FIP}_{\mathrm{ZP}} = \left[\sum_{\alpha} \left| \frac{\gamma_p^{\alpha}}{2} \left(1 + k \frac{\sigma_n^{\alpha}}{\sigma_y}\right) \right| \right]^2 \left(\frac{\sigma_n^{GB}}{\sigma_y^{GB}} \right)^2 \tag{4-1}$$

where σ_n^{GB} and σ_y^{GB} are peak stress normal to the GB segment and GB strength, respectively. Fig. 4-1 illustrates the finite element calculation of the $\mathrm{FIP}_{\mathrm{int}}$, which is evaluated at the GB sandwich including the GB cohesive element and the Tet elements aside for the neighbor grains.

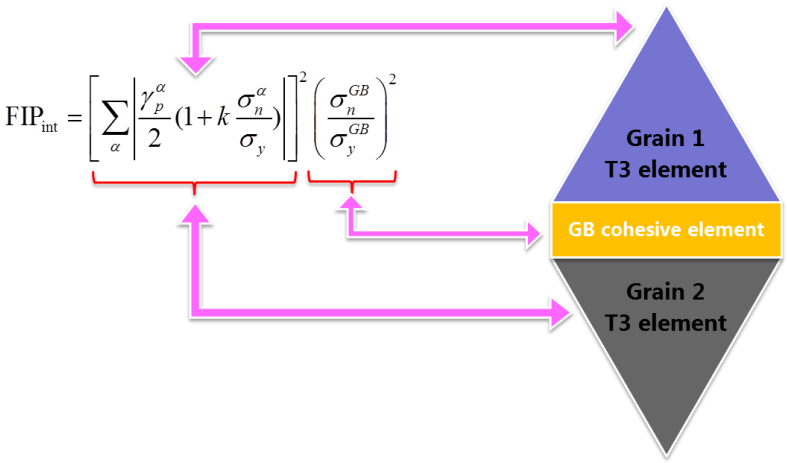

Figure 4-1. FIP evaluation for GB sandwich

4.2.2 Short fatigue crack nucleation and growth equations

For the current study, short fatigue crack is only considered to nucleate transgranularly since this nucleation form is more common even in the corrosive environment (Schijve 2009). Therefore, the nucleation and growth equations of transgranular crack from Chapter 2 are employed here, i.e. Eqs. (2-3 ~ 2-5).

The intergranular growth rate can be expressed as (Castelluccio and McDowell 2014; Miller and McDowell 1992)

$$\left.\frac{da}{dN}\right|_{msc}^{\text{inter}} = \phi_{\text{int}} \exp\left\{-\frac{Q - B\langle PS\rangle}{RT}\right\}\Delta t^{(0.5-\xi)}\mathrm{FIP}_{\text{int}} \tag{4-2}$$

where ϕ_{int} is intergranular proportionality factor in the processing zone, Q is activation energy, B is back stress, PS is maximum principal stress, RT is room temperature, Δt is a time interval of continuous cycle portion, ξ is a departure from parabolic environmental ingress. This formulation accounts for the fact that the diffusion of foreign atoms mediates intergranular crack growth, still driven by an appropriate surrogate measure, $\mathrm{FIP}_{\mathrm{int}}$, computed along GB segments. Literature review in Chapter 1 indicates that elevated temperature can promote the intergranular crack growth. Eq. (4-2) can naturally consider the thermal effect by replacing the RT with a higher temperature with the precondition that the original microstructure is maintained.

Based on the assumption of grain-by-grain crack growth under HCF (Castelluccio and McDowell 2013), stabilized FIPs are taken as constants for potential PSBs in the neighbor grain or GB ahead of the crack tip. Therefore, the number of cycles needed to crack the neighbor grain is calculated by using Eq. (2-5) and Eq. (4-2) without integration since the values for all terms in the equations are known from the crystal plastic simulation except N for a potential PSB or GB.

4.3 Integrated Transgranular and Intergranular Crack Growth Method (ITICGM)

4.3.1 Mesoscale model implementation with CPFEM

A demo-style description is presented here to illustrate the CPFEM implementation, while the procedure itself is general. To consider the grain effect on mesoscale cracking, the microstructures of steel can be artificially generated, such as the Poisson-Voronoi tessellation method, which has been extensively used for modeling polycrystalline material. In the present study, the grains, modeled using T3 plane strain element in ABAQUS, as well as the distributed PSBs are randomly generated using the open-source software Neper (Quey et al. 2011) and some Python codes. Material properties for each grain are assigned using the data for HSLA 50 in the literature (Xie et al. 2004). In the present study, the material model is based upon the crystal plasticity model defined by Huang (Huang 1991). Different from Huang's model, the hardening moduli were updated to three stages of hardening of crystalline materials (Wu et al. 1991) and back stress effect was considered. Each grain is treated as a single crystal with cubic elastic to plastic behavior and pre-defined material orientation. In the present 2D polycrystalline model, the slip surface degrades to the slip line in the planar mode to accommodate plane stress/strain state. To accommodate the random characteristics of the generated microstructure and the stochastic effect of each grain on the overall behavior of the system, the material property is randomly assigned by combining the slip coordinate system and the geometry coordinate system. Specifically, each grain is assumed to have a randomly assigned prime slip orientation, defined by an angle θ subtended from the x geometrical axis, where $0^{\circ} \leq \theta < 360^{\circ}$ (non-directional solidification is assumed). Uniform orientation distribution is considered here without

accounting the effect from the texture. In the present study, only <111>[110] slip systems are activated because it is the most likely slip at around room temperature.

4.3.2 ITICGM under constant amplitude load

The ITICGM consists of the crack initiation phase by crystal plasticity and corresponding FIP, transgranular crack part by PSB model, intergranular crack part by inherent CZM and the manipulation scheme at the grain boundaries. In the initial modeling stage, the grain boundaries are inserted using built-in cohesive elements defined by unloading coupled traction-separation law in ABAQUS (DS SIMULIA 2011). Each grain is divided into several PSBs with inactivated cohesive elements between each other (refer to Fig. 4-2). During the loading process, cracks initiate at the PSB with the largest FIPs and the nucleation life is obtained using Eq. (2-3). One side of the cohesive elements bounding the cracked PSB is activated with reduced strength. The path of the crack extension (transgranular or intergranular) is determined by the minimum number needed to crack the neighbor grain or grain boundary calculated by corresponding FIP-based crack growth rate equations, i.e., Eqs. (2-5, 4-2) (refer to Fig. 4-3, three arrows at the crack tips denote possible paths). If the crack goes in a transgranular mode, a new cohesive element line for cracked PSB will be activated. Otherwise, the part of the intergranular cohesive elements with minimum cycle number to fracture is set to have reduced strength. The general procedure could be summarized as a flowchart shown in Fig. 4-4.

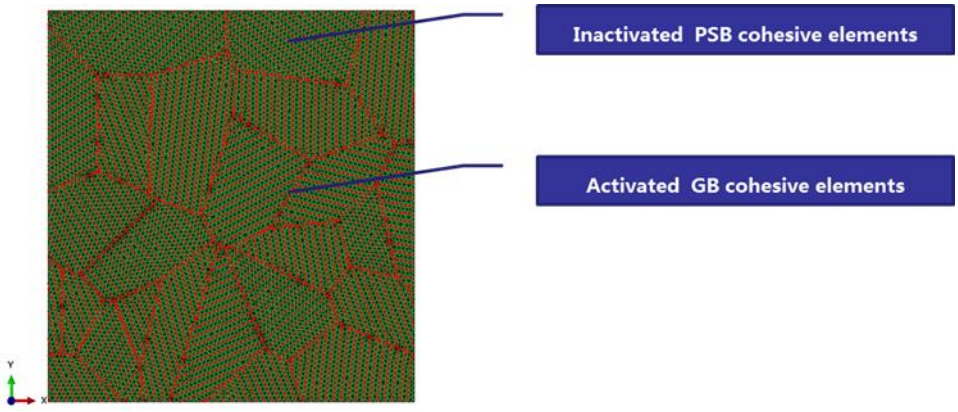

Figure 4-2. PSB/GB cohesive element insertion

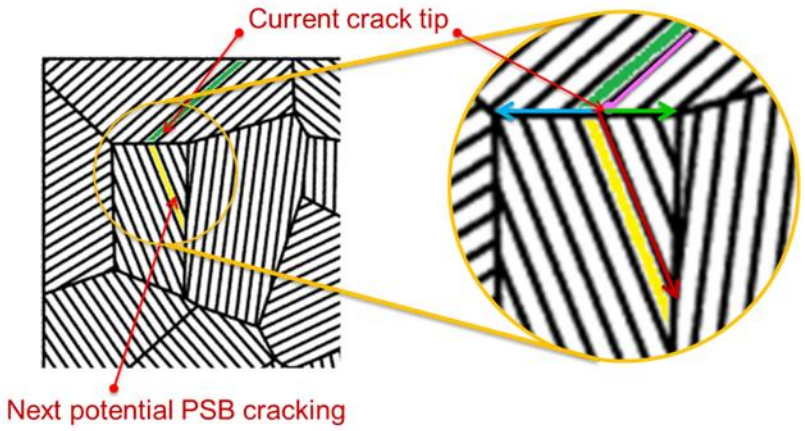

Figure 4-3. Crack path extension scheme

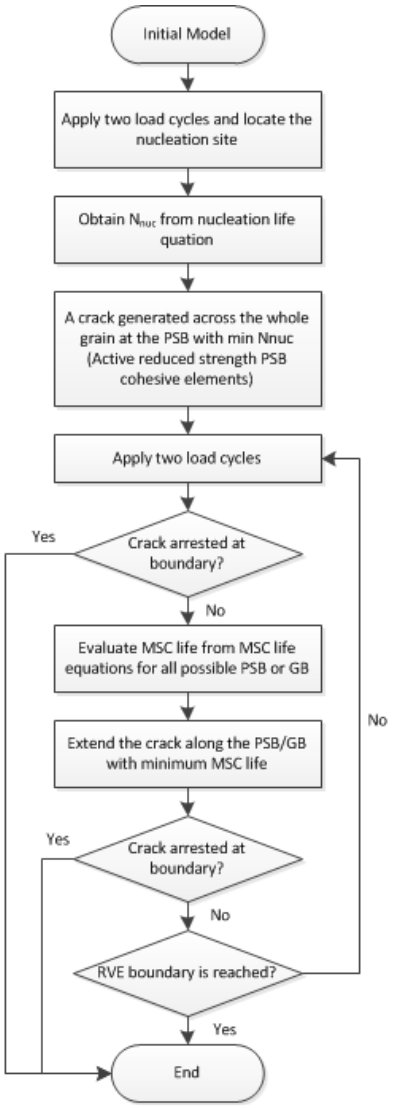

Figure 4-4. Flowchart of ITICGM

4.4 Implementation and Demonstration of Corrosion-informed ITICGM

4.4.1 Corrosion-informed ITICGM and Implementation

With the exposure to corrosive liquid or gas, short fatigue crack nucleation and propagation modeling could become more complex since corrosion mechanism needs to be incorporated. Since the hydrogen embrittlement is recognized as the primary corrosion mechanism for high strength steel, the hydrogen-diffusion informed CZM is used together with the ITICGM to form the Corrosion-informed ITICGM.

Hydrogen generates due to chemical reaction on the surface of the metal in the hydrogen compound, sea, and water. The hydrogen penetrates into the surface and diffuses mainly at the grain boundary (Shintaku et al. 2015). Hence pure grain boundary diffusion is assumed here for simplification. Since the hydrogen diffusion reaches a steady state in a short time and is assumed to keep stable during the short crack regime, Corrosion-informed ITICGM is carried out by two steps in sequence:

1) Steady-state diffusion analysis of GB hydrogen concentration and generate corresponding degraded CZM;
2) Include the updated CZM in original ITICGM approach.

In the mass diffusion module in ABAQUS, the hydrogen concentration c is obtained by Fick's law. The default traction-separation type cohesive element is built in with the bilinear traction-separation law in ABAQUS (DS SIMULIA 2011). Thus the fracture energy G_c is the only independent parameter which equals to the cohesive energy and depends on hydrogen diffusion by Eq. (4-3) (Rimoli and Ortiz 2010; Shintaku et al. 2015),

$$G_c = \left(1 - 1.0467\theta + 0.1687\theta^2\right) G_{c0} \tag{4-3}$$

where $\theta = c/c_s$ is the grain-boundary hydrogen coverage or impurity, c_s is the saturation value of c, G_{c0} is the GB surface energy at $c = 0$. This formulation is based on the first principle calculation by atomic mechanics. Assuming that the surface is saturated, the boundary condition $\theta = 1$ is given on the top face of the SVE. It is worthy to notice here, the parameter α_g, ϕ, and ϕ_{int} in Eqs. (2-3, 2-5, 4-2) can be calibrated by corrosion fatigue experiment data for further acceleration/barrier effect, which will be left for future research.

Being consistent with example information in Section 3, a demonstration of the Corrosion-informed ITICGM has been performed. Some results and discussion are presented in following subsections.

4.4.2 Grain boundary hydrogen diffusion analysis in polycrystalline SVE

This analysis is performed in Fick's law based mass diffusion module of ABAQUS. The diffusion coefficient at the GB is taken as $D_{gb} = 2.53 \times 10^3$ μm^2/s and it inside the grain is assumed to be $D_{in} = D_{gb} \times 10^4$. Since the mass diffusion module in ABAQUS 6.11 does not support the cohesive element, to keep the consistency of node/element number, the PSB element sets adjacent to the GB are used for hydrogen diffusion path, on the same SVE but with all cohesive elements deleted. The result of one simulation of hydrogen diffusion is shown in Fig. 4-5. It can be observed that the hydrogen concentration is decreasing from the top surface (the source), most gathered along the GB as anticipation.

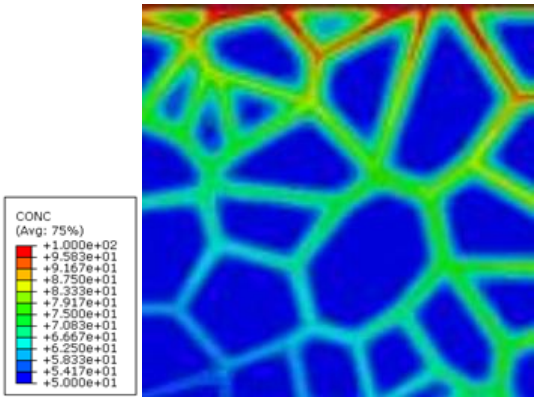

Figure 4-5. GB hydrogen diffusion analysis result

4.4.3 Crack growth, strain, and stress for different crack modes in SVE

In the present study, the random effects from the size, shape, and orientation of the grains are considered in fatigue analysis. Also, the SVE is assumed to be located at the macro hotspot and crack nucleates inside the surface grain (prescribed for one-way crack). All realizations are carried out with the following boundary and loading conditions:

B.C.s: free top surface, bottom surface with vertical support, and periodic boundary for other sides.

Loads: 0.5% peak strain along X axis, triangle loading at 0.5%/sec, $R = 0$.

For comparison, the pure transgranular growth and mixed growth with and without corrosion are simulated for the same SVE with Transgranular Crack Growth Method, ITICGM and Corrosion-informed

ITICGM, respectively. In ITICGM, the critical separation at maximum traction is taken as δ_c = 2 μm and the separation at failure is taken as δ_f = 20 μm, which are reasonable values based on estimations of the yield stress and fracture energy of HSLA 50. G_{c0} is taken as 502 kJ/m in the present study. In Corrosion-informed ITICGM, the hydrogen concentration result from Section 4.2 will degrade the CZM by Eq. (4-3). The whole process of one simulation for pure transgranular growth and mixed growth with and without corrosion is plotted in Fig. 4-6. Crystal strain localization, crack nucleation, stress redistribution, and crack propagation and arrest can be observed. The figure shows that the crack can propagate intergranularly when transgranular propagation gets arrested; mixed behavior is found to induce larger strain and promote the crack nucleation and propagation; the intergranular segments dominate the crack growth when GB is hydrogen degraded.

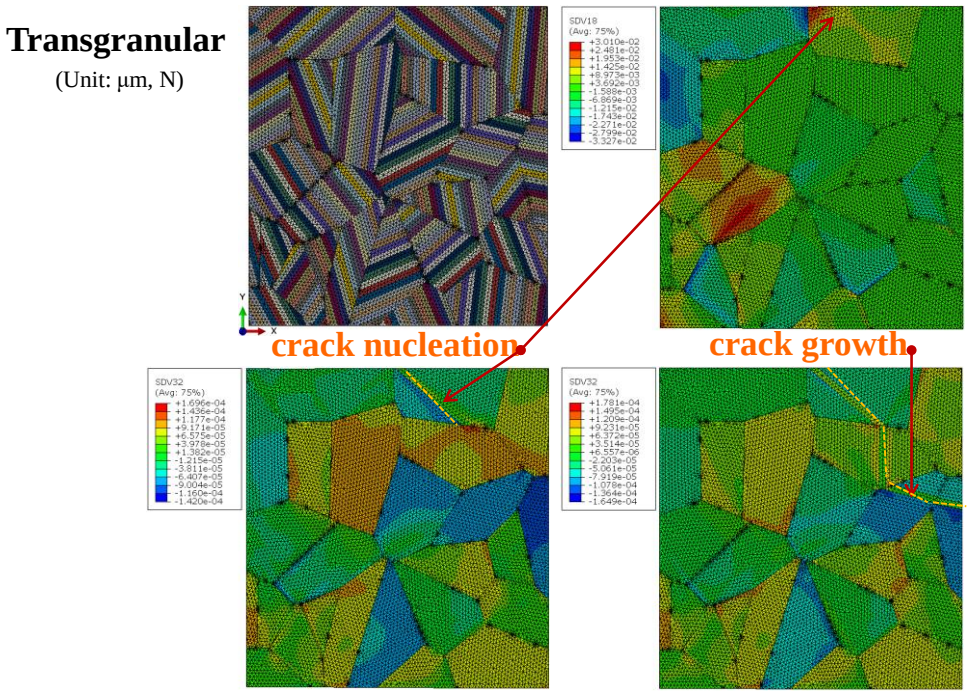

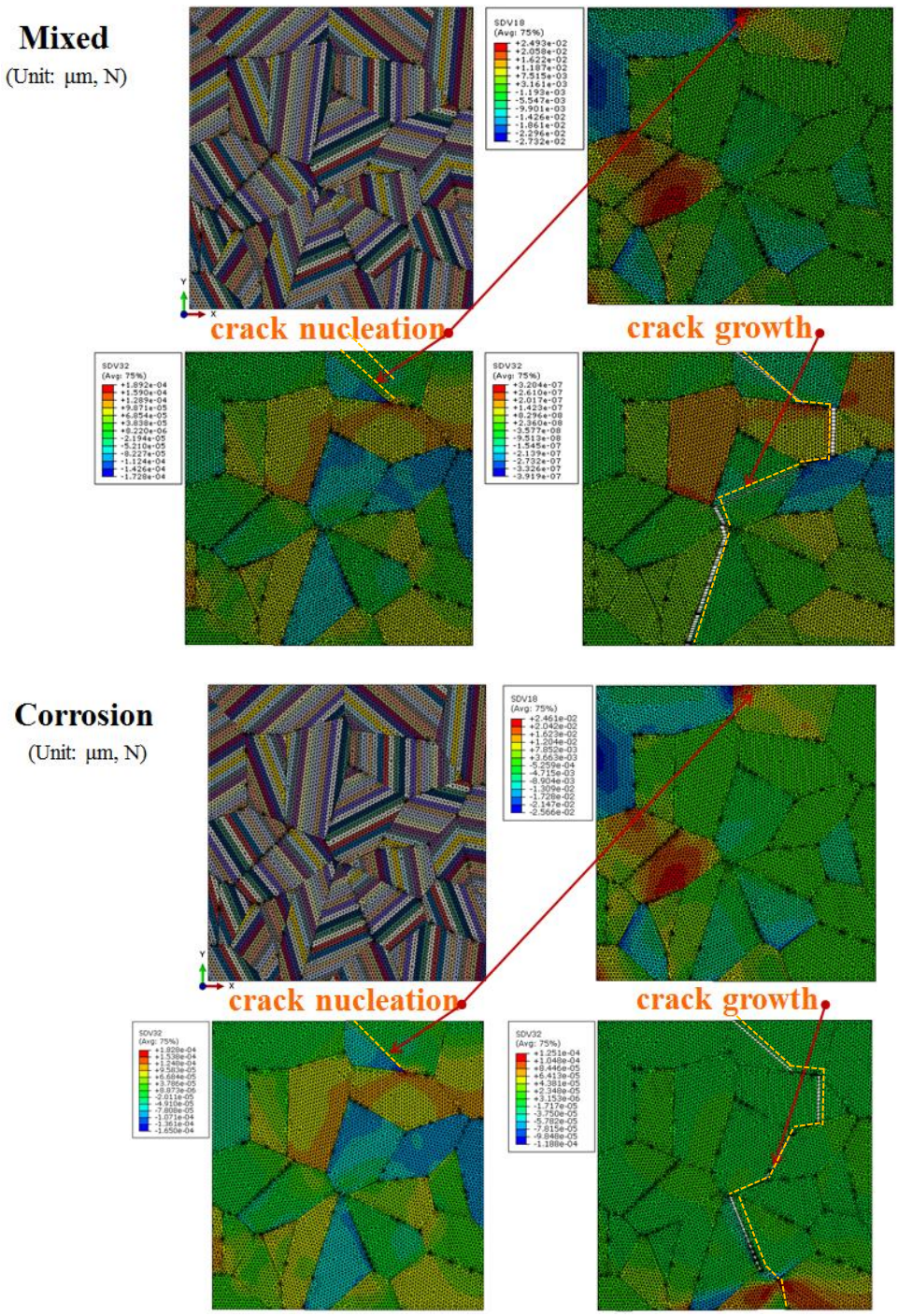

Figure 4-6. Crack growth, strain and stress for one SVE simulation (three crack modes)

(upper left – PSB distribution, upper right – plastic shear strain (SDV18) after 2 load cycles, lower left – resolved shear stress (SDV32) at 2 cycles after nucleation, lower right – MSC path at the end)

4.4.4 Comparison between pure transgranular growth and mixed crack growth with and without corrosion

For the same microstructure, the comparison between pure transgranular growth (yellow), mixed growth (red), and mixed growth under corrosion (blue) is shown in Fig. 4-7. The comparison indicates that the crack can propagate intergranularly when transgranular propagation gets arrested and the transition between two modes is mutual. It is also found that the paths after nucleation could be entirely different. In addition, the mixed growth under corrosion contains more intergranular segments in the entire crack path.

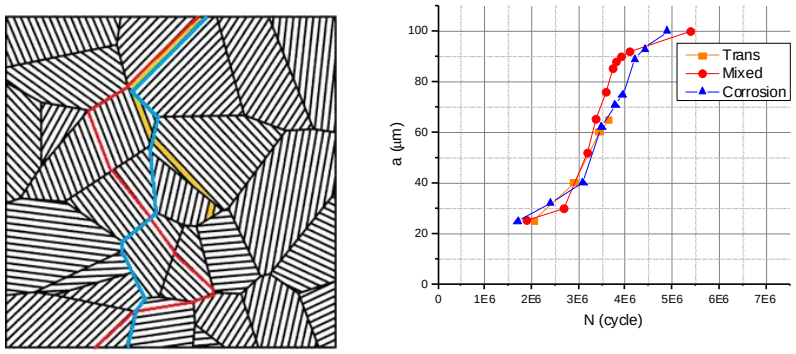

Figure 4-7. Comparison of crack paths and a-N curves (three crack modes)

The *y*-axis projected crack length *a* vs. *N* diagrams from 10 simulations by each method are plotted in Fig. 4-8. Some related statistics are also summarized in Table 4-1. From the figure and table, it can be observed that the scattering phenomenon is different in three methods and the mixed behavior is found to promote the crack nucleation and propagation since high proportion of totally cracked SVE. Mixed growth under corrosion is even more prone to fatigue and contains more intergranular segments in crack paths. Thus, the corrosion accelerates the failure of the SVE in a general trend.

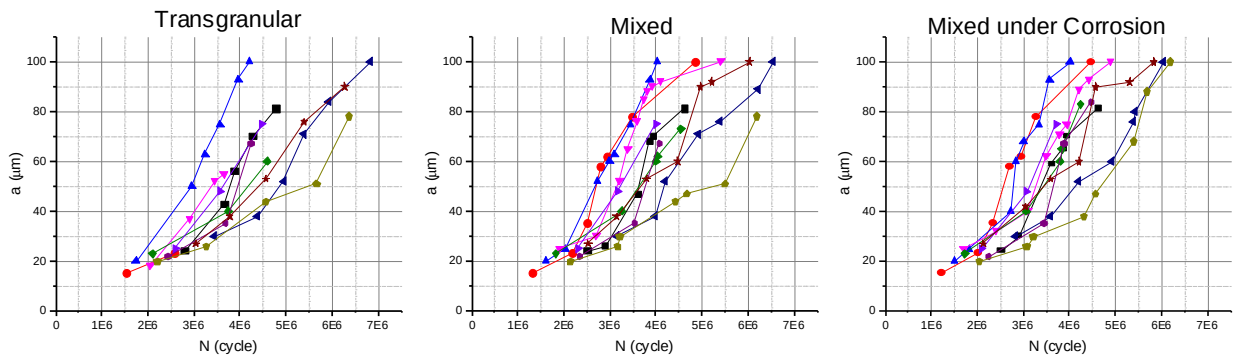

Figure 4-8. Comparison of a-N curves from 10 simulations by three methods

Table 4-1 Some statistics for MSC nucleation and growth by three methods

	Transgranular	Mixed	Mixed under Corrosion
Min N_{nuc}	1,529,173	1,299,797	1,123,519
Max N_{nuc}	3,432,874	3,123,915	3,001,468
Avg. N for 100 μm crack	5,511,907	4,877,593	4,265,743
Avg. number of grain (GB) segments cracked before arrested	4 (0)	3 (2)	2 (5)

4.5 Conclusions

In the present paper, a 2D short crack growth framework built on the microstructure-sensitive model and crystal plasticity based FIP is proposed to simulate the mixed trans-intergranular growth behavior in polycrystalline metal. To be employed in corrosion fatigue problems, the corrosion effect is modeled as the degradation of grain boundary informed by hydrogen diffusion analysis. For demonstration, firstly, a GB diffusion analysis was conducted and hydrogen concentration distribution was obtained. Then a comparison between transgranular-only crack growth and mixed transgranular and intergranular growth (with and without corrosion) was performed on polycrystalline SVE. The crack is found to be able to propagate

intergranularly when transgranular propagation get arrested. Mixed behavior is found to promote the crack nucleation and propagation. Meanwhile, the scattering behavior of the fatigue life can also be achieved, and the hydrogen corrosion on GB induce more intergranular growth. A limitation exists here as the absence of mutual coupling effect between the hydrogen diffusion and stress since they are reciprocal boundary conditions. In addition, the whole framework can serve as a part of multi-scale fatigue prognosis system. However, the calibration and full validation of the model needs extensive statistical technique and physical test data throughout the local microstructure.

CHAPTER 5 QUANTIFICATION OF TIME DISTRIBUTION TO INITIAL LONG CRACK WITH REDUCED ORDER MICROSTRUCTURAL REPRESENTATION ON MICROSTRUCTURALLY SHORT FATIGUE CRACK GROWTH MODEL

5.1 Introduction

Fatigue is one of the primary damage and failure mechanisms of structures or the structural components subjected to cyclic loadings. The current practice in fatigue crack growth assessment for metallic components usually starts with a sufficiently long initial crack, which is a strong and sometimes arbitrary assumption. Beneath that is the bypass of the short crack nucleation and propagation, which is, in fact, worth more attention since short crack regime accounts for about 90% of the structural fatigue life (Krupp 2007). Moreover, some short cracks might not be detectable by current state-of-the-art nondestructive examination methods, which could lead to structural safety concerns since the accelerated crack growth at the long crack ranges could quickly end up with structural component failures. Therefore, it is of great importance to effectively assess fatigue damage in short crack regime. Meanwhile, the uncertainties in this regime also need to be quantified to form a time distribution to initial long crack (TDILC) and provide more confidence fatigue life prediction. The research on the direct quantification of TDILC is somehow very limited. However, several researchers naturally assume a distribution and project to the equivalent initial flaw size (Liu and Mahadevan 2009). Physical-based model of the short fatigue crack regime should be a useful tool to solve this problem.

Several short crack nucleation and propagation methods were developed in a range from macroscale to microscale. To balance the complexity of microscale models (molecular dynamics) and discontinuity-loss in macroscale models (equivalent initial crack or continuum damage mechanics), mesoscale models based on crystal plasticity and continuous dislocation theory were developed. On this scale, the microstructure of polycrystalline material plays a key role in the evolution of micromechanical stresses and strains and consequent development of damage with the evolution of microstructurally short

crack (MSC) with a length scale from 10μm to 1mm. Random grain shapes and sizes, combined with different crystallographic orientations, inclusions, voids, and other microstructural features result in locally anisotropic and highly heterogeneous behavior of the microstructure with direct influence on the damage initialization and evolution. Recently, the microstructure-sensitive model with FIPs has been a promising tool to describe both the MSC nucleation and growth with the non-local measure (Pineau et al. 2016). Due to the complexity of cyclic microplasticity and damage formation in HCF, the FIPs provide a computable parameter with which differing microstructures may be quantified in fatigue analysis. By the multiple realizations of this approach, the MSC growth and uncertainty from microstructural variability can be better quantified for a certain material under different loading scenario.

However, the CPFEM simulation is still time-consuming and the mass Monte Carlo simulations (MCS) are needed to quantify the MSC growth and TDILC. Some computational cost reduction techniques such as reduced order model (ROM) must be employed to achieve an acceptable accuracy with affordable time. There are two categories of the ROM can be induced, i.e. (i) intrusive ROM by reducing the degree of freedom in the CPFEM or by an alternative solver: e.g., asymptotic expansion method (Ghosh et al. 2016), discrete Fourier transform database (Alharbi and Kalidindi 2015), eigenstrain based methods (Zhang and Oskay 2015), and self-consistent cluster based methods (Liu et al. 2016); (ii) nonintrusive ROM by reducing the sampling space in MCS and constructing response surface: e.g., stochastic ROM surrogate methods (Grigoriu 2014) and stochastic collocation methods (Kouchmeshky and Zabaras 2010). However, most intrusive ROMs are targeting on homogenization and sacrificing lots of local information, while the pixel (voxel in 3D) based numerical solver like EVP-FFT under ideal periodic boundary conditions is more prevailing. Even though some methods like self-consistent cluster-based method can retain certain level information of local micromechanical field, the model reduction efficiency is much lower when incorporating crystal plasticity. To be mentioned here, Priddy et al. (Priddy et al. 2017) propose a to perform a rapid assessment of FIP field in statistical volume element (SVE) by combining Materials Knowledge System (MKS) and decoupled integration for the plastic strain. Nonintrusive ROM approach like adaptive sparse grid collocation (Wen and Zabaras 2012) has also been used for investigating the variability of

fatigue indicator parameters. However, fatigue crack growth is more complex since the microstructure configuration will change due to the crack extension, crack tip drastically influences the micromechanical field ahead under grain clustering effect, and the boundary condition is not fully periodic for surface crack. Rovinelli et al. (Rovinelli et al. 2015) studied the influence of microstructure variability on short crack behavior through calculating FIP field when different static elliptical crack inserted but further crystallographic growth is not discussed. Therefore, for MSC problem, a ROM which can provide a faster estimation of the micromechanical field in the changing microstructure under non-fully periodic boundary conditions is needed.

In this paper, a new framework is proposed to quantify the time distribution to initial long crack (TDILC) without the use of intensive CPFEM. The core is to get a fast estimation of the grain-discrete FIP field by pattern recognition and classification technique, Sobol' decomposition for the current study, a method that can be attributed to the nonintrusive ROM class. The paper is organized into four parts. Section 2 is a problem overview about the quantification of TDILC of the interested 2D microstructure. Due to the complexity and larger dimension of randomness inherent in the microstructure (grain size, shape, and orientation) especially the shape quantification which remains unsolved, for the current study, only grain orientation is considered as a random variable. Therefore, the microstructure is simplified to the aggregates of regular hexagonal grain. Section 3 briefly introduces CPFEM based the MSC growth model and implementations developed by the authors in previous research (Yuan et al. 2017a, 2018a). Section 4 details the full process of Sobol' decomposition based ROM (SDROM) implementation for test problem, including training sample generation, pattern identification, grain-based FIP estimation, and finally the moving window method is applied to surface grains of SVE samples to nucleate a crack at the grain with largest estimated FIP and the window move along the possible cracked grain ahead of the crack tip until the grain is fully cracked. Section 5 discusses the effectiveness of the SDROM by a comparative study with brute force MCS. Section 6 makes a summary.

5.2 Problem Overview and A Simpler Test Problem

5.2.1 Problem overview

Consider a 2D polycrystal SVE as shown in Fig. 5-1. Through the CPFEM and MSC growth model (see Section III for details), the outputs are a micromechanical field, crack path, and crack growth diagram (crack length vs. cycle number curve) which can be observed in Fig. 5-1. For one simulation on a sample SVE, these outputs are deterministic, and one point can be obtained in the TDILC under this load. Straightforward, to quantify the TDILC, the deterministic MCSs can be performed with random generated SVEs. This conventional approach has high fidelity and can account for all the uncertainties from grain size, shape, and orientation. However, due to the high-dimensional uncertainty, the approach may be intractable if more load conditions are considered. Assume the grain number is fixed at n, the number of random variables to uniquely determine the 2D SVE status will be $3n$, for grain centroid coordinates (x, y) and grain orientation θ. Moreover, both scalar (i.e., orientation for our problem) and geometric pattern (i.e., grain size and shape) exist as uncertainty forms and are confounded. The variability of the microstructure topology and orientation somehow present favorable pattern for strain/stress/FIP concentration such as GB with large misorientation, SVE boundary-GB joint point, triple joint, and even triple joint clusters. A perfect approach should perform well to examine the SVE and identify most possible crack path and associate FIP field by critical geometry pattern and orientation pattern classification, rather than running fine CPFEM every time. For a demonstration of feasibility, a simpler problem is formed in next subsection to explore and test such a procedure.

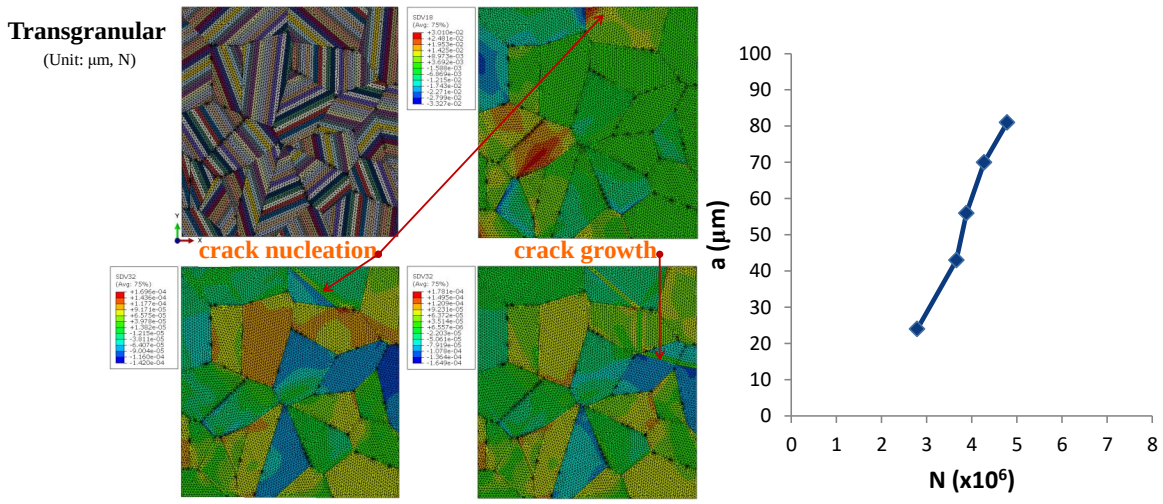

Figure 5-1. Crack growth, strain and stress for one simulation

(upper left – PSB distribution, upper right – plastic shear strain (SDV18) after 2 load cycles, lower left – resolved shear stress (SDV32) at 2 cycles after nucleation, lower right – MSC path at the end)

5.2.2 A simpler test problem

Due to the difficulty to represent the variability of the topology of microstructure, for current pilot research, a simpler problem is considered for using to explore and test following proposed ROM procedure. Therefore, we consider a 2D polycrystal as a tight stack of regular hexagons of uniform size. For example, a 100 μm × 100 μm SVE is shown in Fig. 2., which has almost 25 grains with a uniform size of 20μm and uniformly distributed grain orientations of [0, 180°). The boundary conditions are: left edge free and right edge with *X*-axial support. The cyclic load is *Y*-axial constant amplitude load, for demonstration, 0.5% peak strain, triangle loading at 0.5%/sec, $R = 0$.

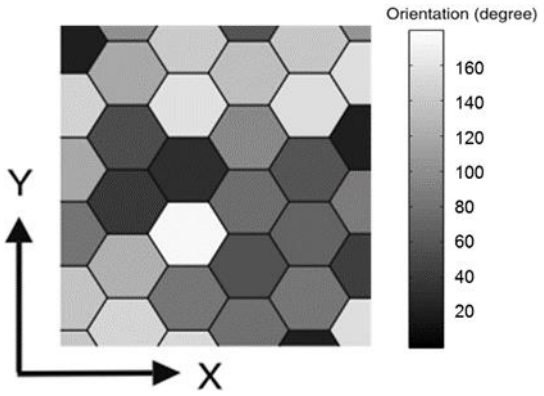

Figure 5-2. 2D SVE for simpler microstructure

After simplification, the random variables reduce to only 25 orientations for the present problem. Moreover, since the grain size becomes a fixed value, the cycle number to crack one grain only depends on the grain-averaged FIP according to Eqs. (2-3, 2-5). Therefore, the final goal of the reduced order modeling is to provide a rapid but satisfactory estimation of the micromechanical field especially ahead of the crack tip.

5.3 Deterministic Solver – Microstructurally Short Fatigue Crack Model

The CPFEM-based MSC model is adopted. The detail of FIP for transgranular crack, short crack nucleation and growth equations, and model implementation has already been elaborated in Chapter 2. Due to the scarcity of material data, the numerical example in Chapter 2 is also adopted here for consistency.

5.4 Reduced Order Modeling by Sobol' Decomposition

5.4.1 General steps for SDROM

(1) Generate random, independent training samples with size to equal to the length scale at which the intergranular interactions die out. All possible pre-crack scenarios behind the grain of interest are exhausted.

(2) Use cubic linear elastic finite element analysis and back calculation of plastic strain to determine micromechanical field and further evaluate FIP. This step builds up the database of FIP field and corresponding orientation variables for each pre-crack scenario.

(3) Identify patterns in the arrangement of crystal grain orientations that result in maximum FIP in the grain of interest, by Sobol' decomposition.

(4) Construct the microstructural pattern space with these patterns as basis vectors and derive the response surface based on these vectors for predicting the FIP in the grain of interest.

(5) Implement a moving window technique to locate the surface crack nucleation and sequentially find FIP in the grain along the possible crack path.

5.4.2 Generation of training data

Specifically, for SVE with five layers of grains in Fig. 5-2, the general training sample template used here is shown in Fig. 3(a), which is trained under uniaxial constant amplitude load. The inclusion of the closest four grains is enough to account for the inter-grain influence (Tan and Arwade 2008). Take Grain #1 as the grain of interest, the specific training samples for crack nucleation from the surface and subsequent growth through four layers of grain is shown in Fig. 5-3(c-g), representing a training case for 0~4 layer pre-cracking scenarios, respectively. Assuming no crack growth between two adjacent grains aligning in the *y*-direction, the possible pre-crack paths can be exhausted easily for each pre-cracked layer case. The red triangle surrounds the possible pre-cracked grains, and yellow lines represent one possible through-centroid crack configuration. Such training is based on finite element analysis of the SVEs, one case of which is shown in Fig. 5-3(b) for 4-layer pre-crack case which consists of about 100 grains. Due to the conflict between the hexagonal grain shape and the straight boundary of SVE, the interface grains between the air and material (most left column of grains in our cases) are assigned with very low stiffness material parameters to accommodate this situation or just deleted leaving behind the sawtooth boundary. The flowchart of the analysis is shown in Fig. 5-4 (refer to Chapter 2 for the detail of each term). This type analysis is only

suitable for HCF problem since the elastic strain is about two orders of magnitude higher than the plastic strain. Also, cyclic stress redistribution and relaxation are neglected in this work, as well as local lattice rotation, since the impact is minimal. Therefore, the plastic strain can be back-calculated from elastic stress field from the cubic linear elastic analysis. A comparison of plastic strain field on an unsimplified SVE by the intact CPFEM and the proposed decoupled approach is shown in Fig. 5-5. It can be observed that the two contours are quite similar (the average error is than 5%), even though some discrepancies exist at some local areas. Moreover, corresponding FIP can be obtained by Eq. (2-1). This analysis procedure is much faster than the CPFEM, with finishing in seconds rather than hourly level. Since the very local field like grain boundary is not our concern, the method is sound to get an acceptable grain-averaged FIP value.

The training samples provide samples of the microstructural response functions for Grain #1, i.e., s_i = FIP$_i$ (θ_1, θ_2,⋯, θ_{N_i}), which gives the FIP as the function of orientation angles θ in all the grains of the training samples with different pre-cracking scenarios. N_i is the total number of grains in pre-cracking scenario i, where i also mean the number of grains (layers) the pre-crack has went through. Shown in Fig. 5-3(c), for nucleation phase, N_0 = 35; for the crack grows though 1~4 layers before Grain #1, N_1 = 43, N_2 = 50, N_3 = 56, and N_4 = 61. The pre-crack path before Grain #1 is exhausted and listed in Table 5-1.

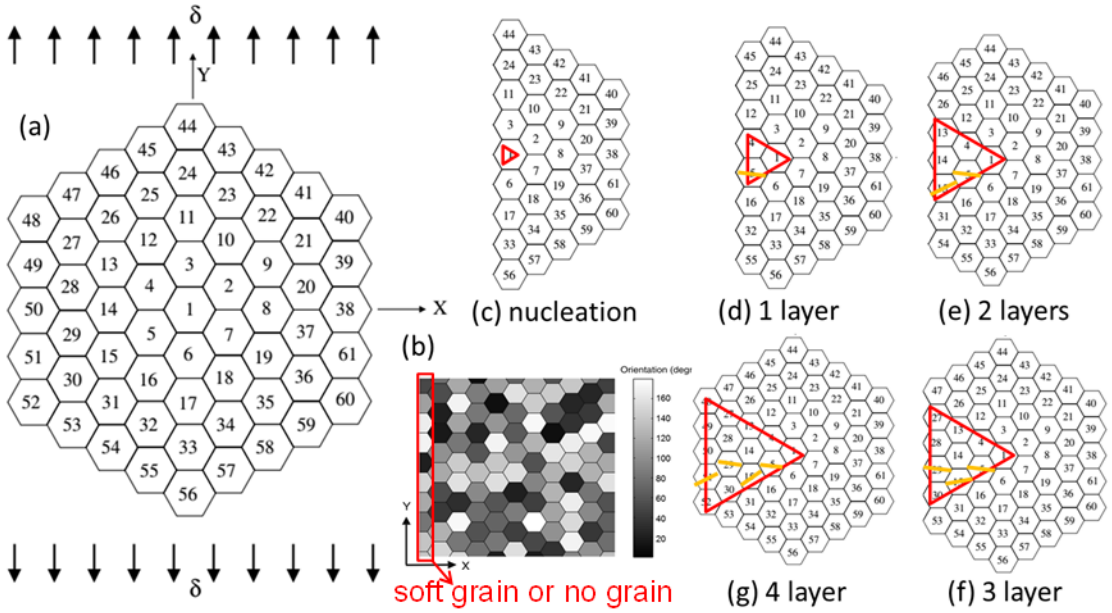

Figure 5-3. Schematic diagram of samples for data training

Table 5-1 List of exhausted pre-crack paths before Grain #1 (symmetry considered)

Case *i*	Pre-cracked layer	Number of grains in a training sample	Possible pre-crack paths	Total number of training cases
1	0	35	—	1
2	1	43	4	1
3	2	50	13-4, 14-4	2
4	3	56	27-13-4, 28-13-4, 28-14-4, 28-14-5	4
5	4	61	48-27-13-4, 49-27-13-4, 49-28-13-4, 49-28-14-4, 49-28-14-5, 50-28-13-4, 50-28-14-4, 50-28-14-5	8
	Total	—	—	16

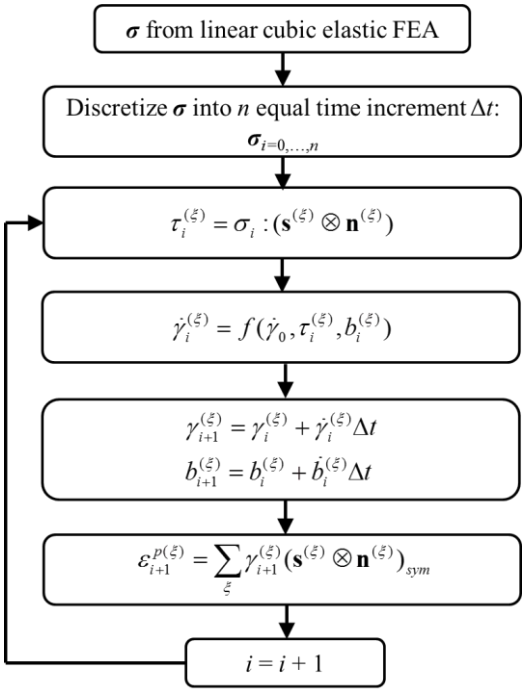

Figure 5-4. Decoupled analysis flowchart to accelerate generation training datasets

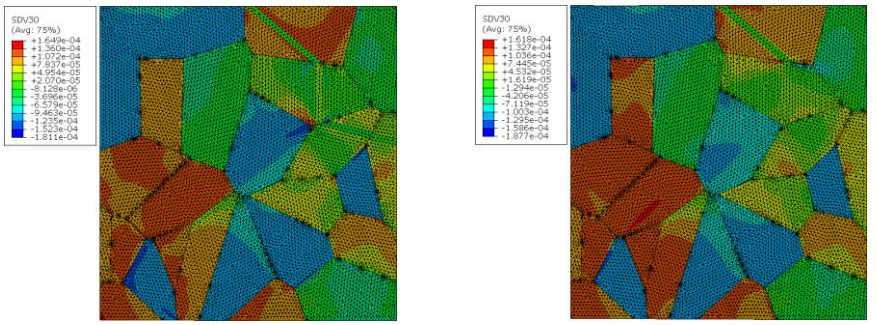

Figure 5-5. Comparison of plastic strain fields

5.4.3 Microstructural pattern extraction by Sobol' Decomposition

After obtaining the training datasets, the microstructural patterns that raise the FIP field can be extracted by Sobol' decomposition/representation. The procedure of Sobol' decomposition is well developed in several papers including Tan and Arwade's framework for a microstructure problem (Tan and Arwade 2008). The conventional Sobol' decomposition is an expansion-type representation of the functions with n independent and uniform distributed input variables in a unit hypercube U^n. For our problem, the procedure is adapted to a hypercubic space of size [0, π). Taken Case 1 (nucleation status with 35-grain SVE, by Fig. 5-3(c)) in Table 1 as a representative, the formulations of the procedure are presented.

The microstructure response function s (θ_1, θ_2,$\cdots$,θ_{35}) can be view as a function linking the FIP response in Grain #1 and 35 independent, uniformly distributed grain orientations. The expansion is as Eq. (5-1) with expressions of mean and first-order terms, which turn out to be sufficient approximation.

$$
\begin{aligned}
s &= s(\theta_1,\theta_2,\cdots,\theta_{35}) = s_0 + \sum_{m=1}^{35}\sum_{1\le i_1<\cdots\le i_m\le 35} s_{i_1\cdots i_m}(\theta_{i_1},\cdots,\theta_{i_m}) \\
s_0 &= \int_{(\pi U)^{35}} s(\theta_1,\cdots,\theta_{35})\pi^{35}\prod_{j=1}^{35} d\theta_j = E_{\theta_1\theta_2\cdots\theta_{35}}\left[s(\theta_1,\cdots,\theta_{35})\right] \\
s_i(\theta_i) &= \int_{(\pi U)^{35-1}} s(\theta)\pi^{34}\prod_{p=j}^{35} d\theta_p - s_0 = E_{\theta_1\theta_2\cdots\theta_{i-1}\theta_{i+1}\cdots\theta_{35}}\left[s(\theta_1,\cdots,\theta_{35})\right] - s_0
\end{aligned}
\tag{5-1}
$$

The variance D, and partial variances and Sobol' indices are formulated as follows, i.e.

$$
\begin{aligned}
D &= E_{\theta_1 \cdots \theta_p \cdots \theta_{35}}\left[s^2\right] - s_0^2 \\
D_{i_1 \cdots i_m} &= E_{i_1 \cdots i_m}\left[s^2_{\theta_1 \cdots \theta_m}\right] \\
S_{i_1 \cdots i_m} &= D_{i_1 \cdots i_m} / D
\end{aligned}
\tag{5-2}
$$

where the Sobol' indices measure the contribution to the total variance from the individual input variables and all possible combinations of them.

The discrete form of above equations for *N*-sample implementation is as follows, i.e.

$$
\begin{aligned}
s_0 &= \frac{1}{N}\sum_{j=1}^{N} s^{(j)}\left(\theta_1^{(j)}, \cdots, \theta_{35}^{(j)}\right) \\
s_i(\hat{\theta}_k) &= \frac{1}{\sum_{j=1}^{N} I_{[\hat{\theta}_k - \Delta\theta \leqslant \theta_i^{(j)} < \hat{\theta}_k + \Delta\theta]}} \sum_{j=1}^{N} I_{[\hat{\theta}_k - \Delta\theta \leqslant \theta_i^{(j)} < \hat{\theta}_k + \Delta\theta]} \\
& \qquad s^{(j)}(\theta_1^{(j)}, \theta_2^{(j)}, \ldots, \theta_n^{(j)}) - s_0 \\
D &= \frac{1}{N}\sum_{j=1}^{N} s(\theta_1^{(j)}, \theta_2^{(j)}, \ldots, \theta_n^{(j)})^2 - s_0^2, \\
D_i &= \frac{1}{N_k}\sum_{k=1}^{N_k} s_i(\hat{\theta}_k)^2.
\end{aligned}
\tag{5-3}
$$

where $N_k = 180, \Delta\theta = \pi/180, \hat{\theta}_k = k\pi/90 + \pi/180, k = 0,1,\cdots,180.$

The response maximizing orientation is obtained as

$$
\theta_{i,\max} = \arg\max_{\theta_i \in [0,\pi)}\left[s_i\left(\theta_i\right)\right] \tag{5-4}
$$

Based on the calculated Sobol' index and response maximizing orientation, the geometric pattern with five influence levels and most critical orientations is extracted as $\{\phi_1, \phi_2, \cdots, \phi_5\}$ and shown in Fig. 5-6. To be noted, the extraction is based on datasets of Case 1 and can only serve for FIP estimation at nucleation stage. Corresponding extractions of similar format are obtained for other stages as well. In total, 16 pattern sets have been extracted for all pre-cracking scenarios listed in Table 5-1. Since all these data are only for our demonstration problem and not rigorously verified, they are not listed here. In fact, the idea behind such geometric pattern extraction for the microstructurally short crack problem is more novel and valuable.

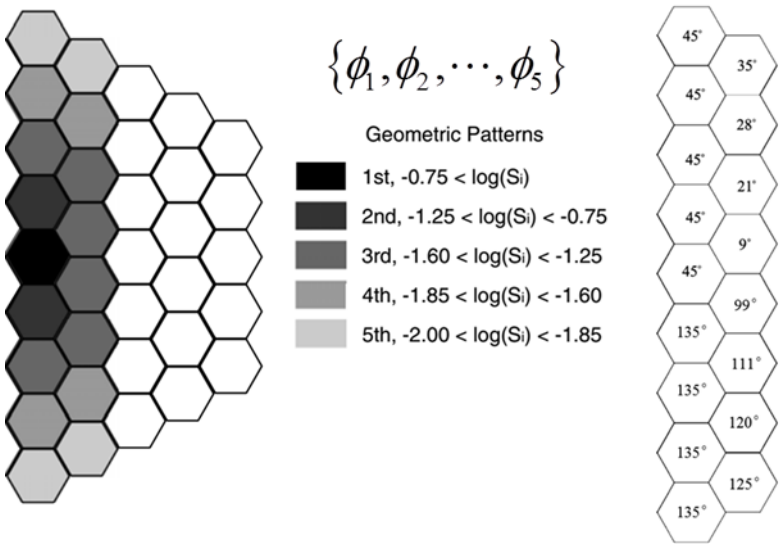

Figure 5-6. Critical pattern of geometry and orientation for Case 1

5.4.4 Reduced order microstructural representation

Still using Case 1 for demonstration, the reduced order microstructural representation is constructed by a projection function from the orientation space $\{\theta_1, \theta_2,\cdots,\theta_{35}\}$ to the geometric pattern space with pattern basis vector $\{\phi_1, \phi_2,\cdots, \phi_5\}$. The projection function Γ and reduced order coordinates $(\psi_1, \psi_2,\cdots, \psi_5)$ are as Eq. (5-5),

$$\begin{aligned} &\left[\psi_1,\psi_2,\cdots,\psi_5\right]=\Gamma\left(\theta_1,\theta_2,\cdots,\theta_{35}\right) \\ &\psi_j=\mathrm{Re}\left\{\sum_{k\in I_j} e^{-2\mathrm{i}\theta_{k,\max}}\cdot e^{2\mathrm{i}\theta_k}\right\},\mathrm{i}=\sqrt{-1} \end{aligned} \tag{5-5}$$

where ψ_j is a scalar quantification of how close the actual orientations to the response maximizing orientations.

Thus, the microstructure response s can be obtained through Sobol' indices weighted linear regression. The equations are

$$\begin{aligned} &s\left(\theta_1,\theta_2,\cdots,\theta_{35}\right)\approx s_{lr}\left(\psi_1,\psi_2,\cdots,\psi_5\right)=\omega_0+\sum_{j=1}^{5}\omega_j w_j\psi_j \\ &w_j=\frac{1}{\sum_{i=1}^{35} I_{\left[i\in I_j\right]}}\sum_{i=1}^{35} I_{\left[i\in I_j\right]}\sqrt{S_i} \end{aligned} \tag{5-6}$$

Similarly, the reduced order microstructural representations can be constructed for all 16 pre-crack scenarios. These derived coefficients are not listed here since the data is for this particular demonstration.

5.5 Results and Comparisons

5.5.1 TDILC by MCS with intact CPFEM

500 grain-scale simulations on random SVEs are performed and 119 simulations render fully cracked SVEs (See Fig. 5-7(a) for crack growth diagram). Regardless of 2D nature, the arrest here is still not real since previous research found that the crack will still advance after far more cycles are accumulated, i.e., reaching VHCF or UHCF, which is governed by other fatigue mechanisms (Jha et al. 2009). Our fatigue model can only capture the MSC-growth controlled condition. The histogram of life of the fully cracked SVEs is plotted in Fig. 5-7(b). According to the shape of the histogram, a lognormal fit by maximum likelihood estimation is performed resulting Lognormal (14.78, 0.09).

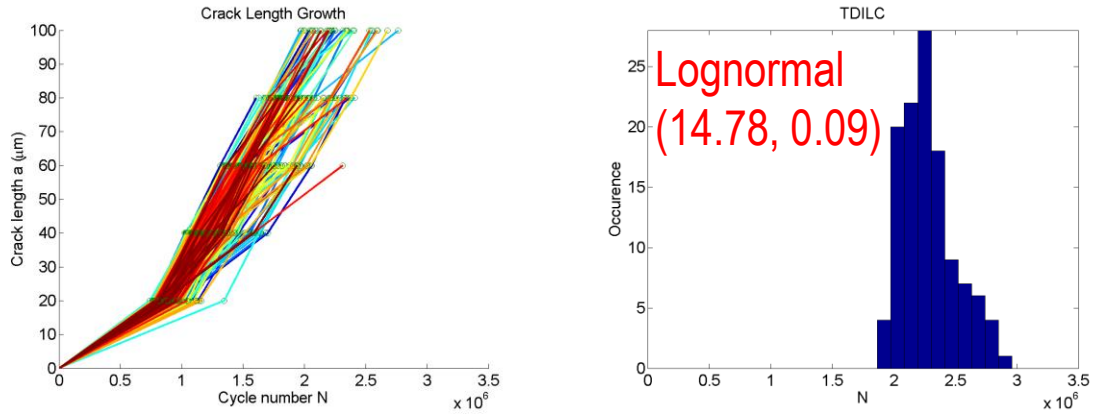

(a) (b)

Figure 5-7. TDILC by brute force MCS with CPFEM

5.5.2 TDILC by MCS with Moving Window and SDROM

The training samples are generated under the same boundary conditions and loads as above brute force method. For time efficiency, the SVEs used in this step are of different sizes for each pre-crack scenario. A schematic representation is shown in Fig. 5-8.

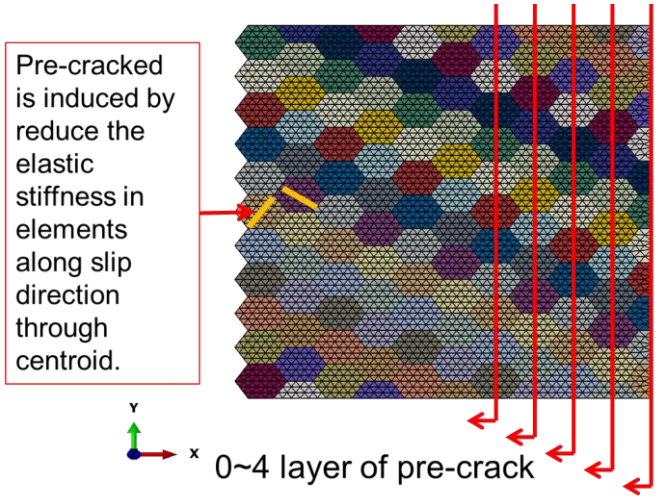

Figure 5-8. SVE used for training sample generation

For comparison with the results by brute force MCS, the counterpart of results from 5000 runs (1476 fully cracked) by SDROM-based moving window technique is plotted in Fig. 5-9 and Lognormal (14.63, 0.11) is fitted for life distribution of fully cracked SVES. In the current pilot study, the results from two methods are found to be quite close. However, the tail portion on two sides is hard to verify since no comparable data by the brute force method there. Moreover, the uncoupled method for the plastic strain to generate the training datasets might not be able to capture the mechanical fields that associated with the tail portion. Therefore, further work is needed for validation and error estimation for proposed methods. Another issue which needs to mention is that the microstructure feature causing pseudo-arrest should be avoided since a large portion of runs rendering only partially-cracked SVEs.

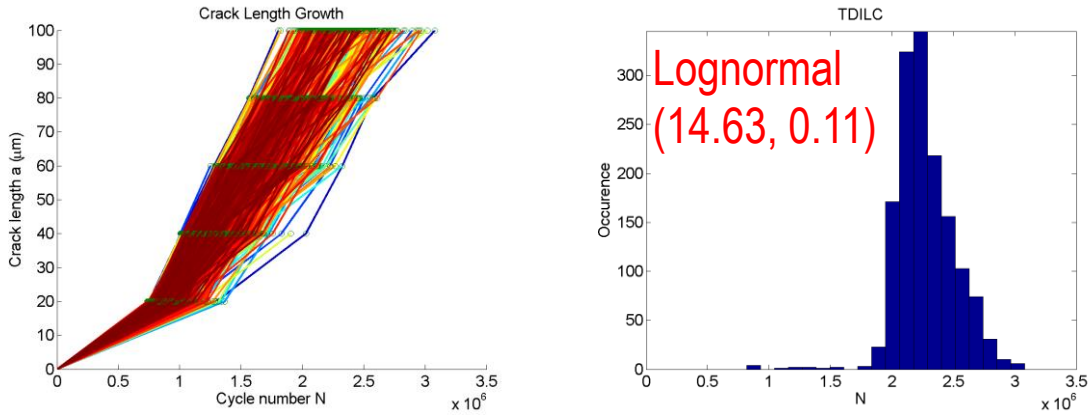

(a) (b)

Figure 5-9. TDILC obtained with SDROM

To highlight the superiority of the proposed framework, the computational expense comparison is summarized in Table 5-2.

Table 5-2 Computational expense comparison

Method	FE-calculations	ROM construction	Moving Window	Total
MCS with CPFEM	410.2 h (500 runs)	—	—	410.2 h
Moving window with ROM	67.4 h (16 x 500 runs for training with decoupled accelerating analysis)	3.3 h	0.9 h (5000 runs)	71.6 h

*Hardware: DELL Precision T7610 Intel ® Xeon ® CPU E5-2687W v2 Dual-core @ 3.4 GHz w/ 64GB RAM

5.6 Conclusions

In the present chapter, a framework to effectively quantify the time distribution to initial long crack is proposed by using a comprehensive procedure based on the reduced order microstructural representation and microstructurally short crack growth model. The 2D short crack growth framework built on the

microstructure-sensitive model and crystal plasticity based FIP is implemented to simulate transgranular growth behavior in polycrystalline metal. To capture the micromechanical field faster, the decoupled plastic strain analysis is proposed with an acceptable approximation. The characteristic geometric patterns with five influence level and most critical orientation arrangement are obtained through Sobol' decomposition/representation. A reduced order representation of the microstructure is developed in essence a projection of the microstructure description (orientation) onto the microstructure pattern. Derived basis vectors are used to construct response surface for predicting the FIP in the grain of interest. A moving window algorithm with SDROM scanning the generated SVE provides predictions of TDILC. The TDILC from Moving window-SDROM and brute force MCS is found to be similar. As future work, the framework can be calibrated and validated with TDILC back-calculated from published fatigue data by stochastic Paris' law with extension to consider the grain size and grain shape variability. To be noted, for our problem, the microstructure feature causing arrest need to be avoided, Sequential Monte Carlo can be a solution. The response surface approach and design of experiments can also be explored for optimal selection of training samples.

CHAPTER 6 FATIGUE CRACK GROWTH SIMULATION FOR PRESSURE VESSELS: FROM MICROSTRUCTURALLY SHORT CRACK TO FINAL FAILURE

6.1 Introduction

The structural integrity and damage tolerance of chemical infrastructures, including vessels and pipes, is critical for the hydrocarbon processing, hydrothermal synthesis, etc., in the chemical industry, one of the sixteen critical infrastructure sectors identified by the Department of Homeland Security (DHS (Department of Homeland Security) 2016). Cracks are responsible for most reported sudden fracture failure of those structures operated under high temperature, high cyclic pressure, and the exposure to corrosive liquid or gas (Annaratone 2007). The origination of cracks is commonly induced by the local stress concentration due to the geometry change in configurations, the pitting corrosion on the wet surfaces, and weldments with flaws and residue stress. From a critical stress hotspot, single crack propagation towards unstable fracture controls the failure of the whole pressure vessel (Vosynek et al. 2014). However, the current practice in fatigue crack growth assessment of pressure vessels usually starts with an empirical assumption that sufficiently long initial crack is present, since the linear elastic fracture mechanics (LEFM) and stress intensity factor range based Paris law only serve for the long crack regime. Moreover, the life consumed towards the initial crack length i.e. crack initiation life is simply obtained by nominal stress approach without explicit consideration of crack (Rudolph et al. 2002). Unfortunately, the crack propagation at early stage i.e. short crack regime, accounting for about 90% of the structural fatigue life (Krupp 2007), is also not detectable by current nondestructive examination methods, which makes it difficult to prevent the accelerated crack growth at the last phase when the crack length increased to the long crack ranges in a timely manner. Meanwhile, the polycrystalline material heterogeneity and severe discontinuities induced by cracks are proven to strongly influence the crack initiation and make the nominal stress approach questionable (Suresh and Ritchie 1984). Therefore, the short crack growth towards the initial long crack needs a better quantification.

Hussain (Hussain 1997) and Bathias & Pineau (Bathias and Pineau 2013) provide comprehensive reviews on the short fatigue crack models considering the microstructure influence and large-scale plasticity effects. Specifically for pressure vessel steel, Wu & Akid (Wu and Akid 1995) proposed plastic zone size based short fatigue crack growth model to consider crack closure effect and short crack deceleration mechanism in the material microstructure. However, the variability of MSC growth requires an approach to render crack growth in realistic microstructures with different attributes such as grain size, morphology, and crystal orientation. Recent microstructure-sensitive models based on crystal plasticity, continuous dislocation theory and fatigue indicator parameters (FIPs) (Castelluccio and McDowell 2015a) are promising tool to describe both the MSC nucleation and growth with a 2D mesoscale finite element simulation framework (Yuan et al. 2017).

It is now well recognized that small pre-existing defects are an inherent feature of structural material even though the forming, fabrication and joining techniques are advanced significantly. However, the size of such defects reduces to the order of microns, like the metallurgical inhomogeneities such as nonmetallic inclusions and voids, or corrosion pits. Therefore the probe of these meso-defects needs to be performed in at least mesoscale simulation. It is also a necessary consideration for short fatigue crack behavior study since these meso-defects can act as a meso-notch, incubation period reducer or arrester to influence the MSC nucleation and growth. Musinski and McDowell (Musinski and McDowell 2012) have adopted 3D crystal plasticity FE model to assess the scatterness of the fatigue life for notched specimens with different notch root radii sizes and random microstructures of equiaxed IN100 and predicted the number of cycles required to propagate an MSC. However, the notch size is still in hundreds of microns, much larger than the SVE size.

In this study, a three-stage fatigue crack growth framework, covering MSC, PSC and LC, is implemented to predict the entire life of the pressure vessel with more physical considerations. For MSC stage, a novel 2D probabilistic mesoscale finite element simulation framework (Yuan et al. 2018a)(Yuan et al. 2018a) is adopted to predict crack evolution in polycrystalline grain aggregates at critical locations of the pressure vessel subjected to cyclic pressure loads. The microstructure-sensitive fatigue model and

crystal plasticity based non-local FIP are used to better describe microstructurally fatigue damage (Castelluccio and McDowell 2014). The simulation process is carried out using ABAQUS with a user subroutine UMAT for crystal plasticity. For PSC stage, Hussain's model (Hussain 1997) is employed to calculate the fatigue life from the typical final MSC length till the initial custom length of LC phase. For the long crack ranges, the fatigue life is obtained according to American Petroleum Institute 579 Fitness-for-Service Level 3 analysis and crack growth software NASGRO (API (American Petroleum Institute) and ASME (The American Society of Mechanical Engineers) 2016; SwRI (Southwest Research Institute) and NASA (National Aeronautics and Space Administration) 2016). The paper is organized in following sections: Section 2 provides details of model for each crack evolution stage. Section 3 presents a framework demonstration on a typical pressure vessel. Section 4 summarizes conclusions.

6.2 Fatigue Crack Growth Models

6.2.1 Three-stage of fatigue crack evolution and single-site damage approach

The total fatigue life in polycrystals can be partitioned into four physically-based regimes: nucleation (10^{-7}m ~ 10^{-5}m), microstructurally small crack (MSC, 10^{-7}m ~ 10^{-5}m), physically short crack (PSC, 10^{-5}m ~ 10^{-4}m), and long crack (LC, > 10^{-3}m) (Castelluccio and McDowell 2014), i.e.

$$N_f = N_{nuc} + N_{msc} + N_{psc} + N_{lc} \tag{6-1}$$

A comprehensive SVE-based short crack model has been developed to provide the physical-based time distribution of initial long crack for further crack growth in the component level simulation (Yuan et al. 2018a; b). In this chapter, the damage evolution in the structural component by a single site damage approach is presented. The single-site damage (SSD) approach is proposed with the assumption that the interaction between each crack is ignored since they are not close enough and appear in a parallel growth configuration. The component is considered to fail while any single crack length reaches a predefined criterion. To obtain the probabilistic prediction of the fatigue life under a certain scenario, firstly, the SVE-based simulations are performed to get the associate lifetime distribution to initial long crack. With

predefined initial crack length such as 0.1mm or 1mm, the PSC or LC growth can be obtained by any sophisticated technique in which the stress intensity factor can be calculated by FEM, or even analytically if under simple loads. Then the total fatigue life distribution is the initiation life distribution plus the deterministic PSC+LC life towards failure. A schematic representation of the three-stage single-site fatigue damage approach.

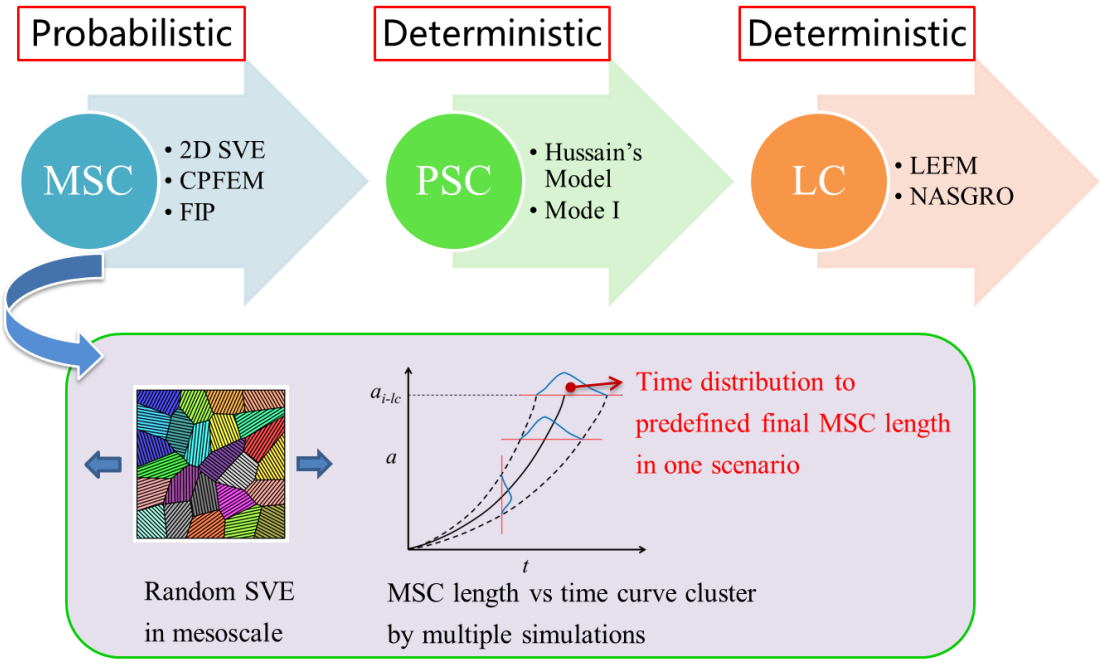

Figure 6-1. Framework of three-stage fatigue crack growth

The pressure vessel is a good representative to apply this approach since its failure is usually defined as penetration of single crack. For the short crack regime, SVE-based simulation can be performed to get the lifetime to the long crack initiation. For the long crack ranges, the fatigue life is obtained according to American Petroleum Institute 579 Fitness-for-Service Level 3 analysis, failure assessment diagram based on BS 7910 Level 2B, and crack growth software NASGRO. Therefore, the entire fatigue life from crack nucleation toward failure can be obtained.

6.2.2 MSC nucleation-growth model and its implementation

Following experimental evidence (Liaw et al. 1997), MSC is assumed to be transgranular and are driven by the cyclic plasticity in the bulk of the grains. This assumption allows us to employ the microstructure-sensitive framework developed by Castelluccio and Mcdowell (Castelluccio and McDowell 2015a) and Fatemi and Socie's FIP (Fatemi and Socie 1988) to assess fatigue crack growth through the microstructure. The detail of the MSC model and its implementation has been elaborated in Chapter 2 and not repeated here.

6.2.3 PSC growth model

Based on Hussain's model for Mode I PSC (Hussain 1997), the fatigue life N_{psc} from final MSC length a_{msc} to initial LC length a_0 can be calculate as

$$N_{psc} = \frac{1}{f\frac{\kappa}{G}\frac{\sqrt{1-n^2}}{n}\Delta\sigma}\left(\ln a_0 - \ln a_{msc}\right) + N_{msc} \tag{6-1}$$

where f represents the degree of irreversibility of slip on each cycle; G is the shear modulus; $\kappa = 1$ for screw dislocation; $\Delta\sigma$ is the applied stress range; n is the measurement of stress concentration ahead of plastic zone and defined as

$$n = \cos\left(\frac{\pi}{2}\frac{\sigma}{\sigma_{\text{comp}}}\right) \tag{6-2}$$

where σ_{comp} is comparison stress which is equal to the flow stress, i.e. yield strength within the plastic zone.

6.2.4 LC growth model

The LC growth model adopted is conventional Paris law which is also the basic version of NASGRO fatigue crack growth rate equation (SwRI (Southwest Research Institute) and NASA (National Aeronautics and

Space Administration) 2016) and specifically from API 579-1/ASME FFS-1 (API (American Petroleum Institute) and ASME (The American Society of Mechanical Engineers) 2016).

6.3 Three-stage Fatigue Crack Growth Simulation of Pressure Vessels: A Demonstration Example

6.3.1 Critical location identification of a typical pressure vessel

A 133.4-cm-ID 1315.7-cm-long vessel, with a centered flange on the south end and an off-centered flange on the north end (as shown in Fig. 6-3) is operated at the pressure from 13.8 MPa to 20.7 MPa. The material is quenched and tempered T-1 steel.

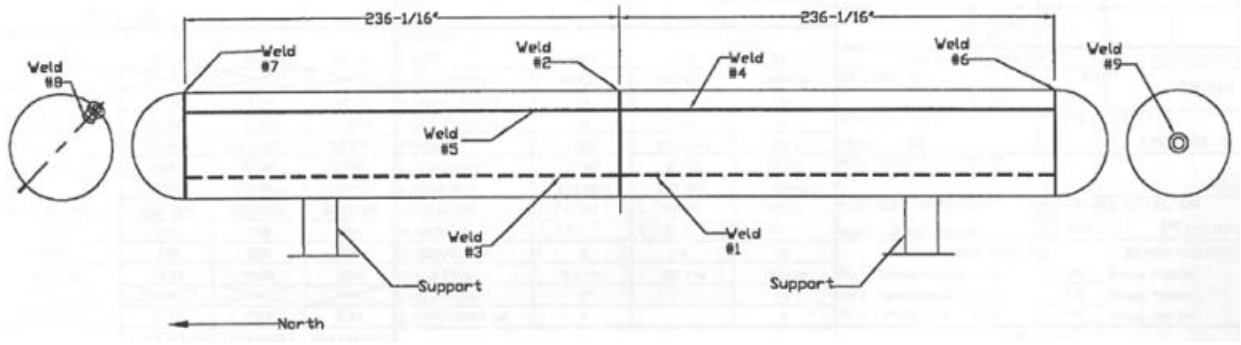

Figure 6-2. Schematic drawing of the pressure vessel

The critical locations for fatigue crack initiation are identified according to von-Mises stress profile from global finite element analysis. Here for example, according to 2D axisymmetric model, one critical location at centered flange outlet-inside corner (stress profile (unit: psi) shown in Fig. 6-4) with maximum normal stress range 151.7 MPa is selected for three-stage fatigue crack growth analysis. The three stages are also schematically visualized in Fig. 6-3. The SVEs for MSC growth simulation are generated for the surface hotspot with uniaxial load along the first principle stress direction.

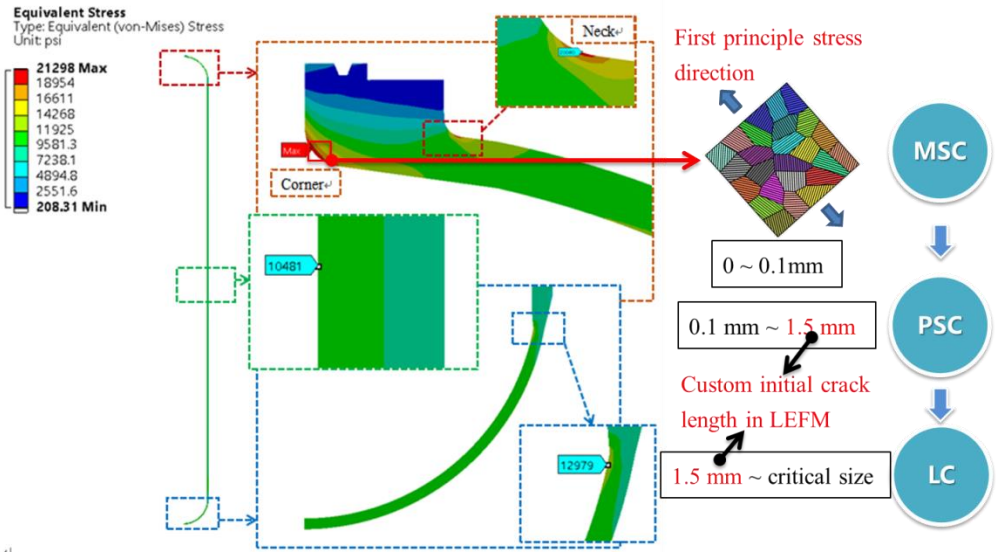

Figure 6-3. 2D axisymmetric FEA for hotspot stress and schematic diagram of subsequent analysis

6.3.2 Simulations of MSC in SVE

For martensitic steel (T-1, QT), lath martensite is close to BCC crystal structure after tempering. A block of lath martensite within a prior austenite grain constitutes a single grain for purposes of assigning grain orientation. The average size of the individual block of lath martensite (grain) is 20 μm. Mesoscale finite element models are built for the critical location with size 100 μm by 100 μm 2D plane strain SVEs. Each grain is divided into several PSBs along {110}<111> slip system. The SVEs are loaded with cyclic uniaxial stress range 151.7 MPa with R = 0.67. Crack growth, strain, and stress in weld zones for one realization is shown in Fig. 6-4.

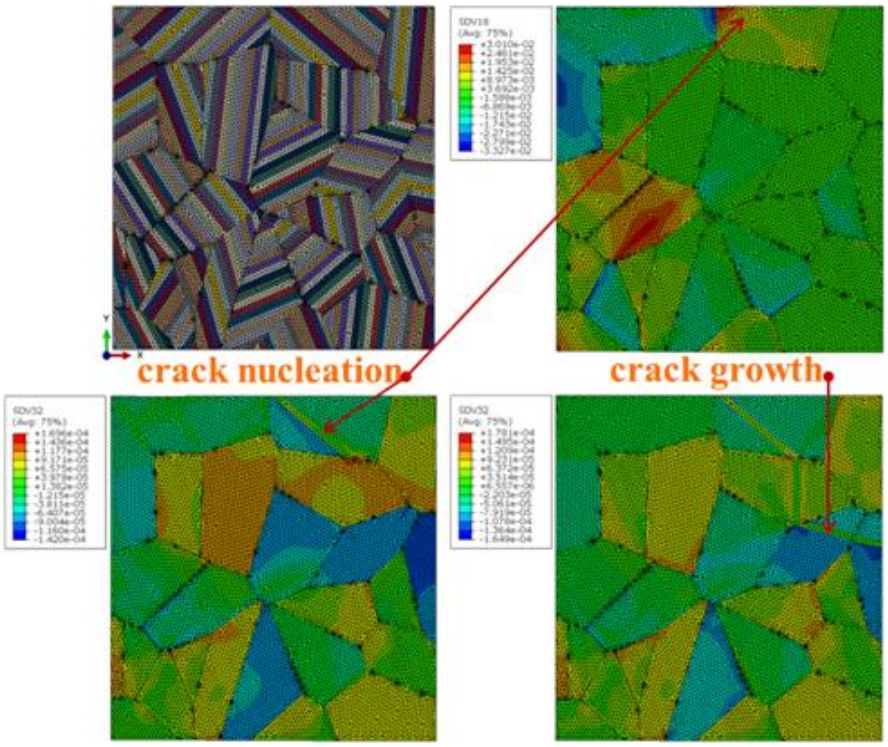

Figure 6-4. Crack growth, strain and stress for one simulation (unit: N, μm)

500 grain-scale simulations on random SVEs are performed, and 384 simulations render fully cracked SVEs (See Fig. 6-5(a) for crack growth diagram). The histogram and lognormal fit of the fully cracked SVE are plotted in Fig. 6-5(b). The time consumed is 443 hours on Dell T7610 workstation.

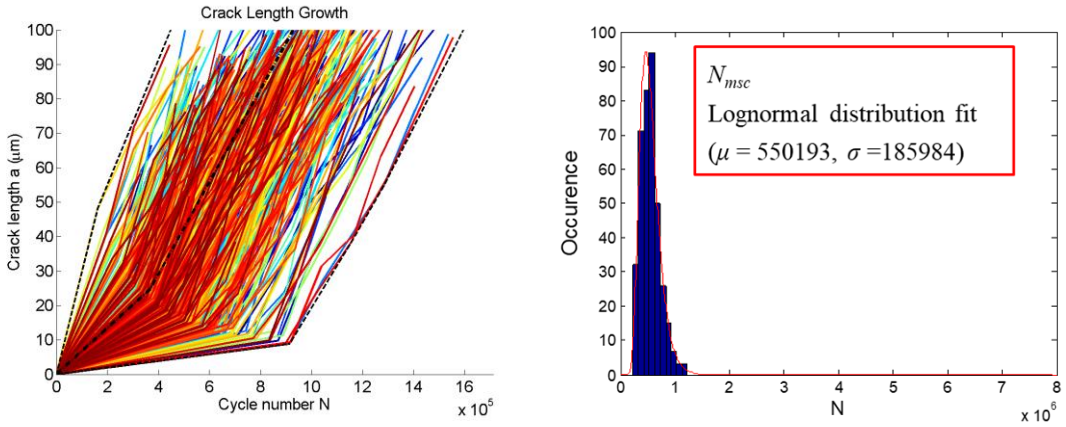

Figure 6-5. Time distribution to final MSC length by grain-scale simulations

6.3.3 Total fatigue life assessment including PSC and LC growth

With T-1 steel mechanical properties (G = 80 GPa, σ_{comp} = 689 MPa) substituting in the Eqs. (6-1, 6-2), f is taken as 0.002 (Hussain 1997) and a_0 = 1.5 mm, then PSC life N_{psc} = 634,002 cycles.

The fatigue crack growth rates used for LC evaluation were taken from Paragraph F.5.3.3 of API 579-1/ASME FFS-1. Stage II of the Paris equation is used, and the equation is:

$$\frac{da}{dN} = 6.60\times10^{-9}(\Delta K)^{2.25} \qquad \text{for martensitic steels (T1)} \tag{6-3}$$

For LC starting from a_0 = 1.5 mm to unstable fracture, the NASGRO analysis on SC02 geometry model gives the LC life N_{lc}= 175,500 cycles. The worksheet is shown in Fig. 6-6.

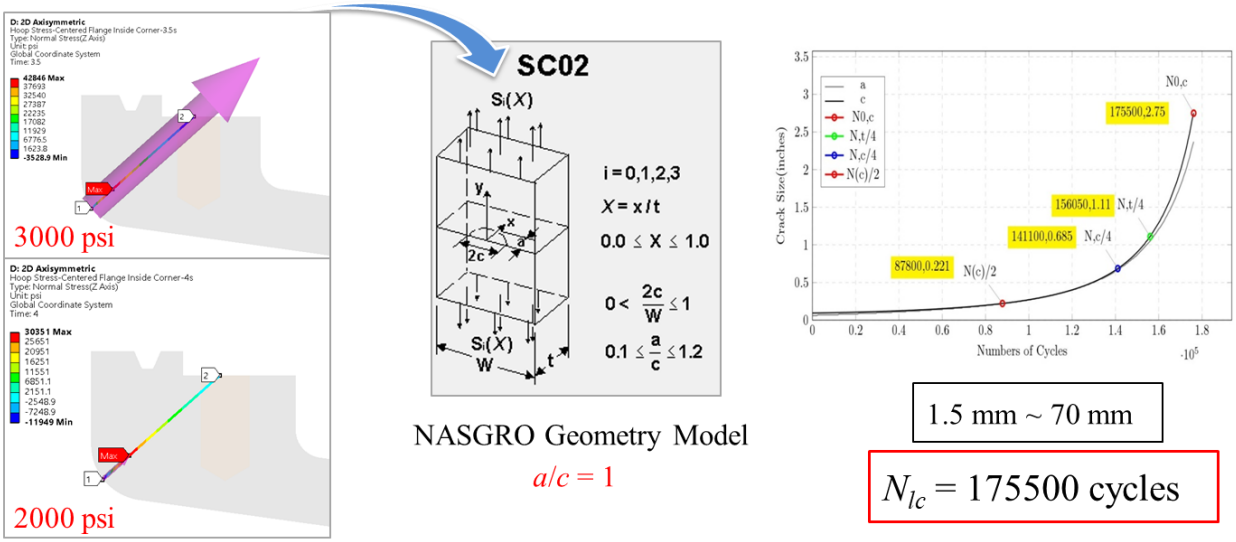

Figure 6-6. Long crack growth by NASGRO

To sum up, the entire fatigue life is N_f = 1,333,349 cycles. Assuming 3 cycles per week, the total life will be 9259 years. To be noticed, the number is only for one critical location which may not be the most critical one.

6.4 Conclusions

In the present paper, a three-stage fatigue crack growth framework covering the MSC, PSC and LC phases is implemented to predict the entire fatigue life of the pressure vessel. A novel 2D small crack simulation

framework built on microstructure-sensitive model and crystal plasticity based FIP is proposed for the single microstructurally short crack evolution. Together with Hussin's model for PSC and NASGRO approach for LC, the entire fatigue life can be obtained. A trial on a typical pressure vessel demonstrates the feasibility of the framework. The uncertainty from the variability of polycrystalline microstructure (including the grain size, morphology, crystal orientatio) are incorporated and reflected on the time distribution to final length of MSC. Future work can be devoted to the evaluation of size&shape effect of meso-notch and other type of meso-defects, and development of an advanced numerical approach for PSC simulation.

CHAPTER 7 MULTI-SITE FATIGUE DAMAGE EVOLUTION AND SURROGATION: FROM SHORT CRACK MODEL TO TIME-DETERIORATE COMPONENT

7.1 Introduction

For structures with redundant components, the local details in these components can endure multi-site fatigue damage, while the overall structural integrity still holds. Visually, the multi-site damage (MSD) refers to the simultaneous presence of multiple fatigue cracks in the same hotspot zone or later in the whole component. The life cycle of MSD can be described as three stages: (i) multiple cracks initiate in the hotspot zone early in the fatigue life, grow, coalesce and tend to form a dominant crack; (ii) the dominant cracks from different hotspot zones may interact and lead to the failure of the whole component; (iii) finally, the entire structure fails due to progressive failure of components. In a complex structure such as orthotropic deck and offshore structure, many components like stiffeners (ribs) or tubular joints are under similar working conditions. In each component, there may be multiple hotspots where multiple cracks may initiate and growth.

Under most circumstances, structures with MSD can work safely for a long time while the detrimental effects from MSD are attenuated by redundant constructional details. A good example is the orthotropic steel deck while MSD is commonly distributed in a large amount of complex welded joints for deck plates and stiffeners (ribs). These components (with joints) are under similar working conditions as redundant details. Each component may contain several hotspot zones and multiple cracks may initiate and grow in each hotspot zone. However, if MSD is not controlled and let develop freely, the resulted failure of components will even change the load paths, and the whole structure will behave far from designed and unforeseeable failure may happen. Therefore, from the view of life-cycle performance, these local damages should be evaluated. With the estimation of the current fatigue crack configuration in the components, the decision maker can decide to arrange an inspection and repair such that the further development of these cracks can be detained and the structure can serve as a renovated assembly for more years safely. On another

aspect, the incorporation of MSD in the structural assessment can provide a more accurate evaluation of the life-cycle performance. Therefore, the research on MSD evolution in the component and surrogation into structural analysis has great significance.

The MSD has been studied in aeronautical engineering since the famous Aloha accident on April 28, 1988 and the MSD approach is developed for the purpose like aging aircraft structural assessment. Millwater summarized the work of predecessors and established a comprehensive computational framework for MSD risk assessment (Millwater 1997). For the appearance of MSD, Jeong and Tong proposed the concept of MSD threshold (Jeong and Tong 1997). MSD under corrosion fatigue is also studied with a comprehensive seven-stage model (Shi and Mahadevan 2003). A probabilistic analysis method based on the statistical theory and fatigue characteristics of each structural detail is developed, and effect from a number of details and stress levels are explored (Zhang et al. 2010). Crack interaction and coalescence are characteristics of MSD. Effect of equivalent initial flaw size distribution in an MSD specimen is studied by using the extended finite element method (XFEM) to consider crack interaction (Kim et al. 2011). Short crack effect in MSD is also studied by quantitative fractographic methods (Tan and Chen 2015). Without the concept of MSD, multiple crack coalescence is limited examined in bridge component and offshore pipe (Ishihara et al. 1985; Wang 1990; Zhang et al. 2015). To be noted, those research on MSD approach is mainly linear elastic fracture mechanics (LEFM) based and the crack growth is studied universally in the long crack regime. Due to the limitation of LEFM, long crack initiation problem has not been tackled well for MSD Stage (i), while when and where a crack will enter the MSD approach is arbitrary or based on specific experiments. In some structures, many identical components are working under similar scenarios, which make using experimental tool to monitor crack initiation even impossible.

Physically in the hotspot zone (identified by the component level finite element analysis), the long crack initiation can be explained as short crack nucleation and growth. The long crack can be considered as initiated when the short crack extends to a characteristic length, after which LEFM can be appropriate (Krupp 2007). There are many factors influencing the multi-crack initiation in the hotspot zone, including microstructure and local geometry, which determine the time-site pair of emerged cracks (Madia et al. 2017;

Tan and Chen 2015). Since the local geometry variability has been discussed by Madia et al. (Madia et al. 2017) and can be more easily reduced with the advance of manufacturing techniques, the main concern is put onto the multi-crack initiation considering microstructure variability. Based on author's previous research (Yuan et al. 2018a), short crack model can be employed for a microstructure-sensitive estimation of transition time from short to long crack of a characteristic length, i.e. time of long crack initiation. Under most circumstances, the microstructure profile of the hotspot zone is unknown and can be taken as a random variable across all components of one kind. Considering microstructure variability, a time distribution of initial long crack (TDILC) for a hotspot zone under one scenarios can be quantified with deterministic Monte Carlo simulation (MCS) (Yuan et al. 2018b).

In this study, an MSD approach handling the multi-crack initiation and growth in the hotspot zone is proposed. The initiation time of multiple cracks are sampled from TDILC of the hotspot zone obtained by implementing a short crack model. The long crack emergence, growth and coalescence are simultaneously captured by long crack growth simulation with stochastic initial crack insertion. Thus, the time-deteriorate component is generated. The surrogation of the time-deteriorate component for structural analysis is also discussed. The paper is organized in following sections: Section 2 provides details of the MSD approach, including short crack model, TDILC obtainment, crack coalescence consideration and the general procedure for time-deteriorate component generation. Section 3 details the long crack simulation approaches to facilitate the time-deteriorate component generation. Section 4 introduces simple damage equivalent surrogates of the time-deteriorate component for incorporation in the structural model. Section 5 presents a framework demonstration on T-joints. Section 6 summarizes some remarkable conclusions.

7.2 Multi-site Damage Approach: From Short Crack Model to Time-deteriorate Component

7.2.1 Short crack model and TDILC

The 2D SVE-based mesoscale short fatigue crack model is adopted. The detail of fatigue indicator parameters, short crack nucleation and growth equations, and model implementation has already been

elaborated in Chapter 2 and not repeated here. To be noted, the short crack here is only microstructurally short crack, and the following physically short crack and mechanically short crack are simply attributed to long crack regime since it is hard to distinguish them from each other and many researchers demonstrated the effectiveness of long crack approach on them (Schijve 2009). To consider microstructure variability in hotspot zones and across the components under almost identical working scenarios, combining the Monte Carlo simulation of short crack growth and practical sampling is an effective and efficient approach to get the short crack damage status of the component at a certain time. The terminology of deterministic Monte Carlo simulation (DMCS) is for this kind of MCS and phrased by MacDonald in the research on corrosion damage simulation (Macdonald and Engelhardt 2012). Generally, DMCS represents the MCS which is performed on the model constrained by the natural law. Specifically, DMCS is performed on SVEs to establish the crack length vs. time curve cluster for different scenarios. From these damage profiles under different scenarios, the short crack length distribution at a certain time and the consumed life distribution of any short crack length can be obtained. However, only the time distribution to initial long crack (TDILC) is the sampling source for the component level analysis. A scheme for such probabilistic damage profile of short crack growth in a scenario is shown in Fig. 7-1. $a_{i\text{-}lc}$ is the initial long crack that can be 0.1 mm, 0.5 mm or 1 mm depending on the material type and the microstructural characteristics. The initiation time distribution of $a_{i\text{-}lc}$ can be fitted to Lognormal or Weibull distribution (Kim et al. 2011). The quantification of TDILC can be performed based on author's previous work (Yuan et al. 2018b) and has also been discussed in Chapter 4.

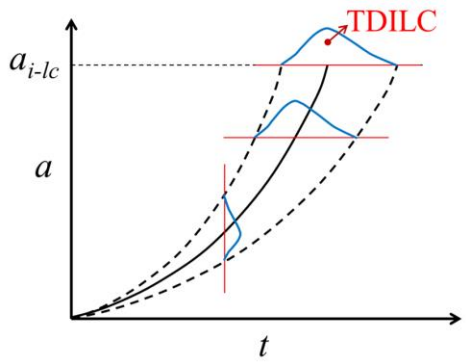

Figure 7-1. Probabilistic damage profile of short crack growth and TDILC in a scenario

7.2.2 Multi-site damage and crack coalescence

The multi-site damage (MSD) is defined as the simultaneous development of fatigue crack at multiple sites in the same structural component; however, these cracks are not independent anymore but leading to coalescence. Crack coalescence often happened in a fast manner and the instantaneous reshaping of crack will promote the further crack growth. In an aircraft structure, the coalescence of short macro-crack near rivet hole is dangerous and may lead to catastrophic failure. Therefore, a reliability analysis is necessary for aging aircraft with MSD. When it comes to MSD on components in steel bridges or offshore structures, the situation is not that critical. Even though MSD may exist on each hotspot of each component, structural redundancy increases the safety, such as the complex component system of an orthotropic steel deck. However, at a certain stage, MSD may evolve to significant long cracks in multiple components. These components with connections will degrade severely and the degradation will lead to stress redistribution and even cause a change of structural configuration. This is the motivation to introduce time-deteriorate component. The approach to generate time-deteriorate component is carried out by coupled stochastic initial crack insertion and long crack growth simulation which will be elaborated in Section 7.2.3.

The process of multiple crack interaction and coalescence is a complex issue. To model the process, analytical approach (such as ASME BPVC code procedure (ASME (The American Society of Mechanical Engineers) 2015)) is still prevailing in the fatigue assessment but mainly for coplanar cracks. The steps are: (i) when two cracks are distant from each other, they grow independently obeying crack growth rate equations like Paris' law. (ii) as the cracks come closer to a characteristic distance, they are considered to coalesce instantaneously and a recharacterization scheme is taken to form a new single crack for further growth. To be noted, the analytical approach neglects both the crack interaction process before step (ii) and the progressive coalescence process, considering their effects are opposite on fatigue life. There are also experiments that address that the effect of crack interaction on two coplanar crack growth is not notable until the tips are very close, while the coalescence will happen very soon (Kishimoto et al. 1989). FEM can

provide more accurate stress intensity factors under crack interactions as input for the analytical crack growth rate equation. However, it requires a computation for each cycle, which hinders the practical applications for high cycle fatigue. It is also worthy to note that the analytical approach is semi-empirical and phenomenological based on experimental observations. It cannot effectively solve non-coplanar crack problem and cannot be used under complex boundary conditions. A fully numerical approach is more predominant, but still underdeveloped especially for fatigue problem. XFEM-aided crack coalescence simulation has been demonstrated to be feasible in the 2D (Budyn et al. 2004; Holl et al. 2013; Ruiz-Muñoz 2018) and only limitedly extended to 3D (Garzon et al. 2014) due to complex enrichment scheme and quadrature.

Since the present study is focused on the incorporation of short fatigue crack profile, analytical approach is taken and only coplanar semi-elliptical cracks perpendicular to maximum principal stress direction (Mode I) are considered for simplicity. One kind of crack coalescence and recharacterization are shown in Fig. 7-2. It shows the recharacterization occurs only when the approaching crack tips physically touch each other (i.e. when interacting tip separation distance $d = 0$). A number of theoretical methods with different recharacterization conditions can be adopted (Tan and Chen 2015). One of them is taken here: $c_{new} = c_1 + c_2$, $a_{new} = \max\{a_1, a_2\}$. The center of the new elliptical crack is the midpoint of the old cracks. When the deepest point of the crack touches the boundary, the crack is instantaneously reshaped to a through-thickness crack with surface length unchanged. Then the conventional through-thickness crack growth model can be implemented. When the surface crack tips of through-thickness crack and semi-elliptical crack touch with each other, they can be merged by directly extending the through-thickness crack to the far-end tip of the semi-elliptical crack.

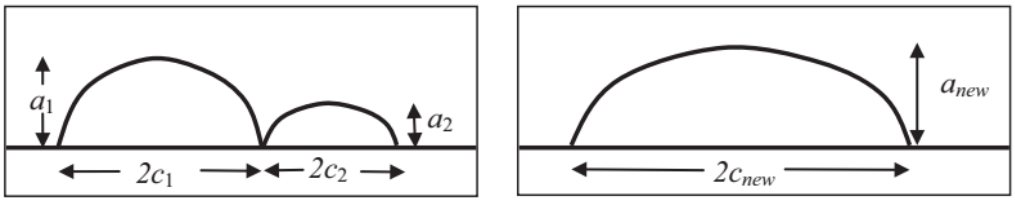

(a) *two coplanar cracks* (i.e. when $d = 0$) (b) *recharacterized crack*

Figure 7-2. Schematic of recharacterization of two coplanar cracks after coalescence

7.2.3 Generation of time-deteriorate components

The MSD development in components includes multiple events happened simultaneously. At a certain time, there could be short crack growth, long crack initiation, long crack propagation and crack coalescence on multiple sites. The two-dimensional Latin hypercube sampling can be used to insert initial cracks in the component model at different time. The time points for each emerged initial crack are sampled from TDILC, while the sites are assumed to be uniform distributed along the hotspot zone. At the same time, long crack growth is performed with analytical method and the crack coalescence are also checked after each extension of the crack. Therefore, to generate an appropriate sample of time-deteriorate component, a 2D schematic illustrating the coupled algorithm is drawn in Fig. 7-3. In this illustration, hotspot zone is divided by short crack density in space. Five initial cracks will be initiated at time $t_1 \sim t_5$ before the present time t_p (not necessarily at the center of cells, figure only for illustration purpose). If t_p is sufficiently large such for an old structure, there will be no new initial crack after t_p. Since the data or study on crack initiation density or spatial distribution is not available, 1/crack density can be taken as three times of initial crack size for conservation, which also guarantees that the maximum number of cracks can initiate independently. By this coupled approach considering MSD, the damage profile from SVE-based simulation and the component damage analysis are integrated.

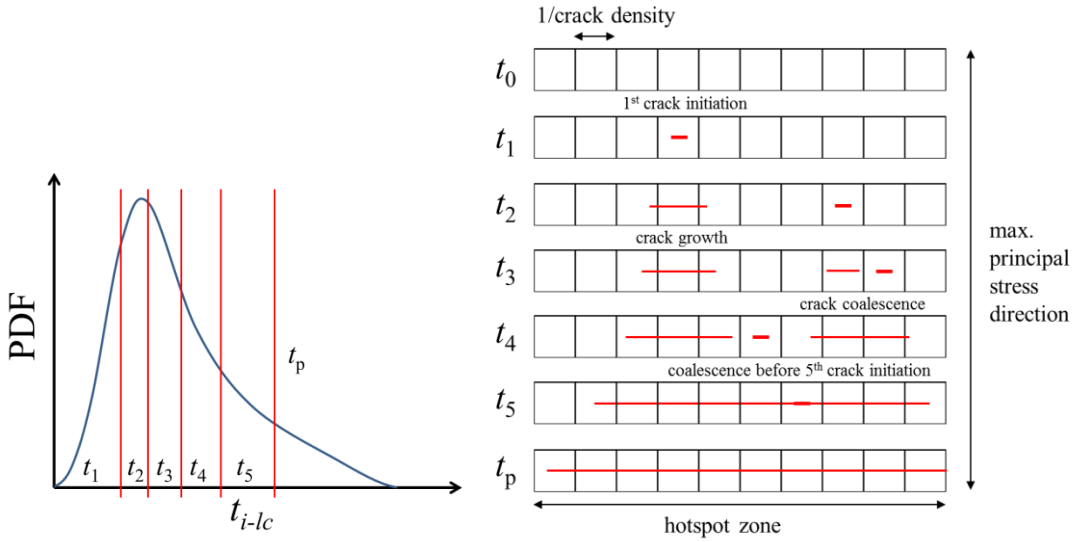

Figure 7-3. MSD approach to generate time-deteriorate components

7.3 Long Crack Growth Simulation Approaches

7.3.1 Analytical approach

For the current study, multiple surface cracks are all assumed to keep semi-elliptical shape under Mode I load, which can make it able to obtain analytical solution of stress intensity factor (SIF) K. Considering the local geometry, the SIF may be multiplied by a magnification factor M_k. Therefore, analytical approach can be implemented to perform rapid estimation of the crack growth.

The analytical approach for crack propagation is based on Paris law, which formulates the growth rate of a fatigue crack as

$$\frac{da}{dN} = C\left(\Delta K\right)^m \tag{7-1}$$

where a is the crack length (or depth) and N is the cycle count; $\Delta K = K_{max} - K_{min}$, is the SIF range; C and m are the Paris constant and exponent, respectively, and are usually experiment-based.

Between any two coalescence events, the cracks grow independently. The crack length, depth and cycle count during that period can be obtained by integrating Eq. (7-1). Based on Section 7.2.3, the crack initiation time and sites are pre-sampled and considered as fixed input for the algorithm of crack growth

simulation. To obtain the multi-crack profile at any time before the present time, the procedure need to iterative to cover every coalescence event. The multi-crack profile at any time can be tabulated as {Crack No., Crack Center, Crack Depth, Crack Half Surface Length, Merged Crack No. Set}. The algorithm of the multi-crack growth based on analytical approach is drawn as Fig. 7-4.

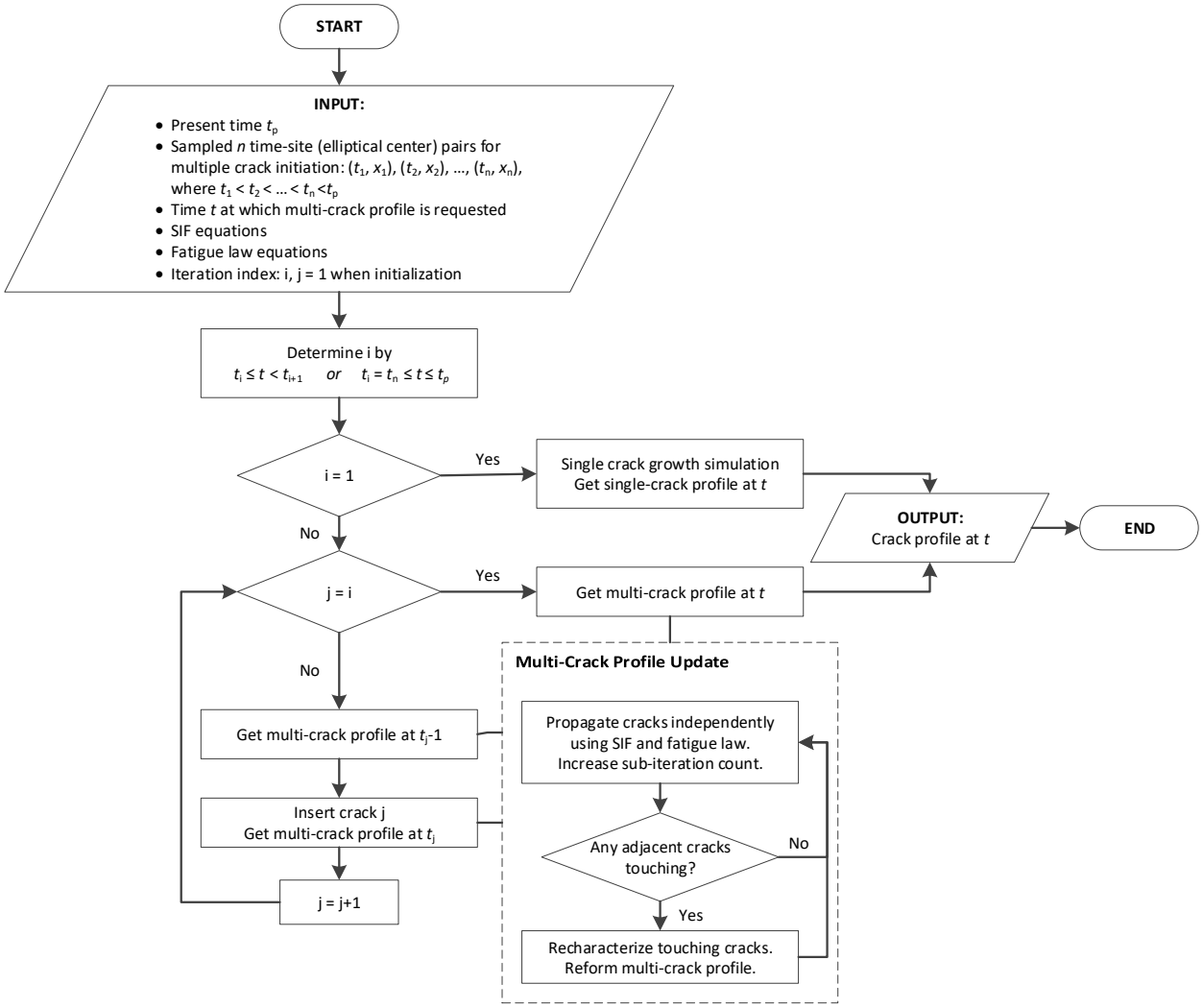

Figure 7-4. Algorithm of the multi-crack growth based on analytical approach

For a straightforward representation, the multi-crack growth process is shown in Fig. 7-5. The line color of reshaped crack front is taken from the largest crack before coalescence. With the multi-crack profile, a finite element model can be built for the time-deteriorate component.

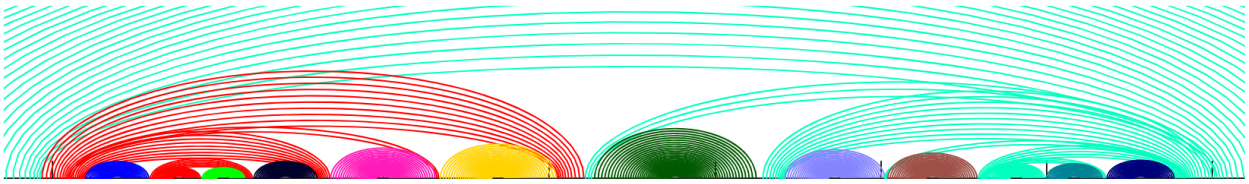

Figure 7-5. An example profile of multi-crack growth process

7.3.2 Cyclic cohesive zone model XFEM approach

This subsection introduces an alternative approach for macroscale fatigue crack growth simulation, which is still under development by the author. It is included in this dissertation since the author has been devoting to develop this promising tool, although it is still infant to be used for the present study. Some essential information and preliminary outcomes are presented here, while details are in the Appendix B.

A cyclic cohesive zone model (CCZM) is used to predict fatigue in an intermediate physical manner by adopting traction and separation law and accumulating damage in the incubation period. With proper input parameters, CCZM is potential to cover the fatigue crack growth in the Paris regime as well as the near-threshold regime (Kuna and Roth 2015; Roth et al. 2014; Xu and Yuan 2009a). Since the traditional cohesive zone model is impractical to predict an arbitrary crack path (Zhai et al. 2004), the CCZM has specially designed shape functions to calculate the discontinuous displacements by using enrichment functions in the XFEM (Belytschko et al. 2014; Wells and Sluys 2001; Xu and Yuan 2009b). Additional virtual degrees of freedom are used for the definition of the crack boundary and approximation of the displacement field. Therefore, it will allow crack nucleation under mixed-load conditions and curved growth without re-meshing. Based on the work of predecessors (Roth et al. 2014; Xu and Yuan 2009a), A 2D implementation program of combining CCZM and XFEM has been developed with ABAQUS and its user subroutines (3D algorithm is in debugging stage), while the CCZM is embedded in the user element (UEL). The 2D CCZM-XFEM program has been applied to predict mixed-mode crack growth in the double cantilever under low cycle fatigue. An example is shown in Fig. 7-6. The crack of CCZM UEL is visualized by overlay element.

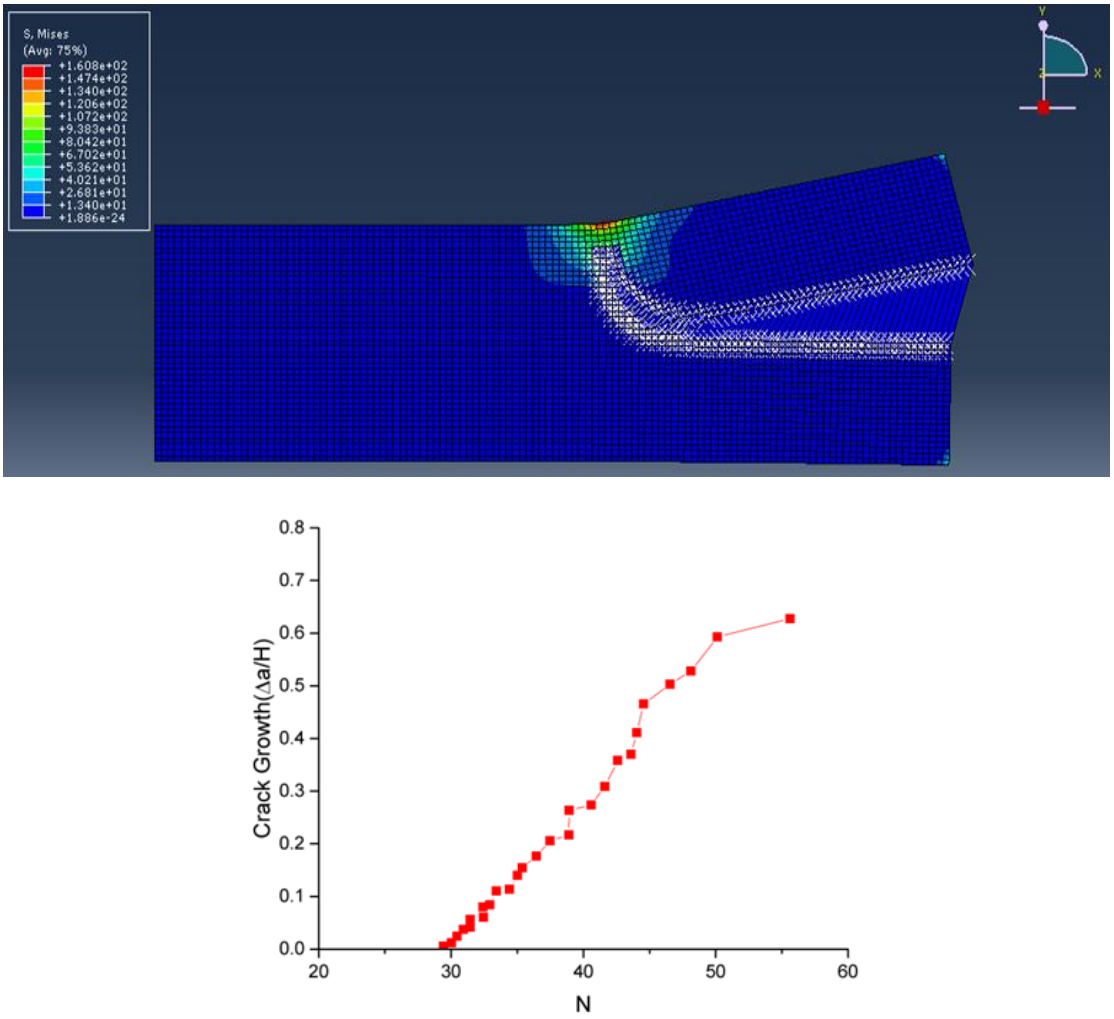

Figure 7-6. Mixed-mode fatigue crack growth of in the double cantilever under low cycle fatigue

To be noted, the current algorithm can only handle crack growth under low cycle fatigue since it is a cycle-by-cycle quasi-static simulation. The cycle jump algorithm or damage extrapolation scheme for application to high cycle fatigue and the incorporation of 3D crack coalescence is still under development.

7.4 Damage Equivalent Surrogates for Structural Model

The FEM models for large structures are mostly built with beam elements with rigid joints or shell elements with shared edges. However, the time-deteriorate component is based on solid element model. To surrogate

and transit the damage information to large structural analysis with multiple time-deteriorate components, the concurrent method is not efficient and damage equivalent surrogate schemes is recommended.

For components constructed with shell element in the structural model, the semi-elliptical crack can take the form as the line spring element in ABAQUS element library to incorporate part-through cracks (flaws) in shell inexpensively. The crack configuration from the obtained time-deteriorate component model can be discrete into node depth series representing the flaw, where line spring element links each pair of facing nodes. A coarser and more conservative equivalent method is directly replacing the crack configuration with a flaw of constant depth as envelope of all cracks. To be noted, line spring element is limited to small-displacement static procedure for the current ABAQUS version. For though-thickness cracks, seam-type crack can be applied to consider the crack opening that reducing the stiffness. The cohesive zone element is also a promising tool to represent crack and link with shell element by multi-point constraints. The direct derivation of damaged stiffness matrix is not effective for shell element since correspondence between solid element model and shell element model of local details is not clear due to the shared boundary and intersection issues. In addition, the complicated shell theory and high degrees of freedom also induce barriers of damage surrogate for shell element model.

In beam/bar element-based model, such time-deteriorate components can affect member section and degrade the rigid node bonding by forming a weaker joint or linkage, even though the global analysis remains in elastic regime. If beam element is used to represent those joints, constructing stiffness matrix with damage consideration is an effective approach to link the performance of cracked component to the behavior as beam element in the structural model. The time-deteriorate component as well as intact component is virtually tested by FEM for different displacements/rotations causing tension, shear, bending, etc. For each DOF pair, the damage coefficient is taken as the ratio of tangential stiffness value from damaged component to that from intact component. Thus, damage equivalent beam element is obtained as by multiplying the element from the conventional stiffness matrix with the corresponding damage coefficient. Besides beam element, joint element, connector element or multi-point constraints can also be used as surrogates representing the equivalent damage.

7.5 A Demonstration Example of T-joint

The end of the component near the beam-beam intersection or beam-rib intersection is prone to MSD due to the complex stress state. In this area, some hotspots can appear at beam web to flange connection or rib to deck connection. T-joint is a common simplification of such connections. Therefore, this section presents a comprehensive example studying MSD evolution and surrogation of T-joint.

The geometry of the T-joint with parametric dimension is shown in Fig. 7-7. It can be interpreted as a single-side welded T-joint with a weld toe crack vertical into the plate. However, in the current study, a homogeneous model is assumed.

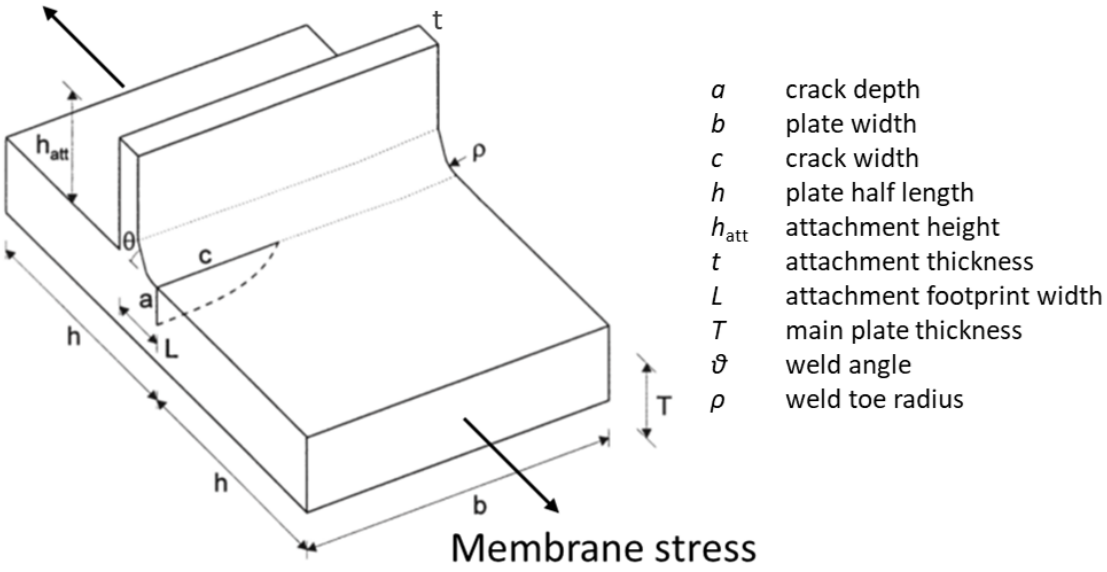

Figure 7-7. Schematic of 3D geometry and dimensions of T-joint with crack

Firstly, FEM of the intact T-joint is built and analyzed to obtain hotspot zone and associated stress.

The values of geometric dimension (unit: mm): b = 50, h = 50, h_{att}= 40, t = 8, L = 14, T = 16, θ = 45°, ρ = 0.

Material properties: linear elastic, elastic modulus E = 200 GPa, Poisson ratio v = 0.25.

The T-joint model undergoes constant amplitude membrane loading: $\Delta\sigma$ = 50 MPa, stress ratio R = 0, period = 2s.

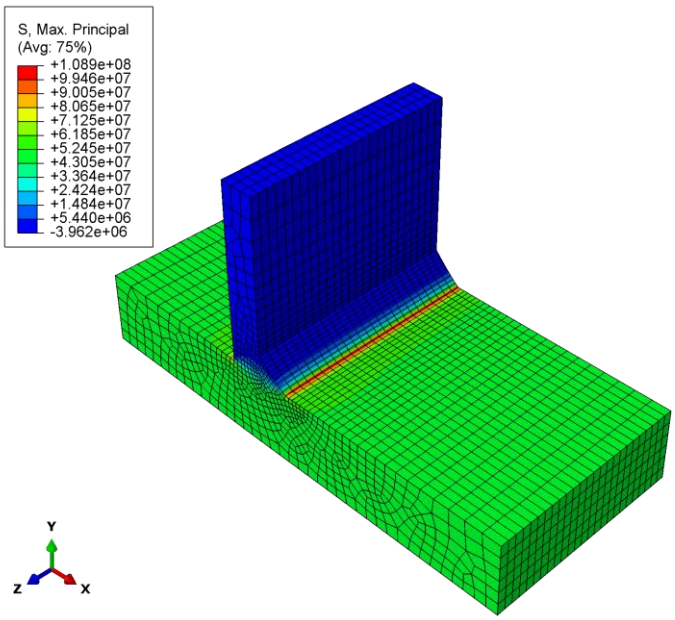

Figure 7-8. Max. principal stress contour of the T-joint at σ_{max} = 50 MPa

From the contour of maximum principal stress, the hotspot zone length is taken as 40 mm to avoid boundary issues. A uniform uniaxial strain range 0.5% assumed for SVE-based short crack model. HAZ microstructure from Chapter 2 is used here. The process to obtain TDILC and demonstrations have been already presented in Chapter 5 and 6. Here, those part of detailed process and results are omitted. The TDILC based on 0.5mm by 0.5mm SVEs is fitted as Lognormal (14.64, 0.2174), mean = 2333804 cycles, std = 513437 cycles.

Assuming initial aspect ratio a/c = 1, the surface length of initial crack is 1 mm, 1/crack density =3 mm. Therefore, in the hotspot zone, 12 cracks are going to be sampled. Assuming t_p = 5000000, which is large enough for using untruncated lognormal distribution for Latin Hypercube sampling. Sites are sampled from interval (5, 45) on the 50 mm plate width (unit: mm). The time-site pairs are listed in Table 7-1.

Table 7-1 Time-site pairs for crack initiation sampled from TDILC and plate width

No.	Time (cycle)	Site (mm)	No.	Time (cycle)	Site (mm)
1	1498563	27.7	7	2290710	32.1
2	1834729	22	8	2426509	43.4

3	1912251	5.3	9	2540153	15.9
4	2049553	10.6	10	2750205	19.3
5	2099595	36.3	11	3033689	31.6
6	2269684	13.3	12	3200330	39.6

For this specific T-joint, analytical solution of Mode I SIF range is based on the empirical solution for plain plate with semi-elliptical crack by Newman and Raju (Newman and Raju 1981) and the local geometry (weld toe) magnification factor M_k based on Bowness and Lee (Bowness and Lee 2000). Alternatively, the SIF range can also be evaluated by the *J*-contour method on fractured FEM shown in Fig. 7-9.

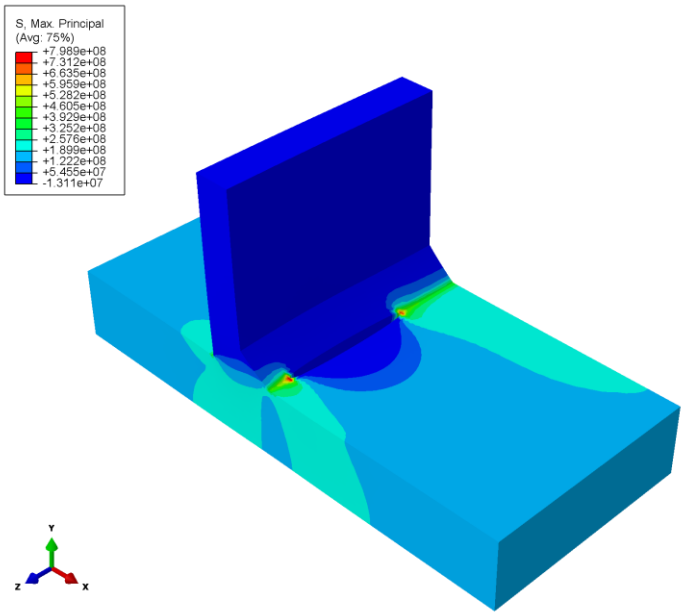

Figure 7-9. Max. principal stress contour of the T-joint with a crack present for SIF evaluation

The SIF range at the crack depth ΔK_a, and the crack surface tip ΔK_c, is given by

$$\Delta K_a = M_{k,a} F \Delta\sigma \sqrt{\pi \frac{a}{Q}} \tag{7-2}$$

$$\Delta K_c = M_{k,c} F \Delta\sigma \sqrt{\pi \frac{a}{Q}} \tag{7-3}$$

where F and Q are complex fitted equations for the geometry of plain plate with semi-elliptical crack; $M_{k,a}$ and $M_{k,c}$ are weld toe magnification factor for crack deepest point and surface crack end, respectively. All these equations are not listed here for conciseness and can refer to literature (Bowness and Lee 2000; Newman and Raju 1981). Since crack aspect ratio is changing when growing, these factors have to be reevaluate accordingly as well.

Paris law constants is taken as $C = 7.943\times10^{-12}$, $m = 3$ (Wang 2017), which is calibrated for rib-plate joints of orthotropic steel deck.

With above as input, the multi-crack growth can be simulated with the algorithm shown in Fig. 7-4. The multi-crack profiles at some characteristic time point around new crack insertion and crack coalescence are shown in Table 7-2. The profiles are drawing on the width-depth face at the weld toe position, which can be interpreted as the real crack configuration.

Table 7-2 Multi-crack profile in the crack growth and coalescence process

Time t	Multi-crack Profiles
1498563 (t_1)	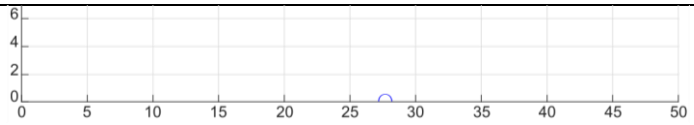
1834729 (t_2)	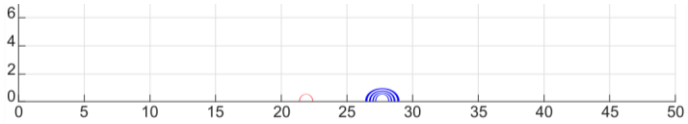
1912251 (t_3)	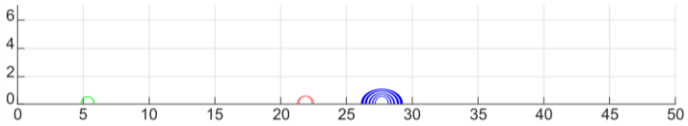
2049553 (t_4)	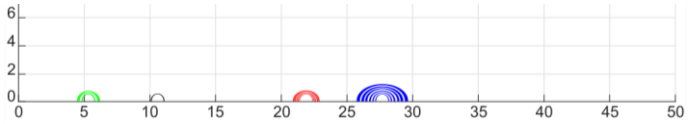
2099595 (t_5)	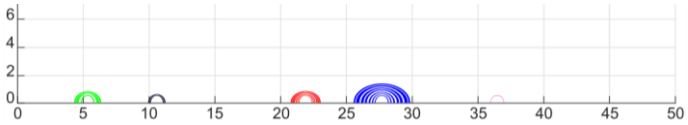

2269684 (t_6)

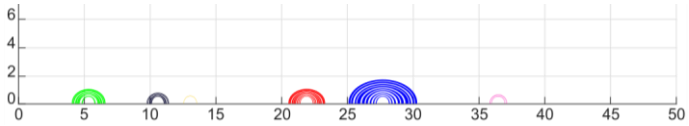

2290710 (t_7)

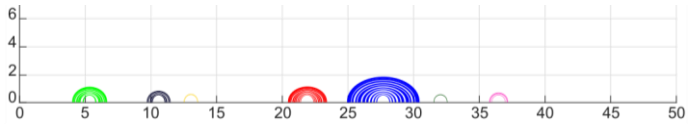

2426509 (t_8)

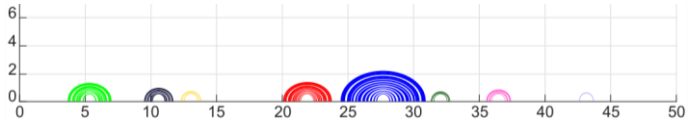

2540153 (t_9)

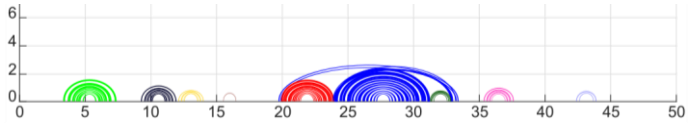

2750205 (t_{10})

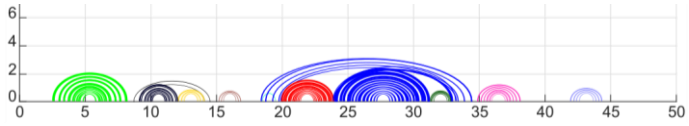

3033689 (t_{11})

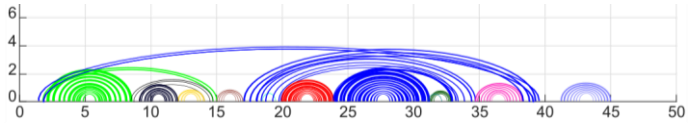

3200330 (t_{12})

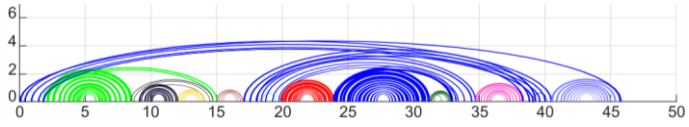

5000000 (t_p)

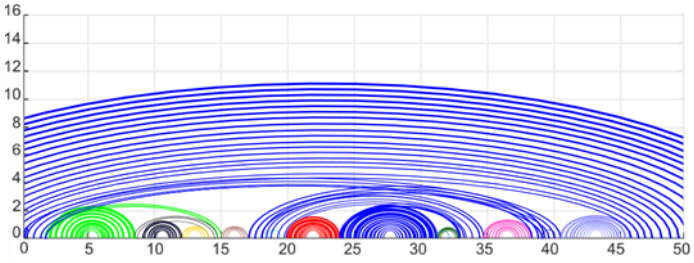

Using the multi-crack profile at t_{11}, the time-deteriorate component – the cracked T-joint is built as FE model in ABAQUS. The cracks are added simply as seams since the model is not used for fracture mechanics study. Both this damaged T-joint and the intact one are tested under axial displacement of 10 mm. The force-displacement curves are shown in Fig. 7-9. A slight reduction can be observed for axial stiffness under damaged condition. By estimation, the axial stiffnesses are k_{11} = 14718 kN/m for the intact

component, k_{11}^{D} = 14162.9 kN/m for the damaged component. Therefore, the damage coefficient $D_{11} = \frac{k_{11}^{D}}{k_{11}}$ = 0.9622. Thus, one damage index is obtained to form the damaged stiffness matrix of the damage equivalent beam element.

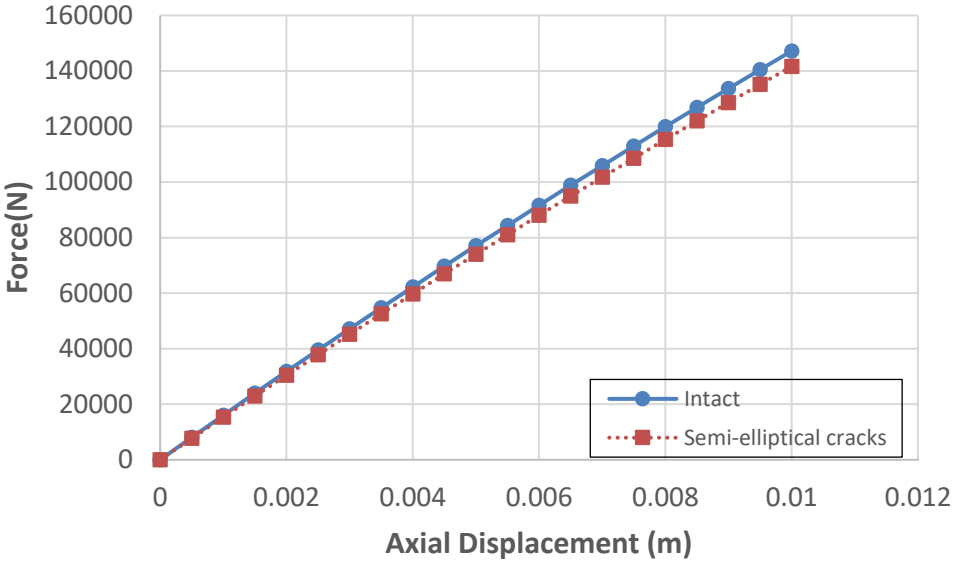

Figure 7-10. Force-displacement curves for both intact and cracked joint

7.6 Conclusions

In the present paper, an MSD approach handling the multi-crack initiation and growth in the hotspot zone is proposed. The initiation time of multiple cracks is sampled from TDILC of the hotspot zone by DMCS on an SVE-based short crack model. The long crack emergence, growth and coalescence are simultaneously captured by long crack growth simulation with stochastic initial crack insertion. As the outcome, the multi-crack profile at any time can be obtained by analytical approach and the time-deteriorate component is generated with FEM. A potential alternative for long crack growth simulation method called CCZM-XFEM, which is under development by the author, is also introduced. The surrogation of the time-deteriorate component for structural analysis is also briefly discussed. Finally, a comprehensive example of T-joint is presented for framework demonstration.

There are several directions for the future work. By statistical learning on this damage profiles in different scenarios, the damage profiles can be functionalized to be damage functions subject to all the sensitive parameters used in the mesoscale model for damage initiation and propagation. This will lead to the damage function analysis and probabilistic fatigue prediction without any more DMCS. Better model is expected to decompose the current long crack growth into physically short crack growth and mechanical short crack growth for more accurate results. If applied for welded joints, the residual stress should be incorporated in current framework. Bayesian updating may be used for rectifying a deviation of SIF from analytical solutions with periodic FEM-based SIF, which may provide more accurate multi-crack profile and time-deteriorate component.

CHAPTER 8 SUMMARY AND FUTURE WORK

8.1 Summary

The study presented in this dissertation provides a novel framework to enable the explicit consideration of the short crack behavior in mesoscale and damage scaling up into macroscale analysis. By the proposed multiscale modeling framework, short fatigue crack damage can be comprehensively analyzed and propagate to component level and structural level analysis, to better estimate the remaining life of the civil infrastructure and provide early warnings in advance for possible catastrophic failures.

Under the SVE scale or the mesoscale, a 2D short crack growth framework built on the microstructure-sensitive model and crystal plasticity based FIP is proposed. Firstly, the transgranular crack growth method under constant amplitude load is developed and applied to weld microstructure as a demonstration. The results show larger deviations of *a*-*N* data for BM than those for HAZ and FZ in MSC regime. Furthermore, the crack growth rate in the FZ has largest variability among the three zones, while the HAZ has the lowest.

With the grain-based Miner's law and rainflow counting method, the variable amplitude load is incorporated in the developed transgranular crack growth method. The grain-by-grain damage accumulation can automatically include the load sequence effect on the grain scale as well as the mean stress effect, damage under macro fatigue limit and the notch effect. The deficiency of the application of Miner's rule in macroscale fatigue damage accumulation is avoided in the model via only applying for the damage accumulation in the sub-grain damage.

Then, the pure transgranular crack simulation algorithm evolves to Integrated Transgranular and Intergranular Crack Growth Method (ITICGM) and further to Corrosion-informed ITICGM. The crack is found to be able to propagate intergranularly when transgranular propagation gets arrested; mixed behavior is found to promote the crack nucleation and propagation; the scattering behavior of the fatigue life can also be achieved; hydrogen corrosion on GB induce more intergranular growth.

To link the short crack damage in the mesoscale to the structural component level, a probabilistic framework is adopted including DMCS (+ROM) in mesoscale, damage profile generation and initial state sampling for components. A reduced order modeling framework is established to faster quantify time distribution to initial long crack for a simplified microstructure. The FEM-aided analytical simulation is adopted to propagates the fatigue crack in components. For single-site damage approach, a three-stage fatigue crack growth framework covering the MSC, PSC and LC phases is implemented to predict the entire fatigue life of the pressure vessel. For multi-site damage in a hotspot, the generation of time-deteriorated status has considered the crack initiation, growth and coalescence in multiple locations simultaneously. By performing numerical tests for different structural level degrees of freedom, the hotspots in the time-deteriorated component are surrogated with specific and damage-equivalent connection for subsequent structural analysis. A walk-through test is performed on the T-joints under membrane tension for demonstration.

The whole framework proposed in this research can serve as a base level of multi-scale fatigue damage prognosis system. It links the physical nature of fatigue to structural assessment, and even further it supports the decision-making process regarding the maintenance and retrofit of civil infrastructures with more confidence. Even though acknowledging the limitations such as 2D simplification, single slip system activation for crack, neglection of subgrain structure, simplified long crack growth FEM, etc., the proposed framework is a novel exploration with promising future, but still a long way to full development. Th calibration and validation are indispensable components in the rigorous development of a numerical model. However, this dissertation aims to explore the possibility of such advanced and promising models for the application in the structural engineering field. Therefore, the dissertation addresses more on the preliminary set-up of the framework and walk-through of the process, while most models and approaches are migrated or developed with the physically correct concept but have only been very limitedly calibrated and validated due to data scarcity. Some additional discussion regarding the model calibration and validation is provided in the Appendix C.

This study results in the following innovations:

- The research proposes an innovative multi-scale simulation scheme spanning from material level to structural level to incorporate the physics-based fatigue damage modeling, which includes the microstructure model, the concept of nonlocal FIP and the approach of crystal plasticity originated from material science, into the civil infrastructure condition assessment.
- The proposed SVE-based simulation framework is an explicit physics-based damage modeling approach that directly quantifies the short fatigue crack nucleation and propagation, which is a tough topic bypassed by most structural fatigue assessment methods. Meanwhile, variable amplitude loads and environmental effects like corrosion are systematically incorporated for fatigue damage evolution under different working conditions.
- Probabilistic damage profiles of crack configuration under different scenarios are prepared for the initial damage states of components by DMCS (+ROM) on SVE. This process acts as the link between SVE scale simulation and components, transferring damage status across scales as well as the accumulated uncertainty.
- The time-deteriorated component model is generated by the analytical approach and simplified to the equivalent connection at the damaged hotspot for structural model. This process establishes the link between the component scale model and the surrogate damages in the structural model.

The proposed framework is applicable to a wide variety of structures – such as pipelines and pressure vessels, offshore platforms, steel bridges, ships, chemical plants, etc. – subject to cyclic fatigue damages developing from very local details in harsh environments. Beyond the applications on the civil infrastructures, the methodologies could advance other fields that have similar complex system topology with multiple spatiotemporal scales and heterogeneous data sources, for example, the aircraft engine or the nuclear reactors.

8.2 Future Work

The following topics are suggested for subsequent studies:

- *3D SVE model for MSC growth*

  The representation and solution of the MSC problem in 2D is a significant simplification. At the hotspot of the material, the 3D information of polycrystalline microstructure, the boundary conditions and possible crack morphology is compromised. The simplification definitely deduces the error in the multi-axial strain solution, full crack arrest detection, and the fatigue life estimation. Even though 2D model does not prevent us from assessing a few key effects of the microstructure on fatigue cracks, some crack behaviors such as crack transfer/arrest cannot be captured more realistically. Based on the 2D framework, future work can devote to extend it to 3D models with multiple slip system activation and transition for crack growth. The optimal SVE size and number of realizations that yield accurate prediction for different microstructures may also be analyzed in future work.

- *Constitutive model informed by physical bottom-up approaches*

  The quality of the constitutive model affects the quantification of the fatigue driving force and introduces some uncertainty. The crystal plasticity model inside the single grain bulk is a continuum description of the crystal behavior that partitions the strain among the slip planes based on the phenomenological description of dislocation glide. The current adopted version of crystal plasticity model is a basic one while other advanced types of crystal plasticity model are available. A better constitutive model for GB is needed to capture slip transfer/pile-up phenomenon and enable more realistic transgranular-intergranular transition. Future work could aim for a better constitutive model with formulation informed by physical bottom-up approaches (such as first principle calculation by atomic mechanics or molecular dynamics). Benefiting from this, mutual coupling effect between the hydrogen diffusion and stress can also be incorporated.

- *Fatigue model formation, verification, calibration and validation*

  The current microstructure-sensitive fatigue model is based on FIPs and irreversibility parameters. Like

Paris' law, the model form needs to be tested by many practices and experiences to be accepted. Regarding the irreversibility coefficients, the quantitative interpretation of the atomistic process in the crack tip zone would help to quantify these parameters with an additional validation from small crack growth tests. As discussed in Section 8.2, there is a clear trend that the calibration and validation need shift to probability-based methods. Future work can include sensitivity analysis of model parameters, deterministic EBSD verification, the calibration and full validation of the model by extensive statistical technique and physical test data throughout different local microstructures. In the fatigue model implementation, the form to explicitly considering cracks and associated damage may also shift from stiffness reduction or cohesive zones to some more advanced forms.

- *A better reduced order model with machine learning for critical microstructural feature identification*

  The current ROM framework can be extended to consider both the grain size and grain shape variability. Other ROM techniques are also alternatives to try out. For our problem, the microstructure feature causing arrest need to be avoided, Sequential Monte Carlo can be a solution. The response surface approach and design of experiments can also be explored for optimal selection of training samples. With further digging into computational geometry and machine learning, the rapid but relative accurate prediction of fatigue crack growth in microstructures can be realized.

- *A better finite element simulation method for PSC + LC crack growth*

  The current finite element method adopted is an aid to get ΔK for analytical analysis of fatigue crack growth. Therefore, it is simple but with limited usage. In reality, the stress status around a crack can be very complex and the crack growth should be fully solution-dependent. XFEM with cyclic cohesive zone model and cycle jump technique can be a good method to propagate high cycle fatigue crack along arbitrary solution-dependent path. This future work can make it more practical to apply to different types of structural components. Even further, the development of multi-level FEM may make it possible to perform fully-coupled analysis of SVE and component.

APPENDIX A. SINGLE CRYSTAL PLASTICITY MODEL

In the present study, the single crystal plasticity model defined by Huang is employed and modified (Huang 1991). Main equations are included here for reference.

The inelastic deformation of a single crystal is assumed to arise only from crystalline slip and the deformation flows via dislocation. The total deformation gradient **F** is

$$\mathbf{F} = \mathbf{F}^{*} \cdot \mathbf{F}^{\mathbf{P}} \tag{A-1}$$

where $\mathbf{F}^{*}$ is the elastic stretch and rigid rotation and $\mathbf{F}^{\mathbf{P}}$ denotes the pure plastic shear.

The plastic velocity gradient can be expressed as,

$$\dot{\mathbf{F}}^{\mathbf{P}} \cdot \mathbf{F}^{\mathbf{P}\text{-}1} = \sum_{\alpha} \dot{\gamma}^{(\alpha)} \mathbf{s}^{(\alpha)} \mathbf{m}^{(\alpha)} \tag{A-2}$$

where $\dot{\gamma}^{(\alpha)}$ is the slipping rate of α slip system, $\mathbf{s}^{(\alpha)}$ and $\mathbf{m}^{(\alpha)}$ are the slip direction and normal of slip plane in the reference configuration.

In the deformed system,

$$\mathbf{s}^{*(\alpha)} = \mathbf{F}^{*} \cdot \mathbf{s}^{(\alpha)}, \ \mathbf{m}^{*(\alpha)} = \mathbf{m}^{(\alpha)} \cdot \mathbf{F}^{*\text{-}1} \tag{A-3}$$

The velocity in the current configuration is,

$$\mathbf{L} \equiv \dot{\mathbf{F}} \cdot \mathbf{F}^{\text{-}1} = \mathbf{D} + \boldsymbol{\Omega} \tag{A-4}$$

$$\mathbf{D} = \mathbf{D}^{*} + \mathbf{D}^{\mathbf{P}}, \boldsymbol{\Omega} = \boldsymbol{\Omega}^{*} + \boldsymbol{\Omega}^{\mathbf{P}} \tag{A-5}$$

$$\mathbf{D}^{*} + \boldsymbol{\Omega}^{*} = \dot{\mathbf{F}}^{*} \cdot \mathbf{F}^{*\text{-}1}, \mathbf{D}^{\mathbf{P}} + \boldsymbol{\Omega}^{\mathbf{P}} = \sum_{\alpha} \dot{\gamma}^{(\alpha)} \mathbf{s}^{*(\alpha)} \mathbf{m}^{*(\alpha)} \tag{A-6}$$

where **D** is the symmetric rate of stretching and **Ω** is the antisymmetric spin tensor, both of them are divided into lattice parts and plastic parts.

Constitutive laws,

$$\overset{\nabla^{*}}{\boldsymbol{\sigma}} + \boldsymbol{\sigma}(\mathbf{I} : \mathbf{D}^{*}) = \mathbf{L} : \mathbf{D}^{*} \tag{A-7}$$

where $\overset{\nabla^{*}}{\boldsymbol{\sigma}}$ is Jaumann rate of Cauchy stress **σ**.

$$\overset{\nabla^{*}}{\boldsymbol{\sigma}} = \overset{\nabla}{\boldsymbol{\sigma}} + (\boldsymbol{\Omega} - \boldsymbol{\Omega}^{*}) \cdot \boldsymbol{\sigma} - \boldsymbol{\sigma} \cdot (\boldsymbol{\Omega} - \boldsymbol{\Omega}^{*}), \ \overset{\nabla}{\boldsymbol{\sigma}} = \dot{\boldsymbol{\sigma}} - \boldsymbol{\Omega} \cdot \boldsymbol{\sigma} + \boldsymbol{\sigma} \cdot \boldsymbol{\Omega} \tag{A-8}$$

Schmid stress is,

$$\boldsymbol{\tau}^{(\alpha)} = \mathbf{m}^{*(\alpha)} \cdot \frac{\rho_0}{\rho} \boldsymbol{\sigma} \cdot \mathbf{s}^{*(\alpha)} \tag{A-9}$$

where ρ_0 and ρ are the mass density in the reference and current states.

And the Schmid stress rate is

$$\dot{\boldsymbol{\tau}}^{(\alpha)} = \mathbf{m}^{*(\alpha)} \cdot \left[\overset{\nabla^{*}}{\boldsymbol{\sigma}} + \boldsymbol{\sigma}(\mathbf{I} : \mathbf{D}^{*}) - \mathbf{D}^{*} \cdot \boldsymbol{\sigma} + \boldsymbol{\sigma} \cdot \mathbf{D}^{*} \right] \cdot \mathbf{s}^{*(\alpha)} \tag{A-10}$$

The viscoplastic constitutive model (plastic flow rule and hardening rules) used in this study is not included here since it has been elaborated in Chapter 2.

APPENDIX B. CYCLIC COHESIVE ZONE MODEL WITH XFEM

B.1 Cyclic Cohesive Zone Model

The Cyclic Cohesive Zone Model (CCZM) developed by Xu and Yuan (Xu and Yuan 2009a) is applied here. In this model, the material strength depends on both fracture strength as well as cyclic accumulative fatigue strength. Rupture of material will be regulated by conventional cohesive law whereas the fatigue failure is governed by a varying linear unloading/reloading accumulative process.

Cohesive law for normal strength and tangent strength is shown in Eq. (B-1). It is considered to be an exponential function of the separation since it is proved experimentally that the crack propagation is dominated by Mode-I fracture. The shear traction is proportional to the tangential separation.

$$\left.\begin{aligned} T_n &= f_t \frac{\delta_n}{\delta_0} \exp\left(-\frac{\delta_n}{\delta_0} - \frac{\delta_t^2}{\delta_0^2} \right) \\ T_t &= G_t \frac{\delta_t}{\delta_0} \\ \delta_n &= \bar{\delta}_n + \delta_0 \end{aligned}\right\} \tag{B-1}$$

δ_n is the effective normal separation. $\bar{\delta}_n$ denotes the normal separation from the FEM computation. δ_0 is the characteristic cohesive length. G_t is the shear stiffness and δ_t is the tangent separation.

The fatigue effect is considered in the damage evolution equation as Eq. (B-2) and updated cohesive strength like Eq. (B-3). The experiment results verify that there is a degradation of strength under cyclic loading condition. It is taken as an irreversible cohesive crack evolution here because the damage and energy dissipation are irreversible.

$$\dot{D} = \frac{|\dot{\delta}_n|}{\delta_\Sigma} \left(\frac{T_n}{f_t} - D_0 \right) H\left(T_n - f_0 \right) \tag{B-2}$$

$$f_t = (1 - D) f_{t0} \tag{B-3}$$

In Eq. (B-2), the Heaviside function H denotes that the damage accumulation starts once the normal cohesive traction exceeds the cohesive strength. D_0 is damage related to cohesive zone endurance limit. Eq. (3) is the damage equation directly from continuum damage mechanics. δ_Σ is the accumulated cohesive length which scales the increment of cohesive separation $\dot{\delta}_n$.

The unloading and reloading are assumed to proceed along a current stiffness, $k_n = f_t/\delta_0$, which is equal to the slope of the current cohesive curve at zero separation. This assumption will lead to the presence of a residual separation. The material damage is presumed to accumulate during the whole process of unloading and reloading, except for the case of compression. For numerical treatment of compression, the material penetration is reduced by enhancing the material compression stiffness. The CCZM scheme is shown in Fig. B-1.

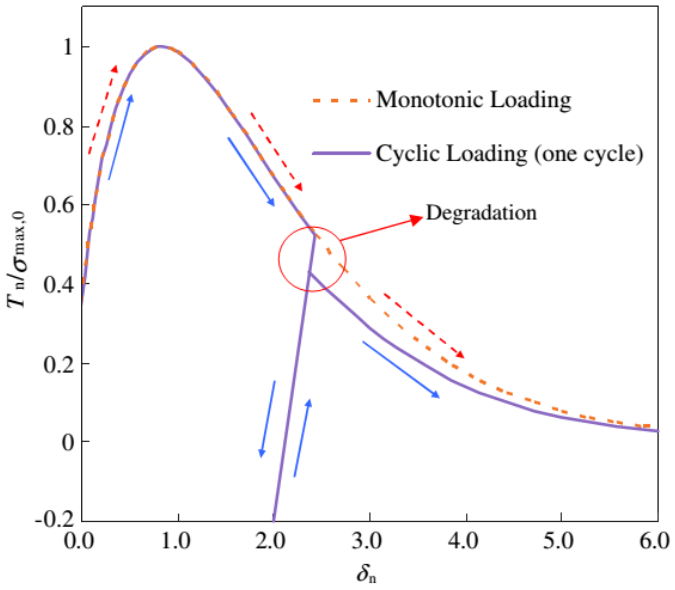

Figure B-1. The CCZM model under pure normal separation

B.2 Integrate CCZM with XFEM

CCZM is combined with XFEM in which strong discontinuity is allowed and the crack can have arbitrary extension path. XFEM is originated from Melenk and Babuska's work (Melenk and Babuška 1996) on the method of partition of unity, which can sufficiently reduce the mesh dependency. Comprehensive review of the XFEM can be found in (Fries and Belytschko 2010; Mohammadi 2008). The key point is that XFEM introduces enriched degrees of freedom in the region of interest, such as the flawed zone or weld zone.

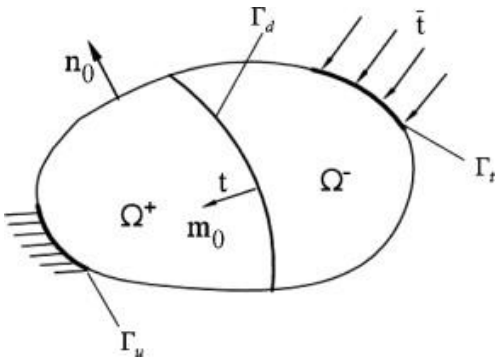

Figure B-2. FEM domain crossed by discontinuity Γ_d

In XFEM, a domain is shown in Fig. B-2. The element shape functions, *N*, fulfil the requirement of partition of unity. The discontinuity, Γ_d is contained in an element which has an additional enriched term as in Eq. (B-4):

$$\mathbf{u} = \mathbf{N}(\mathbf{a} + H_{\Gamma_d}\mathbf{b}) = \bar{\mathbf{u}} + H_{\Gamma_d}\tilde{\mathbf{u}} \tag{B-4}$$

where $\bar{\mathbf{u}}$ is the standard displacement field; $\tilde{\mathbf{u}}$ is the enriched displacement field. **a** and **b** denote the standard and enriched nodal DOF.

The displacement jump is as

$$[\mathbf{u}] = \mathbf{Nb} \mid \Gamma_d \tag{B-5}$$

The equilibrium equation $\nabla \cdot \sigma = 0$ in domain Ω can be converted by using the Galerkin formulation. If the discontinuity is controlled by the cohesive zone, the internal force **t** and tangent stiffness matrix **T** is calculated iteratively as

$$\dot{\mathbf{t}} = \mathbf{T}[\dot{\mathbf{u}}] = \mathbf{T}(\mathbf{N}\dot{\mathbf{b}}) \mid \Gamma_d \tag{B-6}$$

The linearized governing equation combing the CCZM and XFEM can be obtained following the literature (Xu and Yuan 2009a)

$$\begin{bmatrix} \mathbf{K}_{aa} & \mathbf{K}_{ab} \\ \mathbf{K}_{ba} & \mathbf{K}_{bb} \end{bmatrix} \begin{bmatrix} \Delta\mathbf{a} \\ \Delta\mathbf{b} \end{bmatrix} = \begin{bmatrix} \mathbf{f}_{a,ext} \\ \mathbf{f}_{b,ext} \end{bmatrix} - \begin{bmatrix} \mathbf{f}_{a,int} \\ \mathbf{f}_{b,int} \end{bmatrix} \tag{B-7}$$

with

$$\mathbf{f}_{a,int} = \int_{\Omega} \mathbf{B}^T \sigma d\Omega, \mathbf{f}_{a,ext} = \int_{\Gamma_t} \mathbf{N}^T \bar{\mathbf{t}} d\Gamma,$$

$$\mathbf{f}_{b,int} = \int_{\Omega+} \mathbf{B}^T \sigma d\Omega + \int_{\Gamma_d} \mathbf{N}^T \mathbf{t} d\Gamma, \mathbf{f}_{b,ext} = \int_{\Gamma_t+} \mathbf{N}^T \bar{\mathbf{t}} d\Gamma,$$

$$\mathbf{K}_{aa} = \int_{\Omega} \mathbf{B}^T \mathbf{D}\mathbf{B} d\Omega, \mathbf{K}_{ab} = \int_{\Omega+} \mathbf{B}^T \mathbf{D}\mathbf{B} d\Omega$$

$$\mathbf{K}_{ba} = \mathbf{K}_{ab}^T, \mathbf{K}_{bb} = \int_{\Omega+} \mathbf{B}^T \mathbf{D}\mathbf{B} d\Omega + \int_{\Gamma_d} \mathbf{N}^T \mathbf{T}\mathbf{N} d\Gamma$$

In Eq. (B-7), $\Delta\mathbf{a}$ and $\Delta\mathbf{b}$ denote the increment of nodal displacements in an incremental step. **D** is the material constitution matrix and **B** is the strain matrix. **t** and **T** come from the CCZM model. With the discontinuous element, the XFEM formulation still need to be solve in an iterative way even though remesh efforts is avoid.

B.3 CCZM-XFEM Implementation in ABAQUS

CCZM-XFEM model is implemented in ABAQUS via several user subroutines, among which the main component is the user element subroutine (UEL).

For 2D CCZM element, the explicit interface method is used to describe the crack interface. The decomposition for integration is standard in XFEM to make the sub-elements align with the discontinuity. The UEL is developed based on CPE4. The crack is described by a straight line. The whole domain of an intersected element is decomposed to do the integration. Here, two crack patterns are used while the cohesive zone will be a plane. The two crack patterns are shown in Fig. B-3. A cohesive zone plane can cut the quadrilateral into two quadrilaterals (Pattern a), or a triangle and a quadrilateral (Pattern b). The triangle is divide into 3 sub-triangles. One quadrilateral is divided again into 5 triangles, while in each triangle, three Gauss point will be used to get the integration. Therefore, each pattern has 8 sub-triangles (24 Gauss points). For the discontinuity line, 2 integration points are introduced.

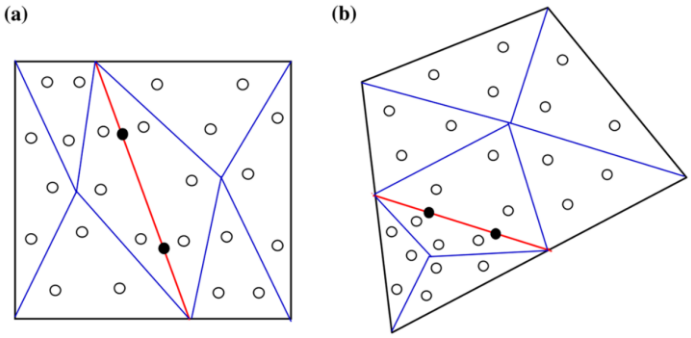

Figure B-3. Decomposition of a quadrilateral (2 patterns)

Above decomposition of 2D element is realized in physical element and all integration points must be projected backward to reference element. However, this method is difficult to expand to 3D because the projection will be non-linear which will require unreasonable time cost. Therefore, for 3D, the discretized level set function is used to describe the crack interface, see Eq. (B-8) and (B-9).

$$\phi^h(x) = \sum_{i \in I} N_i(x)\phi_i = 0 \tag{B-8}$$

$$\gamma(x) = \sum_{i \in I} N_i(x)\gamma_i \le 0 \tag{B-9}$$

where $N_i(x)$ are standard shape function for interpolation; I is the set of all nodes in space Ω; level set function Φ defines the crack path and γ defines the crack tips. The interface is general curved and resulted from finding the roots in the reference element and projecting these points into the physical element geometry. For preliminary development, the 3D CCZM UEL is based on C3D4. The crack interface described by Eq. (B-8) and (B-9) is planar. The whole domain of an intersected element is decomposed to do the integration. Here, two crack patterns are used while the cohesive zone will be a plane. The two crack patterns are shown in Fig. B-4. A cohesive zone plane can cut the tetrahedron into a tetrahedron and a pentahedra (Pattern A), or two pentahedra (Pattern B). One pentahedra is divided again into 3 tetrahedron again. In each tetrahedron, one Gauss point will be used to get the integration. Therefore, Pattern A will consist of 4 sub-tetrahedron (4 Gauss points) while Pattern B has 6 sub-tetrahedron (6 Gauss points). For the discontinuity plane, 3 integration points are introduced.

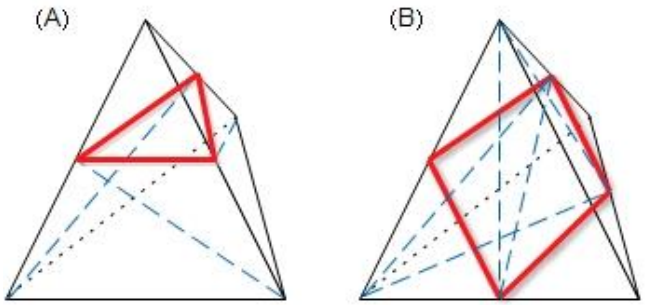

Figure B-4. Decomposition of a tetrahedron (2 patterns)

To be noted, the current algorithm can only handle crack growth under low cycle fatigue since it is a cycle-b-cycle quasi-static simulation. The cycle jump algorithm or damage extrapolation scheme for application to high cycle fatigue and the incorporation of 3D crack coalescence is still under development.

APPENDIX C. DISCUSSION ON MODEL CALIBRATION AND VALIDATION

The calibration and validation (C&V) are indispensable components in the rigorous development of a numerical model. The two major models or approaches in present research are 2D SVE-based short fatigue crack framework and SVE-to-component damage scaling up framework. Due to the nature of multi-level (scale) modeling, the C&V should be conducted in each individual level (scale) and as a multi-level (scale) integration (Panchal et al. 2013). The model with the introduction of corrosion effect also requires multi-physics model C&V. However, the C&V procedure of microstructural level model and the multi-level (scale) model is still underdeveloped according to a report on modeling across scales in the Integrated Computational Materials Engineering (ICME) (TMS (The Minerals Metals & Materials Society) 2015). The report categorizes the framework of model calibration, verification and validation as a research gap, while the filling requires many efforts but with a low probability of success in very recent future. Even worse, fatigue is a kind of performance controlled by rare events – lack of adequate coupling of predictive models and experiments. It is often not tractable from an experimental stand-point, coupling of models and experiments to predict performance is extremely challenging. This is especially an issue when scaling up, for instance, from microstructure and defects to properties and final component or platform performance. The cross-scale fatigue crack model also endures timescale mismatch between length scales, i.e. cyclic loading events are at one time scale (perhaps seconds) whereas the ultimate failure can occur in the timescale of years. Another significant challenge is the dearth of direct measurements of microstructural or interfacial properties, particularly interfacial energy, which is critical to mesoscale fatigue crack modeling. These all cause barriers to real C&V of fatigue model. In addition, validation of models needs to be conducted in a rigorous statistical framework that accurately accounts for uncertainties in experimental measurements and physical-based simulation results at various length and time scales. Technically, a successful C&V relies on some developing preconditions including more readily available data from refined and rigorous experiments and the maturity of multi-level finite element methods. The machine learning techniques can also benefit the uncertainty quantification and propagation in the C&V process.

In another aspect, this dissertation aims to explore the possibility of such advanced and promising models for the application in the structural engineering field. Therefore, the dissertation addresses more on the preliminary set-up of the framework and walk-through of the process, while most models and approaches are migrated or developed with the physically correct concept but have only been very limitedly calibrated and validated due to data scarcity. However, a tentative C&V scheme is presented in the following paragraphs for the comprehension of the dissertation.

For SVE scale model, a tentative plan of experiments is presented to obtain the data needed for C&V. A probabilistic C&V method based on extreme value statistics can be adopted to capture the variability of input parameters and fatigue life roughly. The details can be found in the following two subsections. The damage scaling up framework and component level model needs no validation for the method itself since they are built up with mature techniques and physical-proven models. The cross-scale verification of whole framework effectivity needs the cooperation with large-scale structural analysis, inspection or test, bottom-up calculation, as well as complex system engineering, which is beyond the objective of the present research.

C.1 Experimental procedure

To experimentally study the short fatigue behavior in grain scale for model validation, small flat specimens will be prepared by notching and surface polishing for each material zone. Corroded specimen can also be prepared. Two load ratios (R = 0.1 and -1) will be used in the experiments. Electron backscatter diffraction (EBSD) will be performed for each zone to obtain the grain sizes and its distribution, and the real RVEs will be reconstructed for deterministic simulation. Afterward, the specimen will be tested on the

servohydraulic uniaxial tensile tester and occasionally taken out for scanning electronic microscopy (SEM) observation of short crack nucleation and growth. Enough sampling rate will be ensured to capture the oscillation of the crack growth rate. Finally, the crack length vs. cycle number curves will be used to calibrate the parameters in the model and also serve as a validation for the simulation with calibrated parameters. To understand the random effects of different parameters in mesoscale, such as the grain size, slip band orientation, etc., multiple specimens will be prepared, and tests will be repeated for each configuration with the same cyclic load. A cluster of crack length vs. cycle number curves will form a probabilistic distribution band. The parameters in the simulation framework will be calibrated accordingly in a probabilistic perspective. The statistical data for the stochastic numerical simulation, therefore, can be compared and validated with the group of data from experiments. The tentatively experimental plan is also shown in Fig. C-1. In addition, local stress spectrums obtained from typical loading scenarios – calculated from coupled structural dynamics – will be loaded to the specimen for validation, as well. Data sources include those from numerical simulations of coupled structural dynamic system in our preliminary study and experimental database for typical pressure vessels obtained by Southwest Research Institute (SwRI).

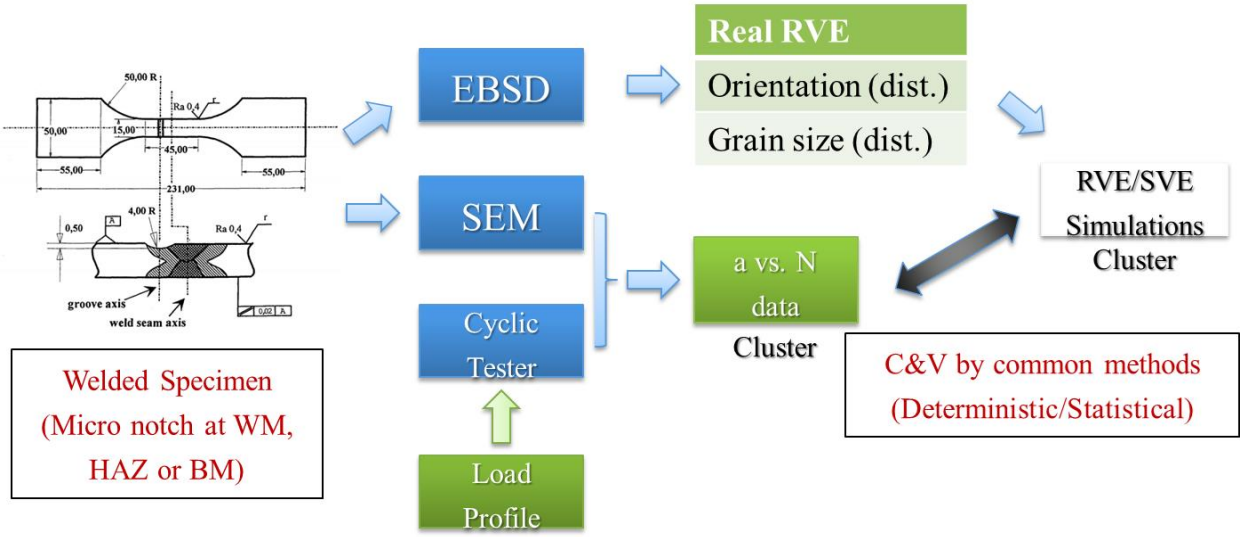

Figure C-1. Experimental procedure scheme (a specimen for weldment is shown)

C.2 Probabilistic calibration and validation procedure

The deterministic C&V is difficult to carry out since many uncertainties in both experiments and modeling make the calibration process very challenging. The smaller scale means larger uncertainties according to uncertainty relationship in physics. Due to these uncertainties and the information loss in modeling the real physical material system, the probabilistic C&V approach for this mesoscale model is more appropriate.

The strategy for computational HCF modeling could focus on the extreme value statistics of the potential sites for microplastic deformation localization since the target probability of failure is very low in most fatigue design scenarios (Przybyla and McDowell 2011). HCF is consequently a localization problem of the extreme value type. Therefore, for the calibration, massive simulations for SVEs can be realized to generate distributions of the extreme value (maximum FIP) to crack each grain. With limited experimental data for the crack length growth, the rough value for the irreversibility parameters can be determined to ensure the order of magnitude of fatigue life prediction. The variability of these parameters may be calibrated only if numerous data are available. Therefore, the validation can also only be coarse by

comparing the crack growth curve clusters with other groups of data qualitatively or with limited quantitative sense.

In contrast to the case for experimental characterization, it has been pointed out in the previous fatigue-related study (Przybyla et al. 2010) that the most relevant distribution of rare events of fatigue crack formation can be much more easily addressed through extreme value statistics of FIPs. The ideas of extreme value sampling from classical extreme value statistics of Gumbel which assumed as a natural rule due to a large population and fitting of extreme value FIP distributions may be a better approach for C&V.

REFERENCES

Adlakha, I., and Solanki, K. N. (2016). "Critical assessment of hydrogen effects on the slip transmission across grain boundaries in α-Fe." *Proceedings of the Royal Society A: Mathematical, Physical and Engineering Science*, 472(2185), 20150617.

Ahmadi, A., and Zenner, H. (2006). "Lifetime simulation under multiaxial random loading with regard to the microcrack growth." *International Journal of Fatigue*, 28(9), 954–962.

AISC (American Institute of Steel Construction). (1963). *Design manual for orthotropic steel plate deck bridges*. (R. Wolchuk, ed.), AISC, New York, NY.

Akid, R., and Miller, K. J. (1991). "Short fatigue crack growth behaviour of a low carbon steel under corrosion fatigue conditions." *Fatigue & Fracture of Engineering Materials & Structures*, 14(6), 637–649.

Alharbi, H. F., and Kalidindi, S. R. (2015). "Crystal plasticity finite element simulations using a database of discrete Fourier transforms." *International Journal of Plasticity*, 66, 71–84.

Alvaro, A., Olden, V., and Akselsen, O. M. (2014). "3D cohesive modelling of hydrogen embrittlement in the heat affected zone of an X70 pipeline steel - Part II." *International Journal of Hydrogen Energy*, 39(7), 3528–3541.

Anderson, T. (2005). *Fracture mechanics: fundamentals and applications, third edition*. CRC Press Taylor & Francis Group, Boca Raton, FL.

Angelova, D., and Akid, R. (1998). "A note on modelling short fatigue crack behaviour." *Fatigue & Fracture of Engineering Materials & Structures*, 21(6), 771–779.

Annaratone, D. (2007). *Pressure vessel design*. Springer-Verlag Berlin Heidelberg, Berlin, Germany.

API (American Petroleum Institute), and ASME (The American Society of Mechanical Engineers). (2016). *API 579-1/ASME FFS-1 fitness-for-service standard*. API Publishing Services, N.W., Washington, D.C.

ASME (The American Society of Mechanical Engineers). (2015). *Boiler and pressure vessel code*. ASME Press, New York, NY.

Azar, A. S., Svensson, L.-E., and Nyhus, B. (2015). "Effect of crystal orientation and texture on fatigue crack evolution in high strength steel welds." *International Journal of Fatigue*, 77, 95–104.

Ballesteros, A. F., Gomes, J. A. P., and Bott, I. S. (2015). "Corrosion evaluation of SAW welded API 5L X-80 joints in H_2S-containing solution." *Materials Research*, 18(2), 417–426.

Bathias, C., and Pineau, A. (Eds.). (2013). *Fatigue of materials and structures: fundamentals*. John Wiley & Sons, Inc., Hoboken, NJ.

Belytschko, T., Liu, W. K., Moran, B., and Elkhodary, K. (2014). *Nonlinear finite elements for continua and structures, 2nd edition*. John Wiley & Sons, Inc., Hoboken, NJ.

Boellinghaus, T. (2000). "Numerical model for hydrogen-assisted cracking." *Corrosion*, 56(6), 611–622.

Boumerzoug, Z. (2010). "Effect of welding on microstructure and mechanical properties of an industrial low carbon steel." *Engineering*, 2(7), 502–506.

Bowness, D., and Lee, M. M. K. (2000). "Prediction of weld toe magnification factors for semi-elliptical cracks in T–butt joints." *International Journal of Fatigue*, 22(5), 369–387.

BSI (British Standard Institution). (2013). *BS7910 - Guide on methods for assessing the acceptability of flaws in metallic structures*. BSI Standard Limited, London, UK.

Buch, A. (1981). "Verification of fatigue life prediction results for notched specimens with short crack propagation phase." *Material Science & Engineering Technology*, 12(8), 272–281.

Budyn, É., Zi, G., Moës, N., and Belytschko, T. (2004). "A method for multiple crack growth in brittle materials without remeshing." *International Journal for Numerical Methods in Engineering*, 61(10), 1741–1770.

Buirette, C., and Degallaix, G. (1998). "Microstructural effects on short fatigue crack initiation and propagation in high strength steel butt welded joints." *Welding in the World*, 41(1), 37–48.

Castelluccio, G. M., and McDowell, D. L. (2012). "Assessment of small fatigue crack growth driving forces in single crystals with and without slip bands." *International Journal of Fracture*, 176(1), 49–64.
Castelluccio, G. M., and McDowell, D. L. (2013). "A mesoscale approach for growth of 3D microstructurally small fatigue cracks in polycrystals." *International Journal of Damage Mechanics*, 23(6), 791–818.
Castelluccio, G. M., and McDowell, D. L. (2014). "Mesoscale modeling of microstructurally small fatigue cracks in metallic polycrystals." *Materials Science and Engineering: A*, 598(6), 34–55.
Castelluccio, G. M., and McDowell, D. L. (2015a). "Microstructure-sensitive small fatigue crack growth assessment: Effect of strain ratio, multiaxial strain state, and geometric discontinuities." *International Journal of Fatigue*, 82, 521–529.
Castelluccio, G. M., and McDowell, D. L. (2015b). "Microstructure and mesh sensitivities of mesoscale surrogate driving force measures for transgranular fatigue cracks in polycrystals." *Materials Science and Engineering: A*, 639, 626–639.
Castelluccio, G. M., Musinski, W. D., and McDowell, D. L. (2014). "Recent developments in assessing microstructure-sensitive early stage fatigue of polycrystals." *Current Opinion in Solid State and Materials Science*, 18(4), 180–187.
Castelluccio, G. M., Perez Ipiña, J. E., Yawny, A. A., and Ernst, H. A. (2013). "Fracture testing of the heat affected zone from welded steel pipes using an in situ stage." *Engineering Fracture Mechanics*, 98, 52–63.
Castelluccio, G. M., Yawny, A. A., Perez Ipiña, J. E., and Ernst, H. A. (2012). "In situ evaluation of tensile properties of heat-affected zones from welded steel pipes." *Strain*, 48(1), 68–74.
Craig, B. D., and Lane, R. A. (2005). "Environmentally-assisted cracking: comparing the influence of hydrogen, stress and corrosion on cracking mechanisms." *The AMPTIAC Quarterly*, 9(1), 17–24.
Dang-Van, K. (1993). "Macro-micro approach in high-cycle multiaxial fatigue." *Advances in Multiaxial Fatigue*, ASTM International, West Conshohocken, PA.
Davis, J. R. (Ed.). (2006). *Corrosion of weldments*. ASM International, Materials Park, OH.
DHS (Department of Homeland Security). (2016). "Critical Infrastructure Sectors." <https://www.dhs.gov/critical-infrastructure-sectors>.
Dmytrakh, I. M., Smiyan, O. D., Syrotyuk, A. M., and Bilyy, O. L. (2013). "Relationship between fatigue crack growth behaviour and local hydrogen concentration near crack tip in pipeline steel." *International Journal of Fatigue*, 50, 26–32.
Döring, R., Hoffmeyer, J., Seeger, T., and Vormwald, M. (2006). "Short fatigue crack growth under nonproportional multiaxial elastic-plastic strains." *International Journal of Fatigue*, 28(9), 972–982.
DS SIMULIA. (2011). *ABAQUS 6.11 Documentation*. Dassault Systèmes, Providence, RI.
Düber, O., Künkler, B., and Krupp, U. (2006). "Experimental characterization and two-dimensional simulation of short-crack propagation in an austenitic–ferritic duplex steel." *International Journal of Fatigue*, 28(9), 983–992.
Dunne, F. P. E. (2014). "Fatigue crack nucleation: Mechanistic modelling across the length scales." *Current Opinion in Solid State and Materials Science*, 18(4), 170–179.
EDF Energy. (2009). *R6: Assessment of the integrity of structures containing defects, revision 4*. EDF Energy, Gloucester, UK.
Endo, M., and McEvily, A. J. (2007). "Prediction of the behavior of small fatigue cracks." *Materials Science and Engineering: A*, 468–470, 51–58.
Engelhardt, G., Macdonald, D. D., Zhang, Y., and Dooley, B. (2004). "Deterministic prediction of corrosion damage in low pressure steam turbines." *PowerPlant Chemistry*, 6(11), 1–18.
Fan, J. L., Guo, X. L., Wu, C. W., and Zhao, Y. G. (2011). "Research on fatigue behavior evaluation and fatigue fracture mechanisms of cruciform welded joints." *Materials Science and Engineering: A*, 528(29–30), 8417–8427.
Fatemi, A., and Kurath, P. (1988). "Multiaxial fatigue life predictions under the influence of mean-stresses." *Journal of Engineering Materials and Technology*, 110(4), 380–388.
Fatemi, A., and Socie, D. F. (1988). "Critical plane approach to multiaxial fatigue damage including out-

of-phase loading." *Fatigue & Fracture of Engineering Materials & Structures*, 11(3), 149–165.
Fatemi, A., and Yang, L. (1998). "Cumulative fatigue damage and life prediction theories: a survey of the state of the art for homogeneous materials." *International Journal of Fatigue*, 20(1), 9–34.
Fong, J., and Fields, R. (Eds.). (1988). *Basic Questions in Fatigue (Vol. 1)*. ASTM International, West Conshohocken, PA.
Fricke, W. (2014). "Recent developments and future challenges in fatigue strength assessment of welded joints." *Proceedings of the Institution of Mechanical Engineers, Part C: Journal of Mechanical Engineering Science*, 229(7), 1224–1239.
Fries, T.-P., and Belytschko, T. (2010). "The extended/generalized finite element method: An overview of the method and its applications." *International Journal for Numerical Methods in Engineering*, 84(3), 253–304.
Garzon, J., O'Hara, P., Duarte, C. A., and Buttlar, W. G. (2014). "Improvements of explicit crack surface representation and update within the generalized finite element method with application to three-dimensional crack coalescence." *International Journal for Numerical Methods in Engineering*, 97(4), 231–273.
Ghahremani, K., Walbridge, S., and Topper, T. (2015). "High cycle fatigue behaviour of impact treated welds under variable amplitude loading conditions." *International Journal of Fatigue*, 81, 128–142.
Ghomashchi, R., Costin, W., and Kurji, R. (2015). "Evolution of weld metal microstructure in shielded metal arc welding of X70 HSLA steel with cellulosic electrodes: A case study." *Materials Characterization*, 107, 317–326.
Ghosh, P. K., Babu, P. N., and Gupta, P. C. (1994). "Microstructure-fatigue crack growth rate correlation in multipass submerged arc C-Mn steel weld deposit." *ISIJ International*, 34(3), 280–284.
Ghosh, S., and Chakraborty, P. (2013). "Microstructure and load sensitive fatigue crack nucleation in Ti-6242 using accelerated crystal plasticity FEM simulations." *International Journal of Fatigue*, 48, 231–246.
Ghosh, S., Weber, G., and Keshavarz, S. (2016). "Multiscale modeling of polycrystalline nickel-based superalloys accounting for subgrain microstructures." *Mechanics Research Communications*, 78(B), 34–46.
Grigoriu, M. (2014). "Response statistics for random heterogeneous microstructures." *SIAM/ASA Journal on Uncertainty Quantification*, 2(1), 252–275.
Heitmann, H. H., Vehoff, H., and Neumann, P. (1984). "Life prediction for random load fatigue based on the growth behavior of microcracks." *Proceedings of the 6th International Conference on Fracture (ICF6)*, International Congress on Fracture, Cassino (FR), Italy, 3599–3506.
Hertel, O., and Vormwald, M. (2011). "Short-crack-growth-based fatigue assessment of notched components under multiaxial variable amplitude loading." *Engineering Fracture Mechanics*, 78(8), 1614–1627.
Hodapp, D. P., Collette, M. D., and Troesch, A. W. (2014). "Stochastic nonlinear fatigue crack growth predictions for simple specimens subject to representative ship structural loading sequences." *International Journal of Fatigue*, 70, 38–50.
Holl, M., Loehnert, S., and Wriggers, P. (2013). "An adaptive multiscale method for crack propagation and crack coalescence." *International Journal for Numerical Methods in Engineering*, 93(1), 23–51.
Huang, Y. (1991). "A user-material subroutine incroporating single crystal plasticity in the ABAQUS finite element program." Harvard University, Cambridge, MA.
Hussain, K. (1997). "Short fatigue crack behaviour and analytical models: A review." *Engineering Fracture Mechanics*, 58(4), 327–354.
Ishihara, S., Shiozawa, K., and Miyao, K. (1985). "Distribution of corrosion fatigue crack lengths in carbon steel." *Bulletin of JSME*, 28(236), 194–201.
Jeong, D. Y., and Tong, P. (1997). "Onset of multiple site damage and widespread fatigue damage in aging airplanes." *International Journal of Fracture*, 85(2), 185–200.
Jha, S. K., Larsen, J. M., and Rosenberger, A. H. (2009). "Towards a physics-based description of fatigue variability behavior in probabilistic life-prediction." *Engineering Fracture Mechanics*, 76(5), 681–

694.
Kartal, M., Cuddihy, M., and Dunne, F. (2014). “Effects of crystallographic orientation and grain morphology on crack tip stress state and plasticity.” *International Journal of Fatigue*, 61, 46–58.
Kim, J., Zi, G., Van, S. N., Jeong, M., Kong, J., and Kim, M. (2011). “Fatigue life prediction of multiple site damage based on probabilistic equivalent initial flaw model.” *Structural Engineering and Mechanics*, 38(4), 443–457.
Kishimoto, K., Soboyejo, W. O., Smith, R. A., and Knott, J. F. (1989). “A numerical investigation of the interaction and coalescence of twin coplanar semi-elliptical fatigue cracks.” *International Journal of Fatigue*, 11(2), 91–96.
Kouchmeshky, B., and Zabaras, N. (2010). “Microstructure model reduction and uncertainty quantification in multiscale deformation processes.” *Computational Materials Science*, 48(2), 213–227.
Krupp, U. (2007). *Fatigue crack propagation in metals and alloys: microstructural aspects and modelling concepts*. Jonhn Wiley & Sons, Inc., Hoboken, NJ.
Krupp, U., Düber, O., Christ, H.-J., Künkler, B., Köster, P., and Fritzen, C.-P. (2007). “Propagation mechanisms of microstructurally short cracks—Factors governing the transition from short- to long-crack behavior.” *Materials Science and Engineering: A*, 462(1–2), 174–177.
Kuna, M., and Roth, S. (2015). “General remarks on cyclic cohesive zone models.” *International Journal of Fracture*, 196(1–2), 147–167.
Künkler, B., Düber, O., and Köster, P. (2008). “Modelling of short crack propagation–Transition from stage I to stage II.” *Engineering Fracture Mechanics*, 75(3), 715–725.
Lautrou, N., Thevenet, D., and Cognard, J.-Y. (2009). “Fatigue crack initiation life estimation in a steel welded joint by the use of a two-scale damage model.” *Fatigue & Fracture of Engineering Materials & Structures*, 32(5), 403–417.
Lee, E. U. (1996). “Corrosion fatigue of AerMet 100 steel.” Naval Air Warfare Center Aircraft Division, Patuxent River, MD.
Lemaitre, J., and Desmorat, R. (2005). *Engineering damage mechanics: ductile, creep, fatigue and brittle failures*. Springer-Verlag Berlin Heidelberg, Berlin, Germany.
Li, Y., Aubin, V., Rey, C., and Bompard, P. (2012). “The effects of variable stress amplitude on cyclic plasticity and microcrack initiation in austenitic steel 304L.” *Computational Materials Science*, 64, 7–11.
Li, Z. X., Chan, T. H. T., and Ko, J. M. (2002). “Determination of effective stress range and its application on fatigue stress assessment of existing briges.” *International Journal of Solids and Structures*, 39(9), 2401–2417.
Liaw, P. K., Yang, C. Y., Palusamy, S. S., and Ren, W. (1997). “Fatigue crack initiation and propagation behavior of pressure vessel steels.” *Engineering Fracture Mechanics*, 57(1), 85–104.
Lillbacka, R., Johnson, E., and Ekh, M. (2006). “A model for short crack propagation in polycrystalline materials.” *Engineering Fracture Mechanics*, 73(2), 223–232.
Liu, Y., and Mahadevan, S. (2007). “Stochastic fatigue damage modeling under variable amplitude loading.” *International Journal of Fatigue*, 29(6), 1149–1161.
Liu, Y., and Mahadevan, S. (2009). “Probabilistic fatigue life prediction using an equivalent initial flaw size distribution.” *International Journal of Fatigue*, 31(3), 476–487.
Liu, Z., Bessa, M. A., and Liu, W. K. (2016). “Self-consistent clustering analysis: An efficient multi-scale scheme for inelastic heterogeneous materials.” *Computer Methods in Applied Mechanics and Engineering*, 306, 319–341.
de los Rios, E. R., Mohamed, H. J., and Miller, K. J. (1985). “A micro-mechanics analysis for short fatigue crack growth.” *Fatigue & Fracture of Engineering Materials & Structures*, 8(1), 49–63.
Lu, Z., and Liu, Y. (2010). “Small time scale fatigue crack growth analysis.” *International Journal of Fatigue*, 32(8), 1306–1321.
Lynn, A. K., and DuQuesnay, D. L. (2002). “Computer simulation of variable amplitude fatigue crack initiation behaviour using a new strain-based cumulative damage model.” *International Journal of Fatigue*, 24(9), 977–986.

Macdonald, D. D., and Engelhardt, G. R. (2012). "A brief review of determinism in the prediction of localized corrosion damage." *Zeitschrift für Physikalische Chemie*, 226(9–10), 871–888.
Madia, M., Schork, B., Bernhard, J., and Kaffenberger, M. (2017). "Multiple crack initiation and propagation in weldments under fatigue loading." *Procedia Structural Integrity*, 7, 423–430.
Maljaars, J., Pijpers, R., and Slot, H. (2015). "Load sequence effects in fatigue crack growth of thick-walled welded C-Mn steel members." *International Journal of Fatigue*, 79, 10–24.
El Malki Alaoui, A., Thevenet, D., and Zeghloul, A. (2009). "Short surface fatigue cracks growth under constant and variable amplitude loading." *Engineering Fracture Mechanics*, 76(15), 2359–2370.
Manonukul, A., and Dunne, F. P. E. (2004). "High- and low-cycle fatigue crack initiation using polycrystal plasticity." *Proceedings of the Royal Society A: Mathematical, Physical and Engineering Sciences*, 460(2047), 1881–1903.
Mansor, N. I. I., Abdullah, S., Ariffin, A. K., and Syarif, J. (2014). "A review of the fatigue failure mechanism of metallic materials under a corroded environment." *Engineering Failure Analysis*, 42, 353–365.
Melenk, J. M., and Babuška, I. (1996). "The partition of unity finite element method: Basic theory and applications." *Computer Methods in Applied Mechanics and Engineering*, 139(1–4), 289–314.
Mikheevskiy, S., Bogdanov, S., and Glinka, G. (2015). "Analysis of fatigue crack growth under spectrum loading - The UniGrow fatigue crack growth model." *Theoretical and Applied Fracture Mechanics*, 79, 25–33.
Miller, K. J. (1987). "The behaviour of short fatigue cracks and their initiation. Part I - A review of two recent books." *Fatigue & Fracture of Engineering Materials & Structures*, 10(1), 75–91.
Miller, M., and McDowell, D. (1992). "A creep-fatigue-oxidation microcrack propagation model for thermomechanical fatigue." *Journal of Engineering Materials and Technology*, 114(3), 282–288.
Millwater, H. R. J. (1997). "A risk assessment method for multi-site damage." The University of Texas at Austin.
Mohammadi, S. (2008). *Extended finite element method: For fracture analysis of structures*. Blackwell Publishing Ltd, Oxford, UK.
Morel, F. (2000). "Critical plane approach for life prediction of high cycle fatigue under multiaxial variable amplitude loading." *International Journal of Fatigue*, 22(2), 101–119.
Moriconi, C., Henaff, G., and Halm, D. (2011). "Influence of hydrogen coverage on the parameters of a cohesive zone model dedicated to fatigue crack propagation." *Procedia Engineering*, 10, 2657–2662.
Mughrabi, H. (2013). "Microstructural fatigue mechanisms: Cyclic slip irreversibility, crack initiation, non-linear elastic damage analysis." *International Journal of Fatigue*, 57, 2–8.
Mughrabi, H., Herz, K., and Stark, X. (1981). "Cyclic deformation and fatigue behaviour of α-iron mono- and polycrystals." *International Journal of Fracture*, 17(2), 193–220.
Murtaza, G., and Akid, R. (2000). "Empirical corrosion fatigue life prediction models of a high strength steel." *Engineering Fracture Mechanics*, 67(5), 461–474.
Musinski, W. D., and McDowell, D. L. (2012). "Microstructure-sensitive probabilistic modeling of HCF crack initiation and early crack growth in Ni-base superalloy IN100 notched components." *International Journal of Fatigue*, 37, 41–53.
Musinski, W. D., and McDowell, D. L. (2016). "Simulating the effect of grain boundaries on microstructurally small fatigue crack growth from a focused ion beam notch through a three-dimensional array of grains." *Acta Materialia*, 112, 20–39.
Navarro, A., and de los Rios, E. R. (1987). "A model for short fatigue crack propagation with an interpretation of the short-long crack transition." *Fatigue & Fracture of Engineering Materials & Structures*, 10(2), 169–186.
Navarro, A., and de los Rios, E. R. (1988). "Short and long fatigue crack growth: A unified model." *Philosophical Magazine A*, 57(1), 15–36.
Newman, J. C., and Raju, I. S. (1981). "An empirical stress-intensity factor equation for the surface crack." *Engineering Fracture Mechanics*, 15(1–2), 185–192.
Panchal, J. H., Kalidindi, S. R., and McDowell, D. L. (2013). "Key computational modeling issues in

Integrated Computational Materials Engineering." *Computer-Aided Design*, 45(1), 4–25.
Park, J., and Nelson, D. (2000). "Evaluation of an energy-based approach and a critical plane approach for predicting constant amplitude multiaxial fatigue life." *International Journal of Fatigue*, 22(1), 23–29.
Piascik, R., and Willard, S. (1994). "The growth of small corrosion fatigue cracks in Alloy 2024." *Fatigue & Fracture of Engineering Materials & Structures*, 17(11), 1247–1259.
Pineau, A., McDowell, D. L., Busso, E. P., and Antolovich, S. D. (2016). "Failure of metals II: Fatigue." *Acta Materialia*, 107, 484–507.
Polák, J., and Man, J. (2014). "Mechanisms of extrusion and intrusion formation in fatigued crystalline materials." *Materials Science and Engineering: A*, 596, 15–24.
Priddy, M. W., Paulson, N. H., Kalidindi, S. R., and McDowell, D. L. (2017). "Strategies for rapid parametric assessment of microstructure-sensitive fatigue for HCP polycrystals." *International Journal of Fatigue*, 104, 231–242.
Przybyla, C. P., and McDowell, D. L. (2011). "Simulated microstructure-sensitive extreme value probabilities for high cycle fatigue of duplex Ti-6Al-4V." *International Journal of Plasticity*, 27(12), 1871–1895.
Przybyla, C. P., Musinski, W. D., Castelluccio, G. M., and McDowell, D. L. (2013). "Microstructure-sensitive HCF and VHCF simulations." *International Journal of Fatigue*, 57, 9–27.
Przybyla, C., Prasannavenkatesan, R., Salajegheh, N., and McDowell, D. L. (2010). "Microstructure-sensitive modeling of high cycle fatigue." *International Journal of Fatigue*, 32(3), 512–525.
Quey, R., Dawson, P. R., and Barbe, F. (2011). "Large-scale 3D random polycrystals for the finite element method: Generation, meshing and remeshing." *Computer Methods in Applied Mechanics and Engineering*, 200(17–20), 1729–1745.
Radaj, D., Sonsino, C. M., and Fricke, W. (2006). *Fatigue assessment of welded joints by local approaches, 2nd edition*. CRC Press LLC, Boca Raton, FL.
Radaj, D., Sonsino, C. M., and Fricke, W. (2009). "Recent developments in local concepts of fatigue assessment of welded joints." *International Journal of Fatigue*, 31(1), 2–11.
Reis, L., Li, B., and de Freitas, M. (2009). "Crack initiation and growth path under multiaxial fatigue loading in structural steels." *International Journal of Fatigue*, 31(11–12), 1660–1668.
Remes, H., Varsta, P., and Romanoff, J. (2012). "Continuum approach to fatigue crack initiation and propagation in welded steel joints." *International Journal of Fatigue*, 40, 16–26.
Rimoli, J. J., and Ortiz, M. (2010). "A three-dimensional multiscale model of intergranular hydrogen-assisted cracking." *Philosophical Magazine*, 90(21), 2939–2963.
Romeiro, F., de Freitas, M., and da Fonte, M. (2009). "Fatigue crack growth with overloads/underloads: Interaction effects and surface roughness." *International Journal of Fatigue*, 31(11–12), 1889–1894.
Roth, S., Hütter, G., and Kuna, M. (2014). "Simulation of fatigue crack growth with a cyclic cohesive zone model." *International Journal of Fracture*, 188(1), 23–45.
Rovinelli, A., Lebensohn, R. A., and Sangid, M. D. (2015). "Influence of microstructure variability on short crack behavior through postulated micromechanical short crack driving force metrics." *Engineering Fracture Mechanics*, 138, 265–288.
Rudolph, J., Schmitt, C., and Weiß, E. (2002). "Fatigue lifetime assessment procedures for welded pressure vessel components." *International Journal of Pressure Vessels and Piping*, 79(2), 103–112.
Ruiz-Muñoz, G. A. (2018). "Method to analyse multiple site damage fatigue before and after crack coalescence." *Engineering Fracture Mechanics*, 188, 416–430.
Sangid, M. D. (2013). "The physics of fatigue crack initiation." *International Journal of Fatigue*, 57, 58–72.
Sangid, M. D., Maier, H. J., and Sehitoglu, H. (2011). "A physically based fatigue model for prediction of crack initiation from persistent slip bands in polycrystals." *Acta Materialia*, 59(1), 328–341.
Sauzay, M., Liu, J., Rachdi, F., Signor, L., Ghidossi, T., and Villechaise, P. (2014). "Physically-based simulations of the cyclic behavior of FCC polycrystals." *Advanced Materials Research*, 891–892, 833–839.
Sauzay, M., and Moussa, M. O. (2013). "Prediction of grain boundary stress fields and microcrack initiation

induced by slip band impingement." *International Journal of Fracture*, 184(1–2), 215–240.
Schijve, J. (2009). *Fatigue of structures and materials, 2nd edition*. Springer Netherlands, Dordrecht, Netherlands.
Sehitoglu, H., Gall, K., and Garcia, A. (1989). "Recent advances in fatigue crack growth modeling." *International Journal of Fracture*, 80(2–3), 165–192.
Shi, P., and Mahadevan, S. (2003). "Corrosion fatigue and multiple site damage reliability analysis." *International Journal of Fatigue*, 25(6), 457–469.
Shintaku, Y., Muramatsu, M., Takase, S., Tsutsumi, S., and Terada, K. (2015). "Cohesive crack model to reflect local chemical action at grain and its boundaries in polycrystalline metals." *Quarterly Journal of The Japan Welding Society*, 33(2), 152s–155s.
Siddiq, A., and Schmauder, S. (2006). "Crystal plasticity parameter identification procedure for single crystalline material during deformation." *Journal of Computational and Applied Mechanics*, 7(1), 1–15.
Sinha, S., and Ghosh, S. (2006). "Modeling cyclic ratcheting based fatigue life of HSLA steels using crystal plasticity FEM simulations and experiments." *International Journal of Fatigue*, 28(12), 1690–1704.
Skorupa, M., and Skorupa, A. (1993). "Significance of crack initiation period in structural steel welds." *Proceedings of the International Conference on Offshore Mechanics and Arctic Enginneering, Vol. III-B, Material Engineering*, The American Society of Mechanical Engineers, New York, NY, 715–720.
Smith, N. J., McGrath, J. T., Gianetto, J. A., and Orr, R. F. (1989). "Microstructure/mechanical property relationships of submerged arc welds in HSLA 80 steel." *Welding Journal*, 68(3), 112s–120s.
Stephens, R. I., Fatemi, A., Stephens, R. R., and Fuchs, H. O. (2000). *Metal fatigue in engineering, 2nd edition*. John Wiley & Sons, Inc., Hoboken, NJ.
Sun, B., and Li, Z. (2014). "A multi-scale damage model for fatigue accumulation due to short cracks nucleation and growth." *Engineering Fracture Mechanics*, 127, 280–295.
Suresh, S., and Ritchie, R. O. (1984). "Propagation of short fatigue cracks." *International Metals Reviews*, 29(6), 445–476.
Susmel, L., and Taylor, D. (2012). "A critical distance/plane method to estimate finite life of notched components under variable amplitude uniaxial/multiaxial fatigue loading." *International Journal of Fatigue*, 38, 7–24.
Susmel, L., Tovo, R., and Socie, D. F. (2014). "Estimating the orientation of Stage I crack paths through the direction of maximum variance of the resolved shear stress." *International Journal of Fatigue*, 58, 94–101.
Sweeney, C. A., Vorster, W., Leen, S. B., Sakurada, E., McHugh, P. E., and Dunne, F. P. E. (2013). "The role of elastic anisotropy, length scale and crystallographic slip in fatigue crack nucleation." *Journal of the Mechanics and Physics of Solids*, 61(5), 1224–1240.
SwRI (Southwest Research Institute), and NASA (National Aeronautics and Space Administration). (2016). "NASGRO 8.0 Fracture Mechanics and Fatigue Crack Growth Software." SwRI, San Antonio, TX.
Tan, J. T., and Chen, B. K. (2015). "Prediction of fatigue life in aluminium alloy (AA7050-T7451) structures in the presence of multiple artificial short cracks." *Theoretical and Applied Fracture Mechanics*, 78, 1–7.
Tan, L., and Arwade, S. R. (2008). "Response classification of simple polycrystalline microstructures." *Computer Methods in Applied Mechanics and Engineering*, 197(13–16), 1397–1409.
Tanaka, K., and Mura, T. (1981). "A dislocation model for fatigue crack initiation." *Journal of Applied Mechanics*, 48(1), 97–103.
TMS (The Minerals Metals & Materials Society). (2015). "Modeling across scales: A roadmapping sudy for connecting materials models and simulations across length and time scales." TMS, Warrendale, PA.
Troitsky, M. S. (1987). *Orthotropic bridges-theory and design-2nd edition*. James F. Lincoln Arc Welding Foundation, Cleveland, OH.
Venkateswaran, P., Ganesh Sundara Raman, S., and Pathak, S. D. (2005). "Short fatigue crack growth

behaviour of a ferritic steel weld metal." *Science and Technology of Welding and Joining*, 10(1), 95–102.
Vosynek, P., Vlk, M., and Návrat, T. (2014). "Review of pressurized vessel structural design – an assessment of total life." *Applied Mechanics and Materials*, 624, 218–222.
Wang, B. (2017). "A multiscale study on fatigue mechanism and life estimation on welded joints of orthotropic steel decks." Ghent University, Tongji University.
Wang, D. (1990). "Fatigue behaviour of mechanically fastened double-angle shear connection in steel bridges." Lehigh University.
Wei, L. W., de los Rios, E. R., and James, M. N. (2002). "Experimental study and modelling of short fatigue crack growth in aluminium alloy Al7010-T7451 under random loading." *International Journal of Fatigue*, 24(9), 963–975.
Wells, G. N., and Sluys, L. J. (2001). "A new method for modelling cohesive cracks using finite elements." *International Journal for Numerical Methods in Engineering*, 50(12), 2667–2682.
Wen, B., and Zabaras, N. (2012). "Investigating variability of fatigue indicator parameters of two-phase nickel-based superalloy microstructures." *Computational Materials Science*, 51(1), 455–481.
Wirsching, P. H. (1984). "Fatigue reliability for offshore structures." *Journal of Structural Engineering*, 110(10), 2340–2356.
Wu, T.-Y., Bassani, J. L., and Laird, C. (1991). "Latent hardening in single crystals - I. Theory and experiments." *Proceedings of the Royal Society A: Mathematical, Physical and Engineering Sciences*, 438(1893), 1–19.
Wu, W., Owino, J., Al-Ostaz, A., and Cai, L. (2014). "Applying periodic boundary conditions in finite element analysis." *Simulia Community Conference*, DS SIMULIA, Providence, RI.
Wu, X. J., and Akid, R. (1995). "Propagation Behaviour of Short Fatigue Cracks in Q2N Steel." *Fatigue & Fracture of Engineering Materials & Structures*, 18(4), 443–454.
Xie, C. L., Ghosh, S., and Groeber, M. (2004). "Modeling cyclic deformation of HSLA steels using crystal plasticity." *Journal of Engineering Materials and Technology*, 126(4), 339.
Xu, Y., and Yuan, H. (2009a). "Computational analysis of mixed-mode fatigue crack growth in quasi-brittle materials using extended finite element methods." *Engineering Fracture Mechanics*, 76(2), 165–181.
Xu, Y., and Yuan, H. (2009b). "Computational modeling of mixed-mode fatigue crack growth using extended finite element methods." *International Journal of Fracture*, 159(2), 151–165.
Xue, Y. (2010). "Modeling fatigue small-crack growth with confidence - A multistage approach." *International Journal of Fatigue*, 32(7), 1210–1219.
Ya, S., Yamada, K., and Ishikawa, T. (2010). "Fatigue evaluation of rib-to-deck welded joints of orthotropic steel bridge deck." *Journal of Bridge Engineering*, 16(4), 492–499.
Yuan, H., Zhang, W., Castelluccio, G. M., Kim, J., and Liu, Y. (2018a). "Microstructure-sensitive estimation of small fatigue crack growth in bridges steel welds." *International Journal of Fatigue*, 112, 183–197.
Yuan, H., Zhang, W., Kim, J., and Liu, Y. (2017a). "A nonlinear grain-based fatigue damage model for civil infrastructure under variable amplitude loads." *International Journal of Fatigue*, 104, 389–396.
Yuan, H., Zhang, W., Kim, J., and Liu, Y. (2017b). "Mesoscale simulation of corrosion fatigue by an integrated transgranular and intergranular crack growth method." *AIAA SciTech Forum - 58th AIAA/ASCE/AHS/ASC Structures, Structural Dynamics, and Materials Conference*, AIAA (American Institute of Aeronautics and Astronautics), Reston, VA.
Yuan, H., Zhang, W., and Liu, Y. (2018b). "Quantification of time distribution to initial long crack by reduced order microstructural representation on microstructurally short fatigue crack growth model." *AIAA SciTech Forum - Non-Deterministic Approaches Conference*, AIAA (American Institute of Aeronautics and Astronautics), Reston, VA.
Zhai, J., Tomar, V., and Zhou, M. (2004). "Micromechanical simulation of dynamic fracture using the cohesive finite element method." *Journal of Engineering Materials and Technology*, 126(2), 179–191.
Zhang, J., Bao, R., Zhang, X., and Fei, B. (2010). "A probabilistic estimation method of multiple site damage occurrence for aircraft structures." *Procedia Engineering*, 2(1), 1115–1124.

Zhang, J., Yang, S., and Lin, J. (2016). “A nonlinear continuous damage model based on short-crack concept under variable amplitude loading.” *Fatigue & Fracture of Engineering Materials & Structures*, 39(1), 79–94.
Zhang, W., Cai, C. S., and Pan, F. (2013a). “Finite element modeling of bridges with equivalent orthotropic material method for multi-scale dynamic loads.” *Engineering Structures*, 54, 82–93.
Zhang, W., Cai, C. S., and Pan, F. (2013b). “Nonlinear fatigue damage assessment of existing bridges considering progressively deteriorated road conditions.” *Engineering Structures*, 56, 1922–1932.
Zhang, W., Cai, C. S., Pan, F., and Zhang, Y. (2014). “Fatigue life estimation of existing bridges under vehicle and non-stationary hurricane wind.” *Journal of Wind Engineering and Industrial Aerodynamics*, 133, 135–145.
Zhang, W., and Yuan, H. (2014). “Corrosion fatigue effects on life estimation of deteriorated bridges under vehicle impacts.” *Engineering Structures*, 71, 128–136.
Zhang, X., and Oskay, C. (2015). “Eigenstrain based reduced order homogenization for polycrystalline materials.” *Computer Methods in Applied Mechanics and Engineering*, 297, 408–436.
Zhang, Y. M., Ariffin, M. Z., Xiao, Z. M., Zhang, W. G., and Huang, Z. H. (2015). “Nonlinear elastic-plastic stress investigation for two interacting 3-D cracks in offshore pipelines.” *Fatigue and Fracture of Engineering Materials & Structures*, 38(5), 540–550.
Zheng, X., Baotong, L., and Tianxie, C. (1994). “Fatigue tests and life prediction of 16 Mn steel butt welds without crack-like defect.” *International Journal of Fracture*, 68(3), 275–285.